Characterisation of the In-vivo Terahertz Communication Channel within the Human Body Tissues for Future Nano-Communication Networks.

YANG, Ke

Characterisation of the In-vivo Terahertz Communication Channel within the Human Body Tissues for Future Nano-Communication Networks

Ke YANG

A thesis submitted to the faculty of the University of London in partial fulfillment of the requirements for the degree of

Doctor of Philosophy

School of Electronic Engineering and Computer Science
Queen Mary, University of London
London E1 4NS
United Kingdom

September 2015

To my family, for their endless love, encouragement and support

Abstract

Body centric communication has been extensively studied in the past for a range of frequencies, however the need to reduce the size of the devices makes nano-scale technologies attractive for future applications. This opens up opportunities of applying nano-devices made of the novel materials, like carbon nano tubes (CNT), graphene and etc., which operate at THz frequencies and probably inside human bodies.

With a brief introduction of nano-communications and review of the state of the art, three main contributions have been demonstrated in this thesis to characterise nano-scale body-centric communication at THz band:

- A novel channel model has been studied. The path loss values obtained from the simulation have been compared with an analytical model in order to verify the feasibility of the numerical analysis. On the basis of the path loss model and noise model, the channel capacity is also investigated.

- A 3-D stratified skin model is built to investigate the wave propagation from the under-skin to skin surface and the influence of the rough interface between different skin layers is investigated by introducing two detailed skin models with different interfaces (i.e.,3-D sine function and 3-D sinc function). In addition, the effects of the inclusion of the sweat duct is also analysed and the results show great potential of the THz waves on sensing and communicating.

- Since the data of dielectric properties for biological materials at THz band are quite scarce, in collaboration with the Blizard Institute, London, UK, different human tissues such as skin, blood, muscle and *etc.* are planned to be measured with the THz Time Domain Spectroscopy (THz-TDS) system at Queen Mary University of London to enrich the database of electromagnetic parameters at the band of interest. In this chapter, collagen, the main constitution of skin was

mainly studied. Meanwhile, the measured results are compared with the simulated ones with a good agreement.

Finally, a plan for further research activities is presented, aiming at widening and deepening the present understanding of the THz body-centric nano-communication channel, thus providing a complete characterisation useful for the design of reliable and efficient body centric nano-networks.

Acknowledgement

My most sincere and deepest gratitude would like to go to my supervisors and mentors: Prof. Yang Hao & Dr. Akram Alomainy, for their endless support, guidance and encouragement throughout my entire Ph.D.. They both set excellent models for me to overcome the difficulties for their unbounded energy and passion to pursue the truth of science, which has given me the strength and confidence necessary for the development of the work. Besides their valuable academic advice and guidance, they are also kind, friendly and helpful as a human being. I would also like to thank my independent examiner, Dr. Khalid Rajab for his positive and fruitful comments, and Prof. Clive Parini for his assistance during my study in Queen Mary University of London.

A special mention would also like to go to Dr. Qammer Hussain Abbassi, his knowledge and willingness to meet and help all the time during my writing-up period did me a great favour. Without his help, I could not finish this thesis. Also, I would like to thank Prof. Josep Miquel Jornet, University at Buffalo, The State University of New York. Although we just spend two weeks together, I learned much from our detailed discussion and so did the communication with his students, which consolidated my research path towards this thesis.

Additionally, I would like to show my appreciation to my colleagues in antenna group, Dr. Rui Yang, Dr. Oscar Quevedo Teruel , Dr. Rhiannon Mitchell-Thomas, Dr. M*é*lusine Pigeon, Dr. Max Munoz, Dr. Jiefu Zhang, Ms. Nishtha Chopra, Mr. Jiandong Lang and *etc.*, from whom I learned how to be both a qualified researcher and a person knowing how to enjoy life. Without them, I would not have an enjoyable Ph.D.. At the same time, I would like to thank my friends: Dr. Fang Mai, Dr. Chen Chen, Dr. Yongfei Cui and Mr. Dong Dong and *etc.*, with whom I broadened my horizon a lot. Our trips to Europe would always be the pearls in my memory and wish you guys a bright future from my deep heart.

Many thanks to China Scholarship Council for the financial support. I would also

extend my thanks to all staff in Queen Mary University of London for their provision of a good working atmosphere.

Above all, I would like to thank all my family. Regardless of physical distance, their support and affection have always been with me. My last thought goes to: my grandparents and my parents who are always standing by me through thick and thin and also my brother. I dedicate this thesis to my family, to honour their unconditional love, endless encouragement and support, and most importantly, firm confidence in me throughout my life.

Ke Yang

London, Semptember 2015

List of Publications

Journal Publications

1. K. Yang, A. Pellegrini, M. Munoz, A. Brizzi, A. Alomainy and Y. Hao, Numerical Analysis and Characterisation of THz Propagation Channel for Body-Centric Nano-Communication, IEEE Transaction on THz Science and Technology, vol. 5, May 2015.

2. K. Yang, Q.H. Abbasi, N. Chopra, M. Munoz, Y. Hao, and A. Alomainy, Effects of Non-Flat Interfaces in Human Skin Tissues on the In-Vivo THz Communication Channel, Nano Communication Network, Nov., 2015.

3. G. Piro, K. Yang, G. Boggia, N. Chopra, L.A. Grieco and A. Alomainy, Terahertz Communications in Human Tissues at the Nano-Scale for Healthcare Applications, IEEE Transactions on Nanotechnology, vol. 14, May 2015.

4. Y.F. Chen, S. Bush, A. Eckford, K. Yang, N. Chopra, A. Alomainy, Y. Hao, G. Piro, A. Aijaz, M. Nakhai, Y. Zhou and P. Kosmas, A Comprehensive Standardized Framework for Nanoscale and Molecular Communication, Proceedings of the IEEE (submitted).

Standard Contribution

1. S.F. Bush, A. Echford, J. Paluh, T. Thai, T. Sato, G. Piro, Y. Chen, K. Yang, V. Rao, V. Prasad, A. Mukherjee, T. Wysocki, E.F. Armay, A. Rafiei, and S. Goel, P1906.1/D1.1 Draft Recommended Practice for Nanoscale and Molecular Communication Framework, IEEE, 2015.

Conference Publications

1. K. Yang, N. Chopra, J. Upton, A. Alomainy, and Y. Hao, Characterizing Skin-Based Nano-Networks for Healthcare Monitoring Application at THz,IEEE APS/USNC-URSI 2015, Vancouver, BC, Canada, 19-24 July 2015.

2. N. Chopra, K. Yang, J. Upton, A. Alomainy, M. Philpott, Y. Hao, Understanding and Characterising Nanonetworks for Healthcare Monitoring Applications, IEEE IMWS-Bio 2014, London, 8-10 December 2014.

3. K. Yang, Q.H. Abbasi, K. Qaraqe, A. Alomainy and Y. Hao, Body-Centric Nano-Networks: EM Channel Characterisation in Water at the Terahertz Band, The 2014 Asia Pacific Microwave Conference (APMC 2014), 4 to 7 November 2014, Sendai, Japan. (Invited).

4. M. Munoz, K. Yang, A. Alomainy and H. Yang, Modelling of skin tissue for body-centric communications at terahertz frequencies, General Assembly and Scientific Symposium (URSI GASS), 2014 XXXIth URSI, Beijing, China, 16-23 Aug. 2014.

5. Ke Yang, Alice Pellegrini, Alessio Brizzi, Akram Alomainy, Yang Hao, Numerical Analysis of the Communication Channel Path Loss at the THz Band inside the Fat Tissue, IEEE IMWS-Bio 2013, Singapore, 9-11 December 2013.

6. Ke Yang, Akram Alomainy and Yang Hao, In-vivo Characterisation and Numerical Analysis of the THz Radio Channel for Nanoscale Body-Centric Wireless Networks, IEEE APS/USNC-URSI 2013, Orlando, Florida, USA, 7-13 July 2013.

7. Richa Bharadwaj, Ke Yang, Akram Alomainy, Clive Parini, Effect of Base Station Configurations and Complexity on the Accuracy of Ultra Wideband Localisation, 2013 IEEE AP-S/USNC-URSI Symposium, July 7- 13, 2013 in Orlando, Florida.

Contents

List of Abbreviations

3D	Three Dimension
AIGN	Additional Inverse Gaussian Noise
ACW	Average Code Weight
BAN	Body Area Network
BER	Bit Error Rate
CIR	Channel Impulse Response
CNT	Carbon Nano-Tube
CPW	Co-Planar Waveguide
DMC	Diffusion-based Molecular Communication
dB	Decibels
EM wave	Electromagnetic wave
FCC	Federal Communications Commission
FDA	Food and Drug Administration
FDTD	Finite-Difference Time-Domain
FFT	Fast Fourier Transform
FIT	Finite Integral Technique
FMC	Flow-based Molecular Communication
Gbps	Gigabits per second
GNR	Graphene Nano-Ribbons
IC	Integrated Circuit
IEEE	Institute of Electrical & Electronics Engineers
IoNT	Internet of Nano-Things
IR-UWB	Impulse Radio Ultra Wide-Band
ISM	Industrial, Scientific and Medical
LoS	Line of Sight
MAC	Medium Access Control

MB-OFDM	Multi-Band Orthogonal Frequency Division Multiplexing
MICS	Medical Implant Communication System
NLoS	Non-Line of Sight
OCT	Optical Coherent Tomography
p.s.d	power spectrum distribution
PEC	Perfect Electronic Conductor
PIFA	Planar Inverted-F Antenna
PL	Path Loss
PML	Perfect Match Layer
PSO	Particle Swarm Optimisation
RF	Radio Frequency
RMS	Root Mean Square
RT	Ray Tracing
SAR	Specific Absorption Rate
SC	Stratum Corneoum
SEM	Scanning Electron Micrscope
SNR	Signal Noise Ratio
Tbps	Tera-bits per second
TDMA	Time Division Multiple Access
THz band	Tera-Hertz band
TS-OOK	Time-Spread On-Off Keying
Tx	Transmitter
UWB	Ultra Wide-Band
WSN	Wireless Sensor Network
VHF	Very High-Frequency

List of Figures

List of Tables

Chapter 1

Introduction

"I want to build a billion tiny factories, models of each other, which are manufacturing simultaneously. . . The principles of physics, as far as I can see, do not speak against the possibility of maneuvering things atom by atom. It is not an attempt to violate any laws; it is something, in principle, that can be done; but in practice, it has not been done because we are too big."

Richard Feynman

1.1 Introduction to Nanotechnology

Nanotechnology has garnered great attention since its first proposal in 1959 by Richard Feynman in his talk *There's Plenty of Room at the Bottom*, where the possibility of synthesis via direct manipulation of atoms was described; but the term "nano-technology" was not used until 1974 by Norio Taniguchi to describe the technology manipulating materials at the nano-meter level [1]. Later in 1986, K. Eric Drexler proposed the idea of a nanoscale "assembler" inspired by Feyman's talk in the book of *Engines of Creation: The Coming Era of Nanotechnology* [2]. Then, through Drexler's popularisation, the nanotechnology has been widely accepted by public and well developed in academic fields.

According to ISO/TS 27686:2008, the nano-scale is defined as the size from 1 nm to 100 nm [3]. Thus, the nanotechnology can be defined as: "Nanotechnology is science, engineering, and technology conducted at the nanoscale, which is about 1 to 100 nanometers. Nanoscience and nanotechnology are the study and application of extremely small things and can be used across all the other science fields, such as chemistry, biology, physics, materials science, and engineering."[4] according to National Nanotechnology Initiative (NNI). Therefore, two other statements should be emphasized to further understand the definition [5]: first, nanotechnology should contain the formation and application of materials, structures, devices, and systems with unique properties due to their nano-scale size; second, nanotechnology should also include the technologies which can control the materials at nano scale.

Three main research areas have been conducted since its proposal: nano-science where the interaction and behaviour of the nano-materials would be studied; nano-materials fabrication which studies the experimental development of nano-materials and computer modelling to study the interactions and properties of nano-materials by simulation. Recently, nanoparticles such as dendrimers, carbon fullerenes (buckyballs) and nano-shells are used to target specific tissues and organs [6] and molecular and genomic tools are used to uncover the complexity of the induced defence signalling networks of plants [7]. And also, molecular-scale filters and pores with well-defined sizes, shapes, and surface properties allow engineering better functionality in molecular sieving [8].

Four generations were proposed for the roadmap of nanotechnology by Mihail Roco in [9]:

- Passive nanostructures: a) Dispersed and contact nanostructures; b) Products incorporating nanostructures;
- Active nanostructures: a)Bio-active, health effects; b) Physico-chemical active;
- Systems of nanosystems
- Molecular nanosystems

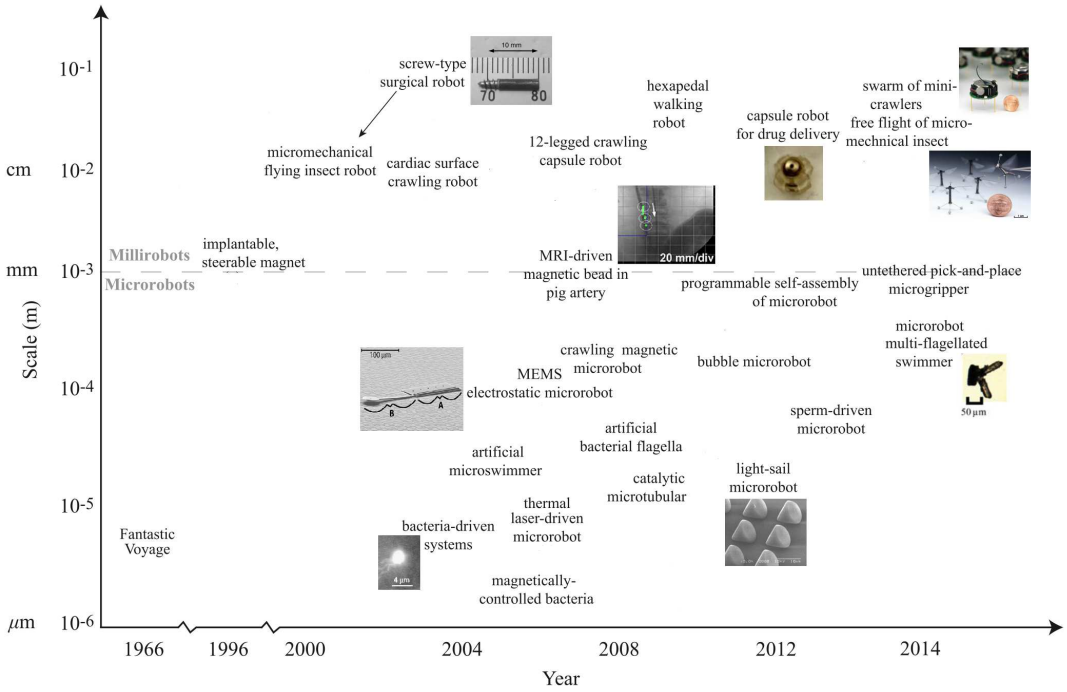

Figure 1.1: Development map of the micro/nano-devices (reproduced from [10])

1.2 Recent Development in Nano-Communication

Based on the general development time-line of nanotechnology, it can be easily seen that the ultimate goal of nano technology would go for nano-network, where the current entire network systems would be shrunk into nanoscale with the nano-robots and molecular machines as the elements in the near future [10]. The development of nano-devices is shown in Fig. 1.1. With the introduction of nanotechnology, the idea of decreasing the size of present sensor network into nano level was also proposed; but at the same time, how to connect the nano-devices in such networks to conduct complex tasks was also questioned, leading to the proposal of the nano-network, followed by the introduction of the concept of nano-communication [11, 12].

The size can make the nano-devices reach the places where current technologies cannot, like in-body environment or some harsh environment [11]. At the same time, the non-invasive method can be realised or the goal of minimal wound would be achieved. Due to the characteristics of iniquitousness and variety of the nano-sensor, different kinds of information can be sensed and gathered together to complete complicated tasks. By using bio-nano-sensors in medicine, e-health monitoring system

[13] can be realised, so is the e-drug delivery system [12] with the aid of nano-robots. The ultimate goal is to connect the nano-network to the internet, by which e-office and e-living house can be fulfilled [14].

Due to the increasingly garnered attention, more and more academic groups have put their focuses on nano-communication since the concept was first mentioned in 2004 by Kaifu Cheng [15]. The NaNoNetworking Center in Catalonia (N3Cat) was set up in 2009 at Universitat Politècnica de Catalunya (UPC), Spain as an initiative of Prof. Ian F. Akyildiz and Prof. Josep Sol-Pareta with the main goal of carrying fundamental research on nanonetworks. Now, three main projects are undergoing: Graphene-enabled Wireless Networks-on-Chip for Massive Multicore Architectures (GWNoCS), Graphene-enabled Wireless Communications and Fundamentals and Applications of Molecular Nanonetworks through Cell Signalling [16]. Later, Nano Communications Centre (NC^2) was established at Tampere University of Technology, Finland to mainly study the molecular communication for nano-network where bacterial nanonetworks, neuronal networks and calcium signalling were investigated [17]. The PhD work of Dr. Josep Miquel Jornet was mainly on EM nano-communication at THz band [18], under the guidance of Professor Ian F. Akyildiz whose another project was on Molecular Nano-Communication Networks (MoNaCo) supported by the National Science Foundation. Meanwhile, as a part of COMNET (Computer Networks) family, a new journal, *i.e.*, Nano Communication Networks, was published in 2010 with Prof. Ian F. Akyildiz as the editor-in-chief, where all aspects of nano-scale networking and communications were covered [19]. In 2014, Josep joined in University at Buffalo, The State University of New York as a professor and built a group whose research emphasis was put on the THz channel characterisation on the basis of the model and design of the graphene-based plasmonic nano-antennas and nano-transceivers. To expand the current ISM and mm-wave work at Queen Mary University of London (QMUL) to nano-scale, the theoretical and numerical studies on the channel performance of nano-communication at THz band was initially investigated [20] [21]. To make nano-network systematic, the IEEE has initiated the standard development project IEEE P1906.1/Draft 1.0 Recommended Practice for Nanoscale and Molecular Communication Framework to provide a definition, common framework, and common parameters for nanoscale communication networks [22], led by S.F. Bush.

1.3 Applications of Nano-Networks [13]

There are a great number of potential applications of nanonetworks, which can be mainly divided into four groups: biomedical, environmental, industrial and military [13][12]. Detailed descriptions of the envisioned applications have been summarised and classified in [12], shown in table 1.1. From it, we can see that nano-networks are born for biomedical fields due to its advantages of size, bio-compatibility and bio-stability. Nano devices spreading over the human body can monitor the human physical movement. For example, nano pressure-sensors distributed in eyes can detect the intraocular pressure (IOP) for the early diagnosis and treatment of glaucoma to prevent vision loss [10]. At the same time, the nano devices deployed in bones can monitor the bone-growth in young diabetes patients to keep them from osteoporosis [10]. Furthermore, nano-robots inside the biological tissues can detect and then eliminate malicious agents or cells , such as viruses or cancer cells, make the treatment less invasive and real time [23]. Moreover, networked nano-devices will be used for organ, nervous track, or tissue replacements, i.e., bio-hybrid implants. While in [14], the concept of intelligent office was proposed, shown in Fig. 1.2. Nano-transceivers are attached to all the elements in the office and even their internal components, which enables them to connect to the Internet all the time; therefore, the user can keep track of the location and status of all the belongings in an effortless fashion. At the same time, all the nano-sensors can detect the user's movement to make essential activity according to the corresponding user's behaviour/needs. The detailed explanation would be given in Appx.A while the specific application such as health monitor, plant monitor and *etc.* will be further explained in Chapter 2 with the structure of the nano-network.

1.4 Research Challenges

To enable nano-devices communicate with each other, many fundamental challenges need to be addressed. As the functional devices shrink into nano-scale, design, fabrication and control of the systems would require design principles which would greatly differ from that of macro-scale [10].

- Nano-addressing is an outstanding physical challenge because of the large amount

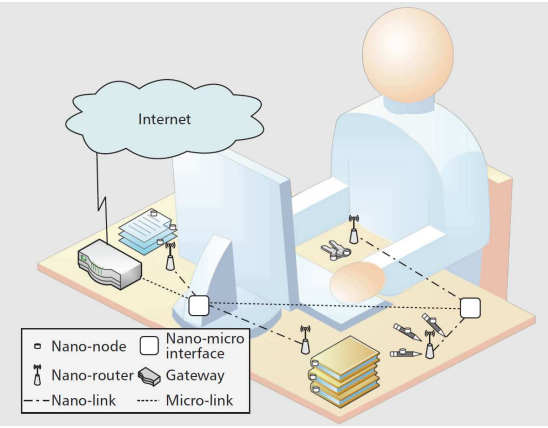

Figure 1.2: Schematics of intelligent office (reproduced from [14])

	Biomedical [6]	Environmental	Industrial	Military
Health Monitor	• Active Visual Imaging for Disease Diagnosis [24] [25] [26] [27] [28] • Mobile Sensing for Disease Diagnosis [29] [30] [31] [32]	Bio-Degradation [13]	Product Quality Control [33]	Nuclear, Biological and Chemical Defences [34]
Therapy	• Tissue Engineering [35] [36] [37] • Bio-Hybrid Implant [38] [39] • Targeted Therapy/Drug Delivery [40] [41] [42] [43] [44] • Cell Manipulation [45] [24] [46] [47] [48] • Minimally Invasive Surgery [49] [50] [51]	Bio-Control [52] [7] [8]	Intelligent Office [14]	Nano-Fictionalized Equipment [53]

Table 1.1: Overview of the envisioned applications [10][12]

of nano-sensors;

- The synchronisation between different devices at nano-scale, another essential aspect of communication, is also a tough job, especially for large-scale distributed networks;
- Reliability and communication speed of the nano-network is another additional challenge because most current communication schemes, e.g. molecular communication, are subject to random processes and diffusion of the molecules;
- Designing the complex nano-scale devices and deploying them is fairly challenging due to the current manufacture technology;
- The interface not among nano-scale components, but also between nano-scale and macro-scale network is also difficult to deal with according to current technology;
- Very limited simulation or analysis tools of nano-scale networks have been put forward. Since the nano-communication is a multidisciplinary topic, the different communication paradigms should work together to complete the full task. However, there is no such simulation platforms to model all the communication methods.

1.5 Research Objectives

The design of reliable and efficient body-centric systems working at THz band requires a detailed analysis of the communication channel. Being the human body a lossy and dispersive medium, the effects of its existence on both antennas and propagation channel have to be properly investigated and modelled.

The initial objectives of this research are summarised as follows:

- Is it possible to use the THz wave for the body-centric nano-communication, especially the in-body communication?
- If so, is it possible to build the corresponding nano-system?

With these two main questions in mind, the following inquiries should be discussed and answered:

- What is the channel performance? Is it different from the traditional ones?
- How can we study the channel? Or what kind of tools can we use to study the channel performance?
- If the nano-system can be built, what is the characteristics of such systems?
- What kind of tools can we use to set up such systems?

1.6 Our Contributions

With the objectives in mind, three key contributions have been achieved, which are summarised below:

- A novel channel model was proposed with the aim to characterise Body-Centric Nano Communication. The path loss values obtained from the simulation have been compared with an analytical model in order to verify the feasibility of the numerical analysis. On the basis of the path loss model and noise model, the channel capacity is also investigated.
- A 3-D stratified skin model is built to investigate the wave propagation from the under-skin to skin surface. Then, the influence of the rough interface between different skin layers is investigated by introducing two detailed skin models with different interfaces (i.e.,3-D sine and 3-D sinc functions). The effects of the inclusion of the sweat duct was studied as well. The results show great potential of the THz waves on sensing and communicating.
- Collagen, main constitute of epidermis of skin, was measured with the THz Time Domain Spectroscopy (THz-TDS) system at Queen Mary University of London (QMUL) to obtain its electromagnetic parameters with the cooperation of Blizard Institute, London UK. At the same time, the double Debye model of the dielectric function at THz band was studied, followed by the investigation of the power loss.

1.7 Thesis Organisation

The rest of the thesis is organised as follows:

Chapter 2 presents the fundamentals of nano communication with a brief introduction to its definition, framework, and various paradigms. The development of the micro/nano-devices is also investigated. Finally, currently available simulation platforms are reviewed.

Chapter 3 gives a brief introduction to EM fundamentals of the communication from the aspects of antennas for body-centric, especially in-body communication, present technology of phantom applied for the study, THz technologies and the corresponding channel performance, and *etc.*.

Chapter 4 presents a thorough investigation of the possibility of THz technology applied to the nano body-centric communication based on the previous studies. A new model is proposed to study the channel performance, *i.e.*, path loss and noise performance. Then the capacity of the channel is studied and numerical models are built to evaluate the proposed model.

Chapter 5 presents a detailed numerical skin model to investigate the effects of the rough interface between different skin layers on the wave performance. First, two skin models with different interfaces defined as 3-D sine and 3-D sinc functions are proposed and compared with a flat model. Then, the sweat duct is included to study the influence of its different states (with sweat as on and without sweat as off). At the same time, the impact of the antenna location is also studied.

Chapter 6 contributes to the database of the EM parameters (mainly dielectric constants) of human tissues at THz band. In this chapter, the collagen, the main constitution of skin, is cultivated and measured by the Time-Domain Spectroscopy system to investigate the suitability to use collagen to represent the skin at the band of interest. Then, an analytical model is proposed based on the measured dielectric constant, *i.e.*, permittivity. Finally, measured power losses of the sample is compared to the theoretical calculation to validate the accuracy of the model presented in Chapter 4.

Chapter 7 provides a summary of the main contributions and findings of the study and concludes the accomplished work. Potential future research activities are also introduced.

References

[1] N. Taniguchi *et al.*, "On the basic concept of nanotechnology," in *Proc. Intl. Conf. Prod. Eng. Tokyo, Part II, Japan Society of Precision Engineering*, 1974, pp. 18–23.

[2] D. K. Eric, "Engines of creation. the coming era of nanotechnology," 1986.

[3] ISO, "Nanotechnologies terminology and definitions for nano-objects nanoparticle, nanofibre and nanoplate, iso/ts 27687:2008, 2008," 2008.

[4] What is Nanotechnology. [Online]. Available: http://www.nano.gov/nanotech-101/what/definition

[5] F. Allhoff, P. Lin, and D. Moore, *Front Matter*. Wiley Online Library, 2010.

[6] R. A. Freitas, "Nanotechnology, nanomedicine and nanosurgery," *International Journal of Surgery*, vol. 3, no. 4, pp. 243–246, 2005.

[7] C. M. Pieterse and M. Dicke, "Plant interactions with microbes and insects: from molecular mechanisms to ecology," *Trends in plant science*, vol. 12, no. 12, pp. 564–569, 2007.

[8] J. Han, J. Fu, and R. B. Schoch, "Molecular sieving using nanofilters: past, present and future," *Lab on a Chip*, vol. 8, no. 1, pp. 23–33, 2008.

[9] M. C. Roco, "Nanotechnology's future," *Scientific American*, vol. 295, no. 2, pp. 39–39, 2006.

[10] M. Sitti, H. Ceylan, W. Hu, J. Giltinan, M. Turan, S. Yim, and E. Diller, "Biomedical applications of untethered mobile milli/microrobots," *Proceedings of the IEEE*, vol. 103, no. 2, pp. 205–224, 2015.

[11] S. F. Bush, *Nanoscale Communication Networks*. Artech House, 2010.

[12] I. F. Akyildiz, F. Brunetti, and C. Blázquez, "Nanonetworks: A new communication paradigm," *Computer Networks*, vol. 52, no. 12, pp. 2260–2279, 2008.

[13] I. F. Akyildiz and J. M. Jornet, "Electromagnetic wireless nanosensor networks," *Nano Communication Networks*, vol. 1, no. 1, pp. 3–19, 2010.

[14] ——, "The internet of nano-things," *Wireless Communications, IEEE*, vol. 17, no. 6, pp. 58–63, 2010.

[15] C. Kaifu, "Nano-photoelectronics devices in nano-communication," *Nanoscience & Technology*, vol. 3, p. 008, 2004.

[16] Homepage of NanoNetworking Center in Catalonia at Universitat Politècnica de Catalunya, Spain. [Online]. Available: http://www.n3cat.upc.edu/index

[17] Homepage of Nano Communications Centre at Tampere University of Technology, Finland. [Online]. Available: http://et4nbic.cs.tut.fi/nanocom/index.html

[18] J. M. Jornet and I. F. Akyildiz, "Fundamentals of electromagnetic nanonetworks in the terahertz band," *Foundations and Trends® in Networking*, vol. 7, no. 2-3, pp. 77–233, 2013.

[19] Homepage of Nano Communication Networks. [Online]. Available: http://www.journals.elsevier.com/nano-communication-networks

[20] G. Piro, K. Yang, G. Boggia, N. Chopra, L. Grieco, and A. Alomainy, "Terahertz communications in human tissues at the nano-scale for healthcare applications," *Nanotechnology, IEEE Transactions on*, 2015.

[21] K. Yang, A. Pellegrini, M. Munoz, A. Brizzi, A. Alomainy, and Y. Hao, "Numerical analysis and characterization of thz propagation channel for body-centric nano-communications," *Terahertz Science and Technology, IEEE Transactions on*, vol. 5, no. 3, pp. 419–426, May 2015.

[22] S. Bush, J. Eckford, A.and Paluh, T. Thai, T. Sato, G. Piro, Y. Chen, K. Yang, V. Rao, V.and Prasad, A. Mukherjee, T. Wysocki, E. F. Armay, A. Rafiei, and S. Goel, "IEEE draft recommended practice for nanoscale and molecular communication framework," *IEEE P1906.1/D1.1, October 2014*, pp. 1–52, Dec 2014.

[23] G. E. Santagati and T. Melodia, "Opto-ultrasonic communications for wireless intra-body nanonetworks," *Nano Communication Networks*, vol. 5, no. 1, pp. 3–14, 2014.

[24] Z. Liao, R. Gao, C. Xu, and Z.-S. Li, "Indications and detection, completion, and retention rates of small-bowel capsule endoscopy: a systematic review," *Gastrointestinal endoscopy*, vol. 71, no. 2, pp. 280–286, 2010.

[25] T. Nakamura and A. Terano, "Capsule endoscopy: past, present, and future," *Journal of gastroenterology*, vol. 43, no. 2, pp. 93–99, 2008.
[26] G. Pan and L. Wang, "Swallowable wireless capsule endoscopy: Progress and technical challenges," *Gastroenterology research and practice*, vol. 2012, 2011.
[27] M. Fluckiger and B. J. Nelson, "Ultrasound emitter localization in heterogeneous media," in *Engineering in Medicine and Biology Society, 2007. EMBS 2007. 29th Annual International Conference of the IEEE*. IEEE, 2007, pp. 2867–2870.
[28] K. Kim, L. A. Johnson, C. Jia, J. C. Joyce, S. Rangwalla, P. D. Higgins, and J. M. Rubin, "Noninvasive ultrasound elasticity imaging (uei) of crohn's disease: animal model," *Ultrasound in medicine & biology*, vol. 34, no. 6, pp. 902–912, 2008.
[29] O. Ergeneman, G. Dogangil, M. P. Kummer, J. J. Abbott, M. K. Nazeeruddin, and B. J. Nelson, "A magnetically controlled wireless optical oxygen sensor for intraocular measurements," *Sensors Journal, IEEE*, vol. 8, no. 1, pp. 29–37, 2008.
[30] J. M. Dubach, D. I. Harjes, and H. A. Clark, "Fluorescent ion-selective nanosensors for intracellular analysis with improved lifetime and size," *Nano Letters*, vol. 7, no. 6, pp. 1827–1831, 2007.
[31] J. Li, T. Peng, and Y. Peng, "A cholesterol biosensor based on entrapment of cholesterol oxidase in a silicic sol-gel matrix at a prussian blue modified electrode," *Electroanalysis*, vol. 15, no. 12, pp. 1031–1037, 2003.
[32] P. Tallury, A. Malhotra, L. M. Byrne, and S. Santra, "Nanobioimaging and sensing of infectious diseases," *Advanced drug delivery reviews*, vol. 62, no. 4, pp. 424–437, 2010.
[33] J. W. Aylott, "Optical nanosensorsan enabling technology for intracellular measurements," *Analyst*, vol. 128, no. 4, pp. 309–312, 2003.
[34] P. Avouris, G. Dresselhaus, and M. Dresselhaus, "Carbon nanotubes: synthesis, structure, properties and applications," *Topics in Applied Physics*, 2000.
[35] S. Tasoglu, E. Diller, S. Guven, M. Sitti, and U. Demirci, "Untethered micro-robotic coding of three-dimensional material composition," *Nature communications*, vol. 5, 2014.
[36] I. J. Fox, G. Q. Daley, S. A. Goldman, J. Huard, T. J. Kamp, and M. Trucco, "Use of differentiated pluripotent stem cells as replacement therapy for treating disease," *Science*, vol. 345, no. 6199, p. 1247391, 2014.
[37] S. Kim, F. Qiu, S. Kim, A. Ghanbari, C. Moon, L. Zhang, B. J. Nelson, and H. Choi, "Fabrication and characterization of magnetic microrobots for three-dimensional cell culture and targeted transportation," *Advanced Materials*, vol. 25, no. 41, pp. 5863–5868, 2013.
[38] K. E. Drexler, *Nanosystems: molecular machinery, manufacturing, and computation*. John Wiley & Sons, Inc., 1992.
[39] R. A. Freitas, "What is nanomedicine?" *Nanomedicine: Nanotechnology, Biology and Medicine*, vol. 1, no. 1, pp. 2–9, 2005.
[40] R. Fernández-Pacheco, C. Marquina, J. G. Valdivia, M. Gutiérrez, M. S. Romero, R. Cornudella, A. Laborda, A. Viloria, T. Higuera, A. García *et al.*, "Magnetic nanoparticles for local drug delivery using magnetic implants," *Journal of Magnetism and Magnetic Materials*, vol. 311, no. 1, pp. 318–322, 2007.
[41] R. A. Freitas, "Pharmacytes: An ideal vehicle for targeted drug delivery," *Journal of Nanoscience and Nanotechnology*, vol. 6, no. 9-10, pp. 2769–2775, 2006.
[42] B. P. Timko, T. Dvir, and D. S. Kohane, "Remotely triggerable drug delivery systems," *Advanced materials*, vol. 22, no. 44, pp. 4925–4943, 2010.
[43] S. Yim and M. Sitti, "Shape-programmable soft capsule robots for semi-implantable drug delivery," *Robotics, IEEE Transactions on*, vol. 28, no. 5, pp. 1198–1202, 2012.
[44] R. W. Carlsen and M. Sitti, "Bio-hybrid cell-based actuators for microsystems," *Small*, vol. 10, no. 19, pp. 3831–3851, 2014.
[45] C.-J. Chen, D. Y. Haik, and J. Chatterjee, "Development of nanotechnology for biomedical applications," in *Emerging Information Technology Conference, 2005.* IEEE, 2005, pp. 4–pp.
[46] E. B. Steager, M. S. Sakar, C. Magee, M. Kennedy, A. Cowley, and V. Kumar, "Automated biomanipulation of single cells using magnetic microrobots," *The International Journal of Robotics Research*, vol. 32, no. 3, pp. 346–359, 2013.

[47] T. Kawahara, M. Sugita, M. Hagiwara, F. Arai, H. Kawano, I. Shihira-Ishikawa, and A. Miyawaki, "On-chip microrobot for investigating the response of aquatic microorganisms to mechanical stimulation," *Lab on a Chip*, vol. 13, no. 6, pp. 1070–1078, 2013.
[48] D.-H. Kim, P. K. Wong, J. Park, A. Levchenko, and Y. Sun, "Microengineered platforms for cell mechanobiology," *Annual review of biomedical engineering*, vol. 11, pp. 203–233, 2009.
[49] K.-C. Kong, J. Cha, D. Jeon, and D.-i. D. Cho, "A rotational micro biopsy device for the capsule endoscope," in *Intelligent Robots and Systems, 2005.(IROS 2005). 2005 IEEE/RSJ International Conference on*. IEEE, 2005, pp. 1839–1843.
[50] P. Miloro, E. Sinibaldi, A. Menciassi, and P. Dario, "Removing vascular obstructions: a challenge, yet an opportunity for interventional microdevices," *Biomedical microdevices*, vol. 14, no. 3, pp. 511–532, 2012.
[51] S. Yim, E. Gultepe, D. H. Gracias, and M. Sitti, "Biopsy using a magnetic capsule endoscope carrying, releasing, and retrieving untethered microgrippers," *Biomedical Engineering, IEEE Transactions on*, vol. 61, no. 2, pp. 513–521, 2014.
[52] M. Heil and J. Ton, "Long-distance signalling in plant defence," *Trends in plant science*, vol. 13, no. 6, pp. 264–272, 2008.
[53] A. M. Andrew, "Nanomedicine, volume 1: Basic capabilities," *Kybernetes*, vol. 29, no. 9/10, pp. 1333–1340, 2000.

Chapter 2

Preliminaries of Nano-Communication

In this chapter, the fundamentals such as the definition, framework, structure and paradigms of nano-communication will be discussed. In addition, a brief review of the development of small-scale devices will be given. In the end, different simulation platforms will also be reviewed briefly with an emphasis on the state-of-art.

2.1 Definition of Nano-Communication

Nano-communication has been a hot topic since its proposal, so is its concept. Below are some explanations on both nano-network and nano-communication from the open literatures:

- "... there are many nano-scale networks embedded within each device that might be otherwise more effectively utilized for communication. ..." (2006) [1]
- "Nanonetworks. i.e., the interconnection of nano-machines are expected to expand the capabilities of single nano-machines by allowing them to cooperate and share information." (2008) [2]

- ”Nanonetworks are communication networks that exist mostly or entirely at the nanometer scale.” (2010) [3]
- ”Nanocommunication is the exchange of information at the nanoscale and it is at the basis of any wired/wireless interconnection of nanomachines in a nanonetwork.” (2011) [4]
- ”As the name indicates, nano-communication encapsulates the communication between devices at the nano-scale applying novel and modified communication and radio propagation principles in comparison to conventional and existing solutions.” (2015) [5]
- ”Nanonetworking is an emerging field, communicating among nanomachines, expanding the capacity of single nanomachine.” (2015)[6]

To make it clearer, four requirements of a nano-scale communication system are summarised [7] as follows:

- At least one essential component of the defined system should be at the nano-scale, even at just one dimension.
- The physical properties applied in the defined system should be different from the ones at macro scale. Take the EM properties as an example, quantum effects can change it at nano scale. The resonant frequency of an antenna would no longer increases when its size decreases at the nano scale; furthermore, the wave propagation velocity would be influenced leading to its reduction below the speed of light.
- The fundamentals of the communication theory should be mapped, where there should be a fully distinguishable transmitter, receiver, medium, message carrier and message.
- Some components of the proposed system should be artificial.

2.2 Framework of Nano-Communication

The model of nano-communication is shown in Fig. 2.1a, which is an enhanced version of the most basic model, i.e., Shannon-Weaver model shown in Fig. 2.1b, of traditional communication. From the figures, it can be seen that the three elemental parts of the traditional communication is reserved while the role of the medium is further considered, focusing on the influences of noise on the messages.

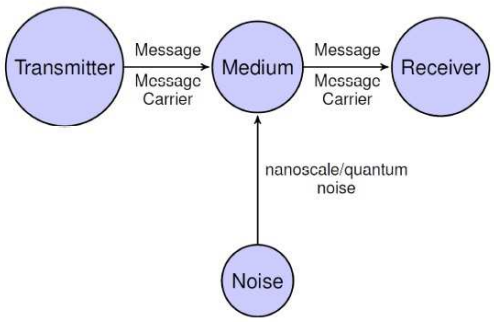

(a) Model of nano-communication

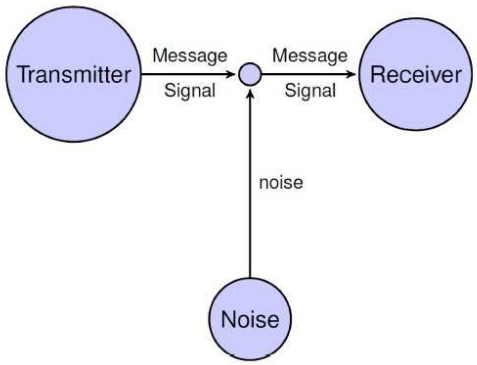

(b) Shannon-Weaver model of communication

Figure 2.1: Various communication models [7]. (The size of the circle indicates the importance of the elements.)

To make it open and broad, the framework of nano-communication is divided into the following 5 parts in IEEE 1906.1[1] [7]:

- Message Carrier: As the name indicates, this component is the physical substance to transmit the message, which can be EM waves, molecular motors or

[1] An IEEE Communications Society sponsored group, which aims to develop the standard such as the definition, framework, simulators and *etc.* for nano-communication. [8]

even nano-bots. Since the message carrier is minute (for molecular communication) or the equipment to produce the carrier is small (for the EM, acoustic communication), the principle at nano scale should be obeyed, for example, huge surface to mass ratio, Brownian motion (for molecular communication) or slow wave propagation and Surface Plasmon Polariton wave along graphene to hugely reduce the antenna size (for EM communication).

- Motion: This part is to make the message carrier move, which can be either active or passive; but the force to move the carrier is not steerable, leading to the random or semi-random motion at the nano-scale.

- Field: Unlike motion part, this element is to guide the message carrier [9], which can be attached to the message carrier or applied externally to the nano-scale communication system. It can be modelled as a mathematical vector field to describe the phenomenon such as organised fluid flow, diffusion gradients, EM fields, microtubule rails, or any other form of well-defined coordinated message carrier organisation.

- Perturbation: Similar to modulation in traditional communication systems, perturbation part could produce controlled variation to introduce the symbols of the message. On the other hand, it should be more abstract and broader because it should contain any controllable modifications in the nano-scale system. To create a message, some aspects of the massage carrier should be modified, which is the process of perturbation. The aspects which can be altered include molecular structure modification, particle concentration variation, voltage level change through nano-wires and specificity change of the receiver. It should be pointed out that unlike macro scale, much more forms of perturbation could exist, besides EM ways.

- Specificity and Sensitivity: These two terms were first proposed to measure the performance of the molecular communication. Specificity measures the proportion of message carrier that are not received by the wrong receiver while sensitivity is to quantify the proportion of message carrier which are received by correctly intended receiver [7]. The reason to put forward such terms is that

in nano bio-systems binding is a natural phenomena but from the communication perspective it should be regarded as message lost when the message carrier binds with another entity along the path to the intended receiver; thus, the goal is to avoid such bindings to the wrong receivers between the transmitters and receivers. To promote these to EM technique, specificity may refer to as the tuning and resonance with the appropriate receiving antenna while the sensitivity is the capability of the receiver to detect the signal.

2.3 State-of-Art Achievement of Devices due to Nano-Technologies

Due to the developments in micro-fabrication and nano-technologies, the limits of the sizes and capabilities of devices have been pushed further and further. A cheap Integrated Chip (IC), whose cost would be less than 1 dollar, was designed by National Applied Research Laboratories, Taiwan using sensor fusion technologies, shown in Fig. 2.2a. From the figure, it can be easily seen that the chip is smaller than a grain of rice. A full-duplex transceiver IC, shown in Fig. 2.2b were presented by Harish Keishnaswamy from Clumnia High-Speed and mm-wave IC Lab (CoSMIC Lab) at the International Solid State Circuits Conference [10] in 2015, whose size is extremely small.

To access the complex and small regions of the human body like gatrointestinal(GI), spinal cord, blood capillaries, the present tethered medical devices are made smaller and smaller. At the same time, the discomfort due to the tissue loss would be decreased. The micro-robots voyaging around human body has been developed recently. For example, a tiny permanent magnet, guided inside the human body by a magnetic stereotaxis system was proposed in [12] while a magnetically driven screw was made to move through tissues [13]. Micro-mechanical flying insect robots were first created in 2000 at University of California, Berkeley [14] and then later a solar-powered crawling robot was realised by Prof. Kristofer S.J. Pister in 2003 [15]. The first medical-used capsule endoscopes, to replace the traditional ones, were applied clinically in 2001 with the FDA's approval. Later the introduction of a crawling mechanism [16] and on-board drug delivery mechanism [17] were marked as another milestone for the development of the capsule endoscopy. A nano-scallop - capable of swimming

(a) Comparison of the chip with a rice (reproduced from [11])

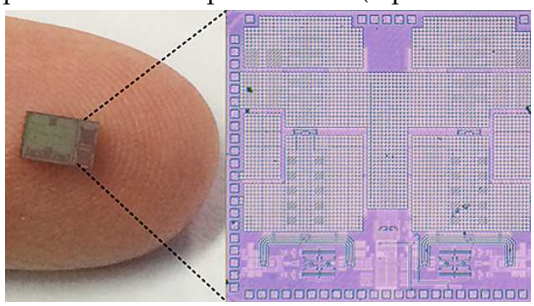

(b) Photo of the full-duplex transceiver IC ©CoSMIC Lab

Figure 2.2: The Realized IC chips

in biomedical fluids - whose size is only a fraction of a millimetre has been developed by the team led by Prof. Peer Fischer at the Max Planck Institute for Intelligent Systems [18], shown in Fig. 2.3a and at the same time a tiny bio-bot powered by skeletal muscle cells, shown in Fig. 2.3b was reported by the engineers at the University of Illinois at Urbana-Champaign [19]. A magnetic helical micro-swimmer was successfully targeted in a wireless way to deliver a single-cell gene to human embryonic kidney whose SEM image is shown in Fig. 2.3c [20].

Besides research on tiny robots, there are also investigations on other applications. A wireless radiation detector was designed by Prof. Babak Ziaie at Purdue University to inject into a tumour to detect the level of the therapeutic radiation received by the tumour [21]. Applying micro-machining techniques, this dosimeter was shrunk to 2 cm long and 2 mm wide. A miniature CO_2 sensor, shown in Fig. 2.4a was developed by the researcher at ETH Zurich based on a novel material whose conductivity would change according to the CO_2 concentration [22]. Nano-switches were realised in the form of multiple patterned nano-islands with 10 nm in thickness and 300 nm in diameter [23], shown in Fig. 2.4b. A nano-wire, around 300 nm wide in diameter, used as

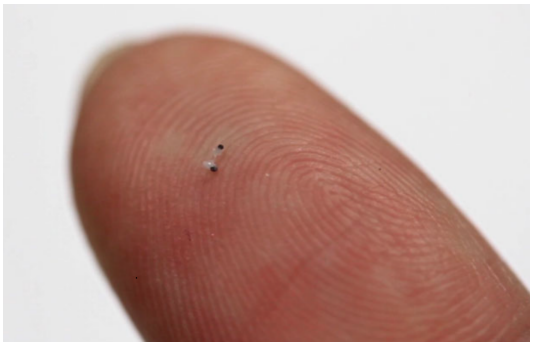

(a) Nano-scallop which can swim in bio-fluids (reproduced from [18])

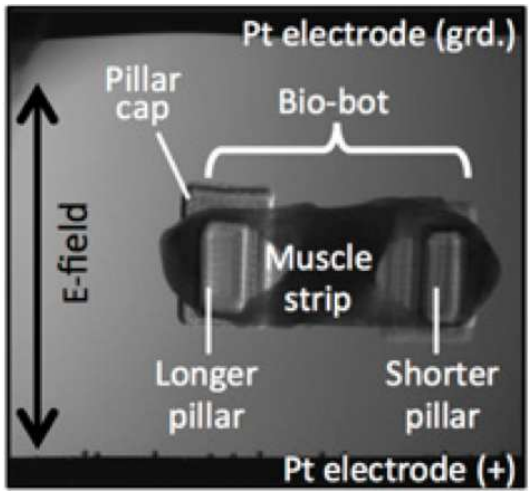

(b) Bio-bot powered by skeletal muscle cells ©UIUC

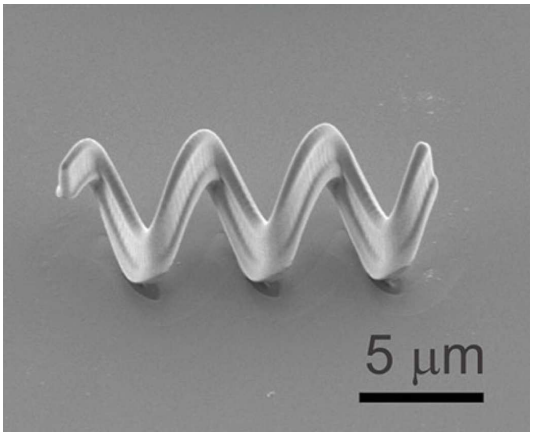

(c) SEM image of the artificial bacterial flagella (reproduced from [20])

Figure 2.3: Photos of the nano-bots which can be used in human body

solar cell was studied in 2007 in Harvard University and it shows a great potential for producing 200 picowatts of electricity, which is believed enough for the nano-devices. The SEM image of this nano-wire was shown in Fig. 2.4c [24]. Also, due to the recent advances in nano-optics, the design and fabrication of the nano-lasers is possible [25], the SEM image and corresponding schematics is shown in Fig. 2.5.

2.4 Various Paradigms of Nano-Communication

To connect the nano-devices, the communication between them need to be completed. According to [2], nano-communication can be divided into two scenarios: (1) Communication between a nano-machine and a larger system such as micro/macro-system, and (2) Communication between two or more nano-devices. Furthermore, the ways of electromagnetic, acoustic, nanomechanical or molecular can all be applied to nano-communications [26] which will be discussed in this section.

2.4.1 Molecular Paradigms

As the origin of the idea of the nano-communication, molecular communication are considered as the most promising paradigm to achieve the nano-communication because there are numerous examples in nature for us to learn and study. In molecular communication, an engineered miniature transmitter releases small particles into a propagation medium while the molecules are applied to encode, transmit, and receive information. Molecular communication can be classified into several categories such as walkway-based where molecules propagate along a predefined pathway via molecular motors, flow-based where molecules propagate in a guided fluidic medium, diffusion-based where molecules propagate in a fluidic medium via spontaneous diffusion and *etc.* [27]. As the most general and widespread scheme found in nature, the diffusion-based molecular communication (DMC) is also the most widely investigated in literature. Some of the most prominent works include mathematical framework for a physical end-to-end channel model for DMC [28], development of an energy model for DMC [29], modeling of diffusion noise [30], channel codes for reliability enhancement [31], and relaying-based solutions for increasing the range of DMC [32, 33]. On

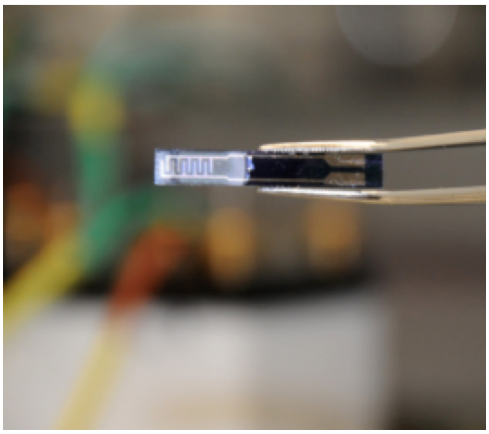

(a) Photo of miniature CO_2 sensor ©ETH Zurich

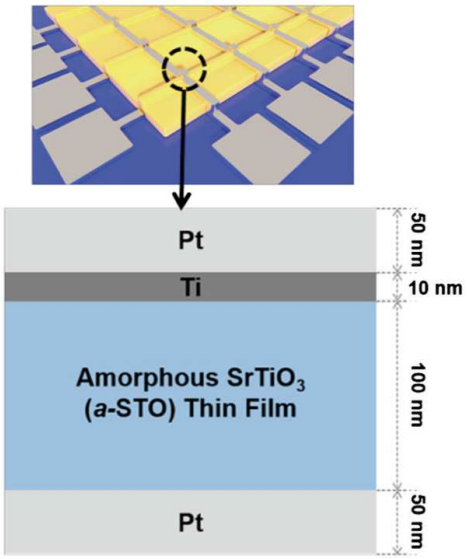

(b) Schematics of the nano-switch (reproduced from [23])

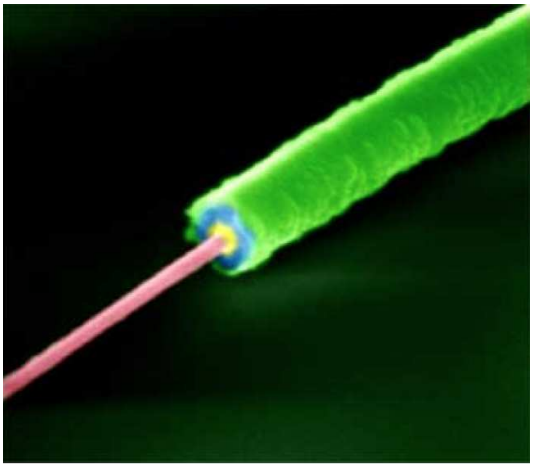

(c) SEM image of the nano-wire ©Harvard University

Figure 2.4: Nano devices for other applications

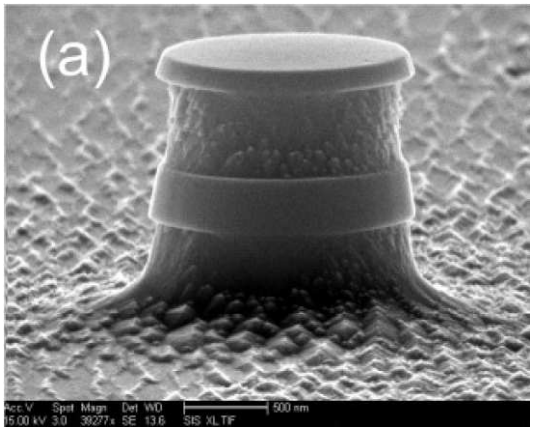

(a) SEM image of the proposed nanolaser

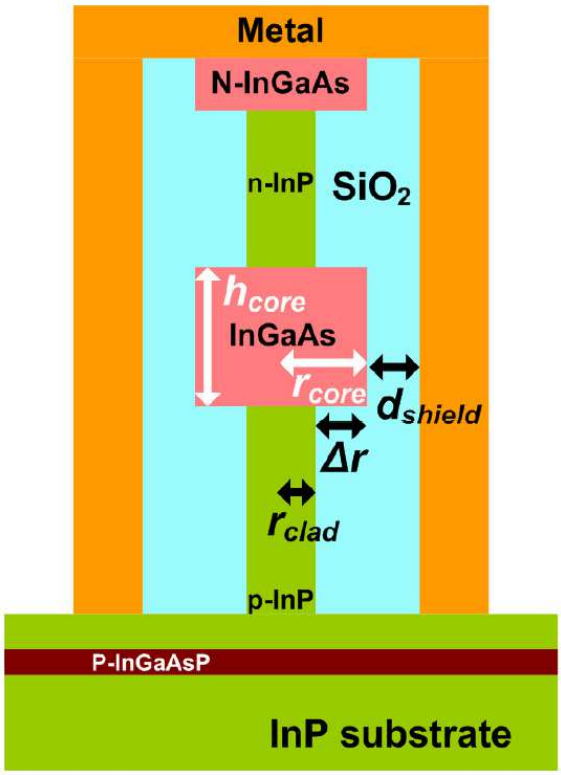

(b) Schematics of the proposed nanolaser

Figure 2.5: SEM image and schematics of the nano-laser with $r_{core} = 750nm$, $r_{clad} = 690nm$ ($\Delta r = 60nm$), and $d_{shield} = 150nm$ with silver coating where r_{core} is the radius of $InGaAs$ gain layer, r_{clad} is the radius of InP cladding. Δr is the difference between r_{core} and r_{clad}. d_{shield} is the thickness of SiO_2 shield layer.(reproduced from [25])

the other hand, the flow-based molecular communication (FMC) is also studied, especially the one of communication in the circulatory system [34, 35].

Diffusion-Based Molecular Communication

In diffusion-based molecular communication, molecules are used to encode, transmit, and receive information, which propagate through spontaneous diffusion in a fluidic medium. Massimiliano and Ian developed a mathematical framework to interpret diffusion-based particle communication in details in 2010 [36], where the general model can be divided into three parts: emission, diffusion and reception. By investigating these three parts individually, the total attenuation and delay was also studied. And the closed-form mathematical expression for the information capacity of DMC was provided later in 2013 [37], which depends on the medium diffusion coefficient, the system temperature, the distance between the transmitter and the receiver, the bandwidth of the transmitted signal and the average transmitted power. Pulse-based modulation scheme [38] was studied, where two detection techniques, energy detection techniques where the nano-receivers measure the energy of the molecular pulse and amplitude detection where the nano-receiver measures the variation of local concentration were compared, showing that energy detection is more robust and suitable for communication over larger communication distances [38, 39]. Fig. 2.6 and 2.7 show two common communication ways in DMC: direct communication and relay communication, whose error performance were analysed in [40].

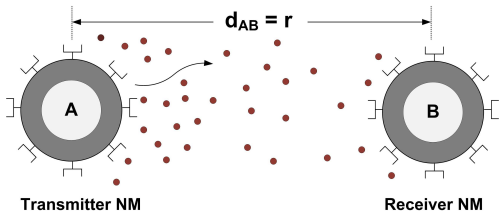

Figure 2.6: A simple diffusion-based molecular nano-network

Flow-Based Molecular Communication

In diffusion-based molecular communication, the propagation medium is assumed to be stationary; however, it is not always accurate in practice. For some applications,

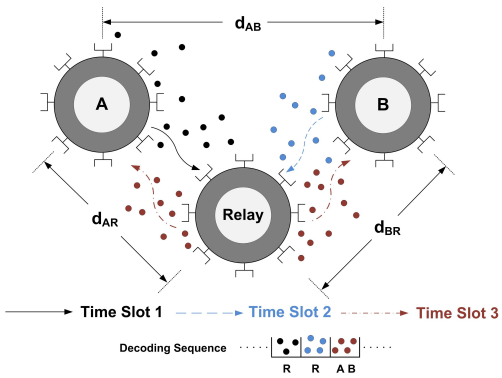

Figure 2.7: A simple nano-network with network coding operation

a drift velocity of the medium may be used to boost the throughput of the molecular communication systems, such as the scenario that the propagation medium are human blood, rivers or wind. Thus, flow-based molecular communication started to catch people's attention. Usually, in molecular communication, information can be encoded in various ways, such as in the release time of the molecules (timing modulation) [41, 42], in the concentration of the molecules or number of molecules per unit area (concentration modulation) [36, 43], in the number of molecules (amplitude modulation) [44], or in the identities of the molecules and *etc.*. [42] first studied the case of molecules with timing modulation in the fluidic medium which refers as to the fact that the messenger molecules propagate in the fluid, propelled by a positive drift velocity and Brownian motion, where the channel was pointed out to be an Additional Inverse Gaussian Noise channel. Then, flow-based molecular communication with concentration modulation was initially analysed by Ian in 2013 [43], where a flow model of microfluidic channel has been proposed and an end-to-end concentration propagation model was developed. To yield the transfer function, the building blocks, shown in Fig. 2.8, of micro-fluidic channel were introduced. Later, flow-based molecular communication with amplitude modulation scheme was investigated [44], where the close form of the probability of error for different schemes (*i.e.*, 2 amplitude levels, 4 amplitude levels and hybrid scheme), was derived. A more general flow-based molecular communication model has been proposed recently which can be applied to both Molecule Shift Keying (MoSK) and Concentration Shift Keying (CSK) [45], where the effects of the moving medium on the signal propagation and Bit Error

Rate (BER) performance was investigated. The noise characterisation was also studied in [46, 47], which shows that it can be divided into two additive elements for the medium Brownian noise $n_b(t) \sim \mathcal{N}(0, s(t))$ [2], caused by the random thermal motion of the molecules which can be described by the Wiener process, and Residual noise $n_r(t) \sim \mathcal{N}(\alpha, \beta)$ [3], caused by messenger molecules existing in the receiver sensing area from previous transmissions or messenger molecules that have been released by the receptors.

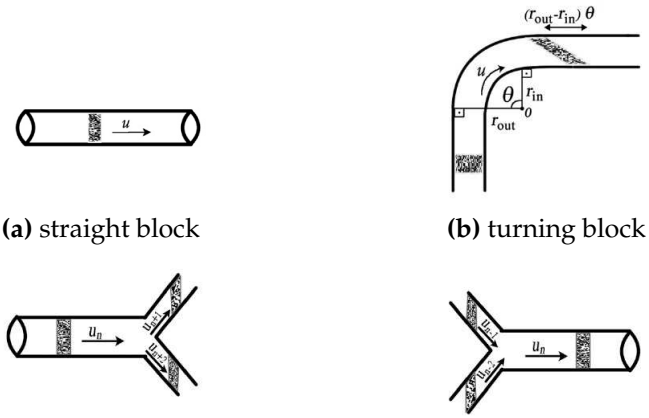

(a) straight block **(b)** turning block

(c) division block **(d)** combination block

Figure 2.8: Building blocks of the microfluidic channels [43]

Based on the development of the nanotechnology, a new paradigm of touch communication (TouchCom) [4] was also proposed in [34], which use a swarm of nano-robots as message carrier for information exchange. In TouchCom, transiet microbots (TMs) [48–50] were applied to carry the drug particles, which can be controlled and tracked by the external macro-unit (MAU) with a guiding force [35, 51]. These TMs would survive some time in body and their pathway would be the channel for the information exchange while the process of loading and unloading is the corresponding transmitting and receiving process. A specific application, illustrated in [34], is shown in Fig. 2.9 while the structure of the applied nano-robots is shown in Fig. 2.10. The channel model of TouchCom was derived by defining the propagation delay, path loss with the angular/delay spectra of the signal strength. Meanwhile, a simulation

[2] $s(t)$ is the mean number of messenger molecules in the receiver sensing area.

[3] α and β depend on the medium and system design factors (such as the propagation area, transmission rate and *etc.*).

[4] Here, touch means the communication (*i.e.*, drug delivery) process is controllable and trackable.

tool was proposed to characterise the movement of the nano-robot swarm in the blood vessel.

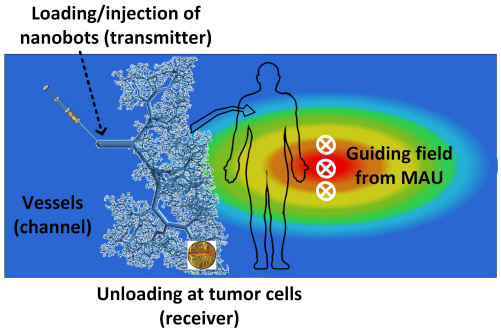

Figure 2.9: Envisioned TouchCom system [34]

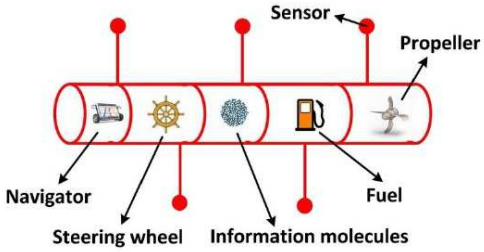

Figure 2.10: Structure of the envisioned nano-robots [34]

2.4.2 Electromagnetic Paradigm

As the name indicates, electromagnetic methods use the electromagnetic wave as the carrier and its properties like amplitude, phase and *etc.* are used to encode the information.

The possibility of EM communication is first discussed in [27], where THz EM waves travelling in the air were thoroughly investigated. THz band was chosen because the emerging new materials like Carbon Nano-Tube (CNT) and Graphene [52] can work at this frequency band as the necessary element to make the nano-transceiver. Later, [53] demonstrates the theoretical model of the nano-network whose nodes are made of CNT. Later, the channel model for THz wave propagating in the air with different concentration of the water vapour was presented in [54] and the corresponding channel capacity was also studied. Based on the characteristics of the channel, a new physical- layer aware medium access control (MAC) protocol, Time Spread On-Off

Keying (TS-OOK), was proposed [55]. Meanwhile, the applications of THz technology in imaging and medical field [56, 57] have also achieved great development and the biological effects of THz radiation are reviewed in [58] showing minimum effect on the human body and no strong evidence of hazardous side effects.

A modified Friis equation has been proposed by Jornet *et al.* in [54] to calculate the path loss of the THz channel in water vapour, which can be divided into two parts: the spread path loss introduced by the expansion of the wave in the medium and the absorption path loss caused by the absorption of molecules in the air:

$$PL = PL_{spr} + PL_{abs} \quad [\text{dB}] \tag{2.1}$$

Later, a more detailed model of THz communication was proposed with the consideration of multi-ray scenario; thus, the propagation models for reflection, scattering and diffraction were considered in [59]. At the same time, the scattering effects of small particles was discussed with the analysis frequency and the impulse responses [60]. Also, the Finite-Difference Time-Domain (FDTD) and the Ray-Tracing (RT) technique were compared to evaluate the reception quality in nanonetwork with the consideration of two cases: line-of-sight (LOS) and multiple objects dispersed near the LOS [61]; then, the conclusion was drawn that at the THz band RT is as good as FDTD. Meanwhile, a discussion of the use of VHF band was conducted with the study of the bit error rate (BER) performance of the nano-receiver made of CNT [62].

The noise power at the receiver can be obtained [54]:

$$\begin{aligned} P_n(f,d) &= \int_B N(f,d)df = k_B \int_B T_{noise}(f,d)df \\ &\simeq k_B \int_B T_{mol}(f,d)df \end{aligned} \tag{2.2}$$

where, T_{mol} is the equivalent noise temperature due to molecular absorption; k_B is the Boltzmann constant; T_o is the reference temperature.

The path loss and molecular noise power of the air with 10% water vapour are shown in Fig. 2.11 and details of EM methods, especially THz wave, will be further discussed in Chapter 3.

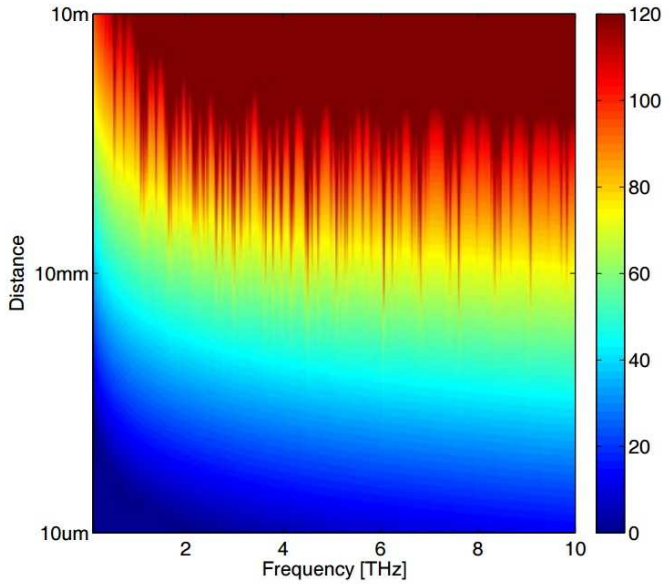

(a) Total path loss $[dB]$ vs. frequency and the distance

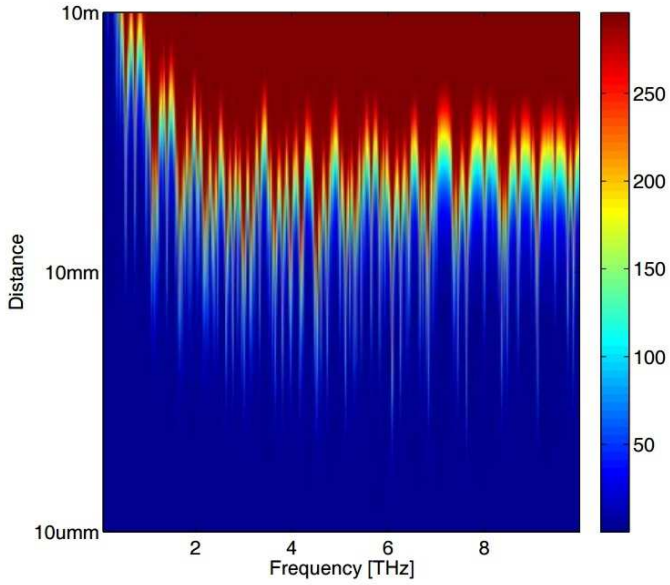

(b) Molecular absorption noise temperature $[K]$ vs. frequency and the distance

Figure 2.11: Path loss and molecular absorption noise temperature for 10% water concentration [54]

2.4.3 Acoustic Paradigm

Acoustic propagation introduces slight pressure variations in the fluid or solid medium, which could satisfy Helmholtz equation when the time dependence is considered [63]:

$$\nabla^2 p(x) + k^2 p(x) = 0 \tag{2.3}$$

where ∇^2 is the Laplace differential operator and $k = \frac{\omega}{c} + i\alpha$ is the complex-valued wave vector with c as the sound speed in the medium and α as the attenuation coefficient of the sound wave in the medium, which is different from medium to medium. By solving Eq. 2.3, the sound pressure can be obtained to describe the sound wave propagation in the medium, where the source of the sound is the motion of the surface in the nano-robot. The behaviour of the nano robots is relevant to their physical properties, surrounding medium and the working frequency. The feasibility of in vivo ultrasonic communication is evaluated by Hogg *et. al.* [64], where communication effectiveness, power requirements and effects on nearby tissue were examined on the basis of discussion on the principles. And an isolated robot, shown in Fig. 2.12a and an aggregated robot were designed to use in blood vessel, whose size are around 10 μm. Later, the nanoscale opto-ultrasonic communications in biological tissues was discussed in [65, 66], where the generation, propagation model were studied and in line with [64] the hazards and design challenges were investigated.

2.5 Structure of Nano-Network to Specific Applications

A simple overview of structure of nano-network was briefly mentioned in Section 2.4.1, where the TouchCom is discussed. Similar to the traditional body-centric communication, the nano-one can also be divided into three parts: in-body, on-body and off-body. An overview of the structure of nano-network can be summarised as below [67]:

- Nano-nodes: they are the smallest and simplest nano-devices. Due to the limited energy, limited memory and reduced communication capabilities, they can only perform simple computation task and can only transmit over very short distances. The nodes could be composed of sensor and communication units,

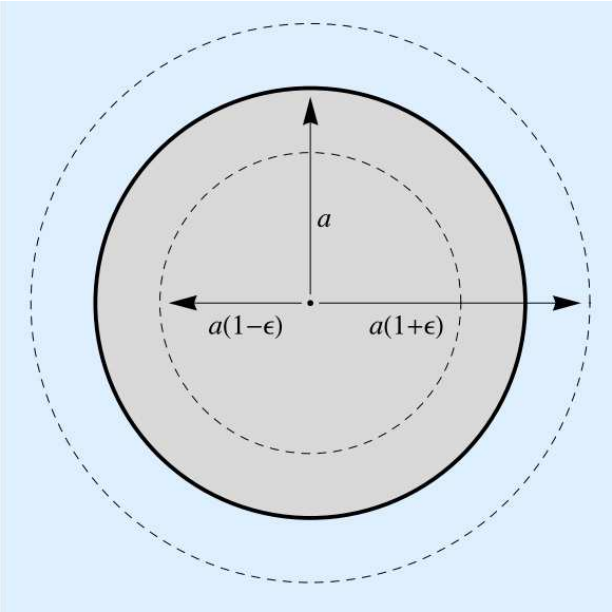

(a) Radial pulsations of a sphere, whose radius changes as $a + a\epsilon\cos(\omega t)$ with $\epsilon << 1$. The ϵ in [64] ranges from 10^9 to 10^3.

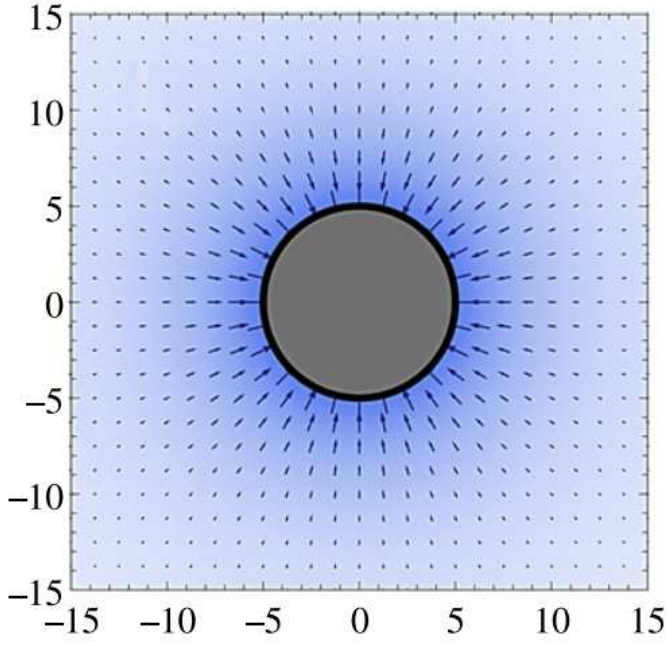

(b) Sound from a $5\mu m$ radius sphere at $f = 10MHz$

Figure 2.12: Schematic and simulation results of the pulse sphere [64]

which is shown in 2.14.

- Nano-routers: since they are nano-devices with slightly larger computational resources than nano-nodes, they can aggregate information from limited nano-machines and also can control the behaviour of nano-nodes by sending extremely simple order (such as on/off, sleep, read value, *etc.*). However, this would increase their size; thus, their deployment would be more invasive.

- Nano-micro interface: they are used to collect the information forwarded by nano-routers and send the information to the micro-scale devices. At the same time, they can send the information from micro-scale to nano-scale by the same way. Nano-micro interfaces are hybrid devices not only able to communicate in the nano-scale using the nano-communication techniques shown in Section 2.4 but also can use classical communication paradigms in micro/macro communication networks.

- Gateway: it makes the users to control or monitor the entire system remotely over the Internet.

Fig. 2.13 shows an example of health monitor system with nano-network: the nano-machines spreading over the clothes can sense the change of the surrounding and make the corresponding response to protect the user or make the user comfortable; the nano-sensors inside the body can sense the body information to indicate the health level, for example, nano-sensors around the heart can monitor the activity of the heart to indicate the health level of the host while the ones in neuro-system can also detect the abnormal situation such as stroke and pain to help the host in time; nano-phones can entertain the user in the process of exercise or make a phone call, but much more importantly, it can be used as the nano-micro interface and the nano social tags inside the users' body can be used as the identity which could make the communication between people much more convenient.

The network architecture of the e-office, part of internet of nano-things (IoNT) is shown in Fig. 2.14. In the e-office, every single element normally found in an office and even its internal components are provided with a nano devices which allows them to be permanently connected to the Internet. As a result, the location and status of all

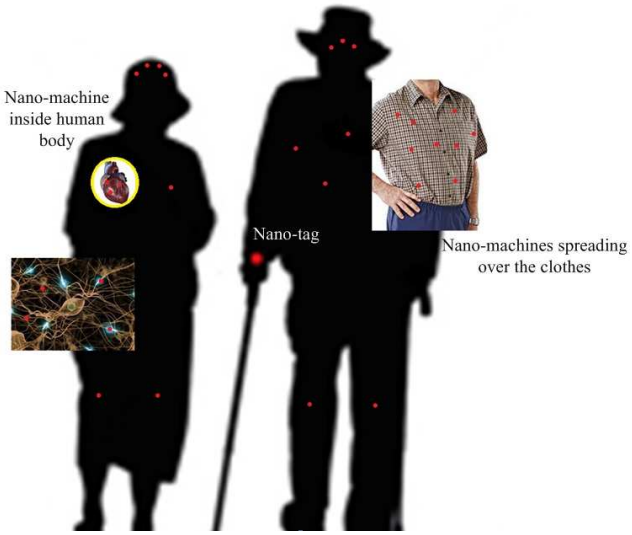

Figure 2.13: Architecture of a health monitor nano-network

its belongings can be tracked effortlessly. Furthermore, by analysing all the information obtained both from the intra-body network and from the off-body, the actuator can be enabled to change the environment such as the temperature, the light and *etc.*, seamlessly in order to make office pleasant and intelligent.

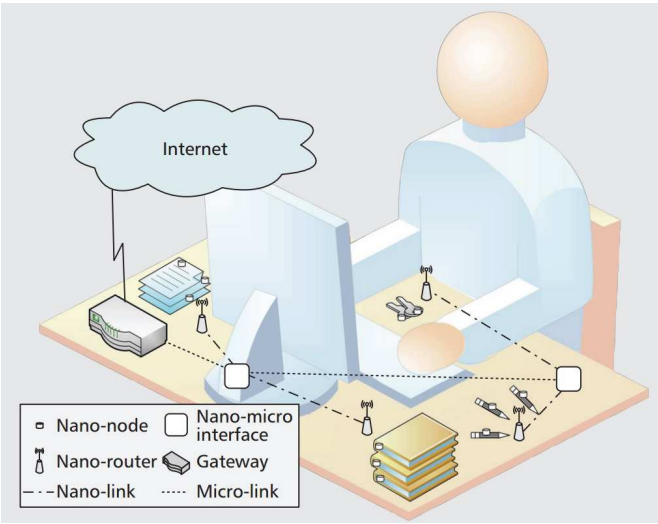

Figure 2.14: Network architecture of the e-office [67]

A conceptual network model of IoNT, based on On-Off Keying (OOK) protocol and TDMA framework, was done in [6], where the nano sensors were randomly deployed at organs of the human body and may be moved by body fluid. The suggested

model assumes hexagonal cell-based nano-sensors deployed in cylindrical shape 3-D hexagonal pole, which is closer to the shape of organs. The network architecture of the IoNT for intra-body disease detection is shown in Fig. 2.15a. As normal, the network contains nano-sensors, nano-routers, nano-micro interface and gateway. When nano-sensors detect specific symptoms or virus by means of molecules [52] or bacteria behaviours [68], simple data (e.g., 1 for detection or 0 for non-detection) will be transmitted over short ranges to nano-routers to inform the existence of symptoms or virus because of the limited capacity of the nano-sensors. Because of the relatively more computational resources, nano-routers can aggregate the data and send the related information to the nano-micro interface. The gateway (i.e., micro-scale device) enable the remote control of the entire system over the Internet possible. Each cell, the smallest living unit of organs, is considered as a hexagonal shape cell, shown in Fig. 2.15b, resulting a 3-D structure for the nano-sensor networks. A 3-D space for the individual target organ, for example, heart, lungs, and kidney, is constructed by the accumulated unit layers which consist of unit cells. As many nano-sensors as possible are put in the model where each hexagonal cell has one active nano-sensor.

Nano-sensors within each layer construct a cluster, where the information sensed by each nano-sensor can be transmitted to the nano-micro interface through the nano-router of each cluster. Each hexagonal cell may have more than one nano-sensors. To make the load of the energy consumption evenly distributing in the nano-networks, only the nano-sensor with the most energy can be selected as the active nano-sensor while the others will go into the sleep mode which would be used for the next data transmission. The information detected by the nano-sensors would be transmitted within the occurrence layer to the nano-router at the center cell (annulus A_0) of the same layer which are also served as an active nano-sensor. Then the data collected by the nano-router of each layer are sent to layer 0's nano-router which will forward the collected data to the nano-micro interface to communicate with micro scale devices, *i.e.*, gateway. From Fig. 2.15, it can be seen that there are three transmission methods:

- Direct data transmission: the data would be sent directly from the nano-sensor to the corresponding nano-router [69].
- Multi-hop data transmission: the data would be sent to the adjacent nano-sensors

which locate in the neighbour cell and is randomly selected until the corresponding nano-router is reached in the way of annulus by annulus hierarchically.

- Hybrid data transmission: the data can be sent by combining the multi-hop and direct transmission methods. First, a threshold range is defined. Then, within the threshold range, every nano-sensor sends the data directly to the nano-router in the same layer. Otherwise, the multi-hop transmission should be used when the nano-sensor is outside the range.

Similarly, there are also three data transmission methods between layers, shown in Fig. 2.15b.

Fig. 2.16 shows an example of using nano-network for agricultural crop-monitor [70]. The chemical compound released by plants can be caught by the nano-sensors and such information can be sent to the micro-devices to analyse the knowledge of environmental conditions and plant interaction patterns; thus, an enhanced chemical defence systems could be developed or the underground soil condition can be retrieved by using plants as sensors. A large numbers of nano-devices equipped with chemical nano-sensors and THz radio units are deployed on the plant, which can transfer the data detected to a micro-scale networking device over a short distance, where the transmission frequency can be dynamically selected in order to optimise throughput of the network. The hierarchical structure of this monitoring network is illustrated in Fig. 2.16a where numerous nano-sensors are situated on the plant through suspension in a spray applied to the plants [70]. The chemical nano-devices deployed in the nano-network comprise a power block and a communication block along with relevant sensors, processing and storage units. The nano-devices are supposed randomly scattered on the plant leaves and cluster are formed based on their location and proximity to micro-devices which are located at specified points on the stem to manage clusters of nano-devices, shown in Fig. 2.16b. The information can only be sent by single-hopped way which means that there is no NLoS.

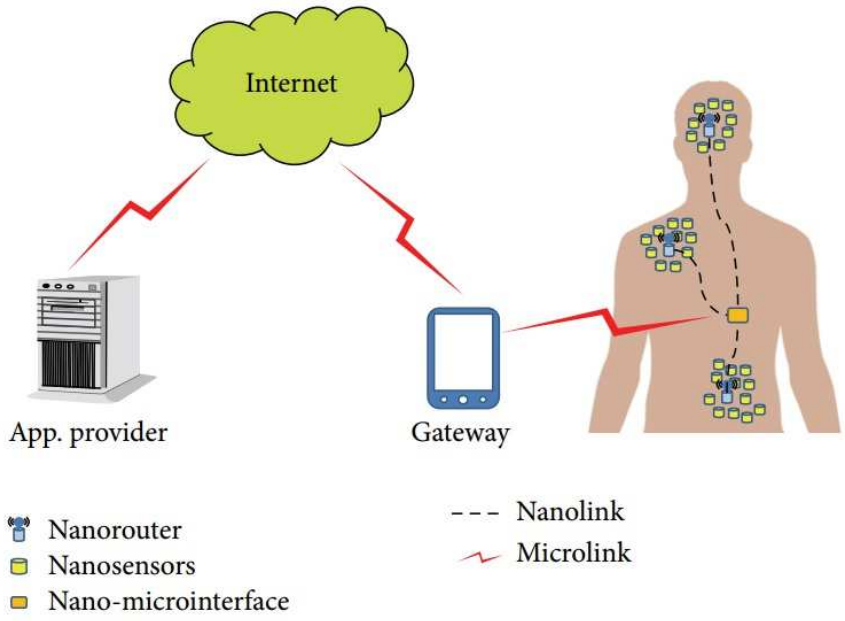

(a) Network structure of the proposed IoNT

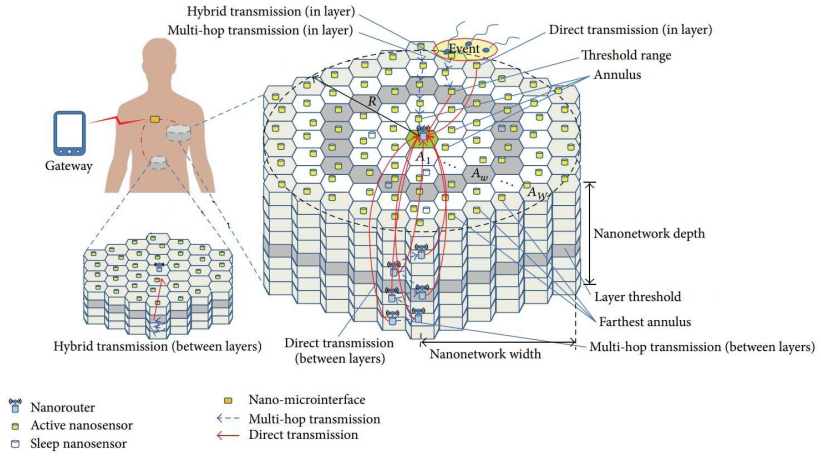

(b) Structure of the nano-cell of IoNT

Figure 2.15: Details of the network architecture of the proposed IoNT [6]

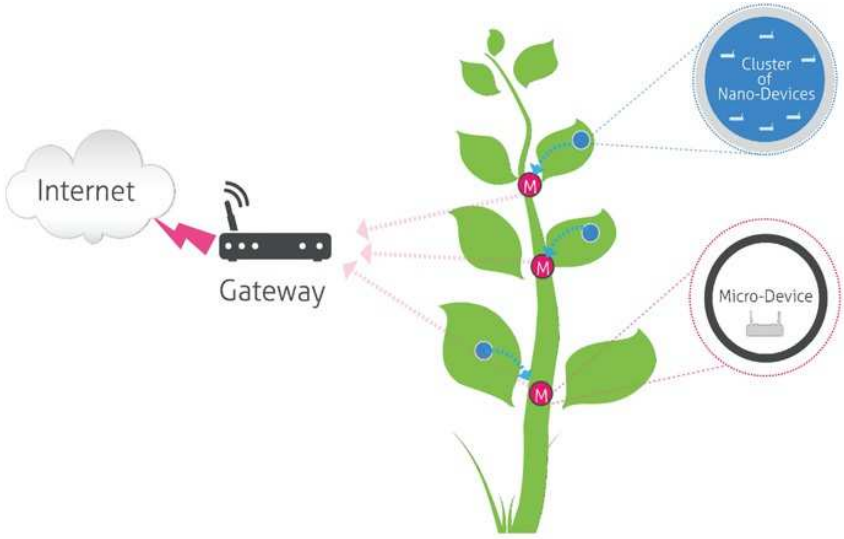

(a) Hierarchical structure of nano-networks for the plant monitoring application

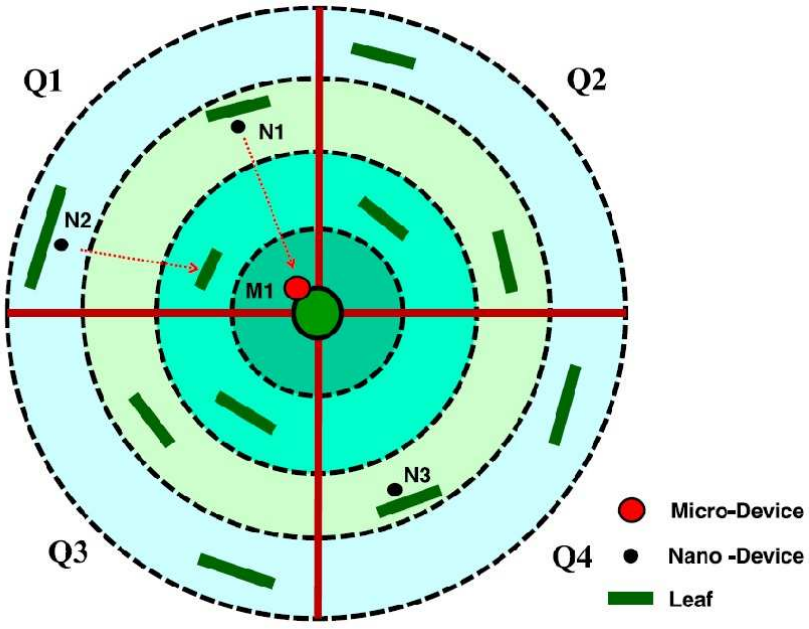

(b) Details of the nodes distribution

Figure 2.16: Nano-network for plant monitoring [70]

2.6 Available Simulators of Nano-Communication

With the wide acceptance of nano-communication, increasingly numerous researches are on the exploration of novel protocol stacks, network architectures, algorithm communication paradigms and channel access procedures to be adopted at the nanoscale [3, 67, 71]; therefore, a modular and freely available simulation platform is indispensable to enable research activities to achieve the final goal of nano-communication. NanoNS [72] and N2Sim [73] are simulators for molecular diffusion based on Brownian motion among immobile nano-devices. A simulator of Brownian motion was investigated in [74] where a dual time-step approach was adopted to manage the runtime complexity to deal with the large number of the simulated particles: for the particle far from the destination, its movement is simulated in a coarse-grained time steps; and when it comes closer to the destination, the fine-grained time steps would be applied. The simulator development of molecular diffusion using High Level Architecture (HLA) is reviewed in 2013 [75] while [76] proposed a generic simulation platform to fit in with multiple nano-devices, channel models, molecular propagation models and nano-devices mobility models. However, the platforms mentioned above are all related to short-range molecular communication. To accommodate the long-range communication, the neuron-based communication platform was developed and evaluated in [77]. At the same time, an open source simulator for EM-based nano-networks, namely Nano-Sim, is proposed in [78, 79], implemented on the top of the Network Simulator 3 (NS-3) platform [80]. Nano-Sim was designed as an open source modular tool to allow the community to devise, add, and test new functionalities and solutions intended for the Terahertz wireless communications. Unfortunately, none of these simulators could capture all features characterising the nano-communication as one completed platform; thus, a novel simulation tool is being developed as a reference simulation model in IEEE P1906.1 [7] which is open-source and extensible.

2.7 Summary

In this chapter, a brief overview of the nano-communication was given starting from what is nano-network, followed by a brief summary of how to build a nano-network. Then, current developments of small-scale devices were summarised and various

paradigms of nano-communication were illustrated where the emphasis was put on three main methods: molecular communication (DMC and FMC), EM communication and acoustic communication. Additionally, the structure of nano-network was analysed with the consideration of specific applications. Finally, a brief introduction to the available simulation platform was summarised to make the whole concept of nano-communication complete.

References

[1] S. F. Bush and Y. Li, "Nano-communications: A new field? an exploration into a carbon nanotube communication network," *GE Global Research Technical Report*, 2006.

[2] I. F. Akyildiz, F. Brunetti, and C. Blázquez, "Nanonetworks: A new communication paradigm," *Computer Networks*, vol. 52, no. 12, pp. 2260–2279, 2008.

[3] S. F. Bush, *Nanoscale Communication Networks*. Artech House, 2010.

[4] I. F. Akyildiz, J. M. Jornet, and M. Pierobon, "Nanonetworks: A new frontier in communications," *Communications of the ACM*, vol. 54, no. 11, pp. 84–89, 2011.

[5] K. Yang, A. Pellegrini, M. Munoz, A. Brizzi, A. Alomainy, and Y. Hao, "Numerical analysis and characterization of thz propagation channel for body-centric nano-communications," *Terahertz Science and Technology, IEEE Transactions on*, vol. 5, no. 3, pp. 419–426, May 2015.

[6] S. J. Lee, C. A. Jung, K. Choi, and S. Kim, "Design of wireless nanosensor networks for intrabody application," *International Journal of Distributed Sensor Networks*, vol. 2015, 2015.

[7] S. Bush, J. Eckford, A.and Paluh, T. Thai, T. Sato, G. Piro, Y. Chen, K. Yang, V. Rao, V.and Prasad, A. Mukherjee, T. Wysocki, E. F. Armay, A. Rafiei, and S. Goel, "IEEE draft recommended practice for nanoscale and molecular communication framework," *IEEE P1906.1/D1.1, October 2014*, pp. 1–52, Dec 2014.

[8] "IEEE P1906.1," https://standards.ieee.org/develop/project/1906.1.html.

[9] S. Bush and S. Goel, "Persistence length as a metric for modeling and simulation of nanoscale communication networks," *Selected Areas in Communications, IEEE Journal on*, vol. 31, no. 12, pp. 815–824, 2013.

[10] J. Zhou, T.-H. Chuang, T. Dinc, and H. Krishnaswamy, "19.1 receiver with¿ 20mhz bandwidth self-interference cancellation suitable for fdd, co-existence and full-duplex applications," in *Solid-State Circuits Conference-(ISSCC), 2015 IEEE International*. IEEE, 2015, pp. 1–3.

[11] Multi-sensing ic for internet of things produced in taiwai. [Online]. Available: http://technews.tw/2015/03/24/multi-sensor-soc-made-by-narlabs/

[12] D. C. Meeker, E. H. Maslen, R. C. Ritter, and F. M. Creighton, "Optimal realization of arbitrary forces in a magnetic stereotaxis system," *Magnetics, IEEE Transactions on*, vol. 32, no. 2, pp. 320–328, 1996.

[13] K. Ishiyama, M. Sendoh, A. Yamazaki, and K. Arai, "Swimming micro-machine driven by magnetic torque," *Sensors and Actuators A: Physical*, vol. 91, no. 1, pp. 141–144, 2001.

[14] J. Yan, S. Avadhanula, J. Birch, M. Dickinson, M. Sitti, T. Su, and R. Fearing, "Wing transmission for a micromechanical flying insect," *Journal of Micromechatronics*, vol. 1, no. 3, pp. 221–237, 2001.

[15] S. Hollar, A. Flynn, C. Bellew, and K. Pister, "Solar powered 10 mg silicon robot," in *Micro Electro Mechanical Systems, 2003. MEMS-03 Kyoto. IEEE The Sixteenth Annual International Conference on*. IEEE, 2003, pp. 706–711.

[16] M. Quirini, A. Menciassi, S. Scapellato, C. Stefanini, and P. Dario, "Design and fabrication of a motor legged capsule for the active exploration of the gastrointestinal tract," *Mechatronics, IEEE/ASME Transactions on*, vol. 13, no. 2, pp. 169–179, 2008.

[17] S. Yim and M. Sitti, "Design and rolling locomotion of a magnetically actuated soft capsule endoscope," *Robotics, IEEE Transactions on*, vol. 28, no. 1, pp. 183–194, 2012.

[18] T. Qiu, T.-C. Lee, A. G. Mark, K. I. Morozov, R. Münster, O. Mierka, S. Turek, A. M. Leshansky, and P. Fischer, "Swimming by reciprocal motion at low reynolds number," *Nature communications*, vol. 5, 2014.

[19] C. Cvetkovic, R. Raman, V. Chan, B. J. Williams, M. Tolish, P. Bajaj, M. S. Sakar, H. H. Asada, M. T. A. Saif, and R. Bashir, "Three-dimensionally printed biological machines powered by skeletal muscle," *Proceedings of the National Academy of Sciences*, vol. 111, no. 28, pp. 10 125–10 130, 2014.

[20] F. Qiu, S. Fujita, R. Mhanna, L. Zhang, B. R. Simona, and B. J. Nelson, "Magnetic helical microswimmers functionalized with lipoplexes for targeted gene delivery," *Advanced*

Functional Materials, vol. 25, no. 11, pp. 1666–1671, 2015.
[21] C. Son and B. Ziaie, "A wireless implantable passive microdosimeter for radiation oncology," *Biomedical Engineering, IEEE Transactions on*, vol. 55, no. 6, pp. 1772–1775, 2008.
[22] C. Willa, J. Yuan, M. Niederberger, and D. Koziej, "When nanoparticles meet poly (ionic liquid) s: Chemoresistive co2 sensing at room temperature," *Advanced Functional Materials*, vol. 25, no. 17, pp. 2537–2542, 2015.
[23] H. Nili, S. Walia, A. E. Kandjani, R. Ramanathan, P. Gutruf, T. Ahmed, S. Balendhran, V. Bansal, D. B. Strukov, O. Kavehei *et al.*, "Donor-induced performance tuning of amorphous srtio3 memristive nanodevices: Multistate resistive switching and mechanical tunability," *Advanced Functional Materials*, 2015.
[24] B. Tian, X. Zheng, T. J. Kempa, Y. Fang, N. Yu, G. Yu, J. Huang, and C. M. Lieber, "Coaxial silicon nanowires as solar cells and nanoelectronic power sources," *Nature*, vol. 449, no. 7164, pp. 885–889, 2007.
[25] J. H. Lee, M. Khajavikhan, A. Simic, Q. Gu, O. Bondarenko, B. Slutsky, M. P. Nezhad, and Y. Fainman, "Electrically pumped sub-wavelength metallo-dielectric pedestal pillar lasers," *Optics express*, vol. 19, no. 22, pp. 21 524–21 531, 2011.
[26] A. M. Andrew, "Nanomedicine, volume 1: Basic capabilities," *Kybernetes*, vol. 29, no. 9/10, pp. 1333–1340, 2000.
[27] I. F. Akyildiz and J. M. Jornet, "Electromagnetic wireless nanosensor networks," *Nano Communication Networks*, vol. 1, no. 1, pp. 3–19, 2010.
[28] M. Pierobon and I. Akyildiz, "A Physical End-to-End Model for Molecular Communication in Nanonetworks," *IEEE J. Sel. Areas Commun.*, vol. 28, no. 4, pp. 602–611, May 2010.
[29] M. kr Kuran, H. B. Yilmaz, T. Tugcu, and B. zerman, "Energy Model for Communication via Diffusion in Nanonetworks," *J. Nano Commun. Networks*, vol. 1, no. 2, pp. 86 – 95, 2010.
[30] M. Pierobon and I. Akyildiz, "Diffusion-Based Noise Analysis for Molecular Communication in Nanonetworks," *IEEE Trans. Signal Process.*, vol. 59, no. 6, pp. 2532–2547, June 2011.
[31] P.-J. Shih, C.-H. Lee, P.-C. Yeh, and K.-C. Chen, "Channel Codes for Reliability Enhancement in Molecular Communication," *IEEE J. Sel. Areas Commun.*, vol. 31, no. 12, pp. 857–867, December 2013.
[32] A. Einolghozati, M. Sardari, and F. Fekri, "Relaying in Diffusion-based Molecular Communication," in *IEEE International Symposium on Information Theory (ISIT)*, July 2013, pp. 1844–1848.
[33] T. Nakano and J.-Q. Liu, "Design and Analysis of Molecular Relay Channels: An Information Theoretic Approach," *IEEE Trans. NanoBioscience*, vol. 9, no. 3, pp. 213–221, Sept 2010.
[34] Y. Chen, P. Kosmas, P. Anwar, and L. Huang, "A touch-communication framework for drug delivery based on a transient microbot system," *Nanobioscience, IEEE Transactions on*, vol. 14, no. 4, pp. 397–408, 2015.
[35] I. Khalil, V. Magdanz, S. Sanchez, O. Schmidt, L. Abelmann, and S. Misra, "Magnetic control of potential microrobotic drug delivery systems: Nanoparticles, magnetotactic bacteria and self-propelled microjets," in *Engineering in Medicine and Biology Society (EMBC), 2013 35th Annual International Conference of the IEEE*, July 2013, pp. 5299–5302.
[36] M. Pierobon and I. F. Akyildiz, "A physical end-to-end model for molecular communication in nanonetworks," *Selected Areas in Communications, IEEE Journal on*, vol. 28, no. 4, pp. 602–611, 2010.
[37] ——, "Capacity of a diffusion-based molecular communication system with channel memory and molecular noise," *Information Theory, IEEE Transactions on*, vol. 59, no. 2, pp. 942–954, 2013.
[38] I. Llatser, A. Cabellos-Aparicio, M. Pierobon, and E. Alarcon, "Detection Techniques for Diffusion-based Molecular Communication," *IEEE J. Sel. Areas Commun.*, vol. 31, no. 12, pp. 726–734, December 2013.
[39] A. Aijaz and A.-H. Aghvami, "Error Performance of Diffusion-Based Molecular Communication Using Pulse-Based Modulation," *IEEE Trans. NanoBiosci*, vol. 14, no. 1, pp.

146–151, Jan 2015.
[40] A. Aijaz, A. Aghvami, and M. Nakhai, "On Error Performance of Network Coding in Diffusion-Based Molecular Nanonetworks," *IEEE Trans. Nanotechnol.*, vol. 13, no. 5, pp. 871–874, Sept 2014.
[41] A. W. Eckford, "Molecular communication: Physically realistic models and achievable information rates," *arXiv preprint arXiv:0812.1554*, 2008.
[42] K. Srinivas, A. W. Eckford, and R. S. Adve, "Molecular communication in fluid media: The additive inverse gaussian noise channel," *Information Theory, IEEE Transactions on*, vol. 58, no. 7, pp. 4678–4692, 2012.
[43] A. O. Bicen and I. Akyildiz, "System-theoretic analysis and least-squares design of microfluidic channels for flow-induced molecular communication," *Signal Processing, IEEE Transactions on*, vol. 61, no. 20, pp. 5000–5013, 2013.
[44] A. Singhal, R. K. Mallik, and B. Lall, "Performance of amplitude modulation schemes for molecular communication over a fluid medium," in *Personal, Indoor, and Mobile Radio Communication (PIMRC), 2014 IEEE 25th Annual International Symposium on*. IEEE, 2014, pp. 785–789.
[45] H. ShahMohammadian, G. G. Messier, and S. Magierowski, "Nano-machine molecular communication over a moving propagation medium," *Nano Communication Networks*, vol. 4, no. 3, pp. 142–153, 2013.
[46] M. Pierobon and I. F. Akyildiz, "Diffusion-based noise analysis for molecular communication in nanonetworks," *Signal Processing, IEEE Transactions on*, vol. 59, no. 6, pp. 2532–2547, 2011.
[47] H. ShahMohammadian, G. G. Messier, and S. Magierowski, "Optimum receiver for molecule shift keying modulation in diffusion-based molecular communication channels," *Nano Communication Networks*, vol. 3, no. 3, pp. 183–195, 2012.
[48] S.-W. Hwang, H. Tao, D.-H. Kim, H. Cheng, J.-K. Song, E. Rill, M. A. Brenckle, B. Panilaitis, S. M. Won, Y.-S. Kim *et al.*, "A physically transient form of silicon electronics," *Science*, vol. 337, no. 6102, pp. 1640–1644, 2012.
[49] S. Martel, M. Mohammadi, O. Felfoul, Z. Lu, and P. Pouponneau, "Flagellated magnetotactic bacteria as controlled mri-trackable propulsion and steering systems for medical nanorobots operating in the human microvasculature," *The International journal of robotics research*, vol. 28, no. 4, pp. 571–582, 2009.
[50] S. Martel, O. Felfoul, J.-B. Mathieu, A. Chanu, S. Tamaz, M. Mohammadi, M. Mankiewicz, and N. Tabatabaei, "Mri-based medical nanorobotic platform for the control of magnetic nanoparticles and flagellated bacteria for target interventions in human capillaries," *The International journal of robotics research*, vol. 28, no. 9, pp. 1169–1182, 2009.
[51] Y. Chen, P. Kosmas, and R. Wang, "Conceptual design and simulations of a nano-communication model for drug delivery based on a transient microbot system," in *Antennas and Propagation (EuCAP), 2014 8th European Conference on*. IEEE, 2014, pp. 63–67.
[52] M. R. da Costa, O. Kibis, and M. Portnoi, "Carbon nanotubes as a basis for terahertz emitters and detectors," *Microelectronics Journal*, vol. 40, no. 4, pp. 776–778, 2009.
[53] C. E. Koksal and E. Ekici, "A nanoradio architecture for interacting nanonetworking tasks," *Nano Communication Networks*, vol. 1, no. 1, pp. 63–75, 2010.
[54] J. M. Jornet and I. F. Akyildiz, "Channel modeling and capacity analysis for electromagnetic wireless nanonetworks in the terahertz band," *Wireless Communications, IEEE Transactions on*, vol. 10, no. 10, pp. 3211–3221, 2011.
[55] J. M. Jornet, J. C. Pujol, and J. S. Pareta, "Phlame: A physical layer aware mac protocol for electromagnetic nanonetworks in the terahertz band," *Nano Communication Networks*, vol. 3, no. 1, pp. 74–81, 2012.
[56] C. S. Joseph, A. N. Yaroslavsky, V. A. Neel, T. M. Goyette, and R. H. Giles, "Continuous wave terahertz transmission imaging of nonmelanoma skin cancers," *Lasers in Surgery and Medicine*, vol. 43, no. 6, pp. 457–462, 2011.
[57] E. Jung, H. Park, K. Moon, M. Lim, Y. Do, H. Han, H. J. Choi, B.-H. Min, S. Kim, I. Park *et al.*, "Thz time-domain spectroscopic imaging of human articular cartilage," *Journal of*

Infrared, Millimeter, and Terahertz Waves, vol. 33, no. 6, pp. 593–598, 2012.
[58] G. J. Wilmink and J. E. Grundt, "Invited review article: current state of research on biological effects of terahertz radiation," *Journal of Infrared, Millimeter, and Terahertz Waves*, vol. 32, no. 10, pp. 1074–1122, 2011.
[59] C. Han, A. Bicen, and I. Akyildiz, "Multi-ray channel modeling and wideband characterization for wireless communications in the terahertz band," *Wireless Communications, IEEE Transactions on*, vol. PP, no. 99, pp. 1–1, 2015.
[60] J. Kokkoniemi, J. Lehtomaki, K. Umebayashi, and M. Juntti, "Frequency and time domain channel models for nanonetworks in terahertz band," *Antennas and Propagation, IEEE Transactions on*, vol. 63, no. 2, pp. 678–691, Feb 2015.
[61] K. Kantelis, S. Amanatiadis, C. Liaskos, N. Kantartzis, N. Konofaos, P. Nicopolitidis, and G. Papadimitriou, "On the use of fdtd and ray-tracing schemes in the nanonetwork environment," *Communications Letters, IEEE*, vol. 18, no. 10, pp. 1823–1826, Oct 2014.
[62] J. Lehtomaki, A. Bicen, and I. Akyildiz, "On the nanoscale electromechanical wireless communication in the vhf band," *Communications, IEEE Transactions on*, vol. 63, no. 1, pp. 311–323, Jan 2015.
[63] A. L. Fetter and J. D. Walecka, *Theoretical mechanics of particles and continua*. Courier Corporation, 2003.
[64] T. Hogg and R. A. Freitas Jr, "Acoustic communication for medical nanorobots," *Nano Communication Networks*, vol. 3, no. 2, pp. 83–102, 2012.
[65] G. E. Santagati and T. Melodia, "Opto-ultrasonic communications in wireless body area nanonetworks," in *Signals, Systems and Computers, 2013 Asilomar Conference on*. IEEE, 2013, pp. 1066–1070.
[66] ——, "Opto-ultrasonic communications for wireless intra-body nanonetworks," *Nano Communication Networks*, vol. 5, no. 1, pp. 3–14, 2014.
[67] I. F. Akyildiz and J. M. Jornet, "The internet of nano-things," *Wireless Communications, IEEE*, vol. 17, no. 6, pp. 58–63, 2010.
[68] Y.-M. Lin, C. Dimitrakopoulos, K. A. Jenkins, D. B. Farmer, H.-Y. Chiu, A. Grill, and P. Avouris, "100-ghz transistors from wafer-scale epitaxial graphene," *Science*, vol. 327, no. 5966, pp. 662–662, 2010.
[69] M. Pierobon, J. M. Jornet, N. Akkari, S. Almasri, and I. F. Akyildiz, "A routing framework for energy harvesting wireless nanosensor networks in the terahertz band," *Wireless networks*, vol. 20, no. 5, pp. 1169–1183, 2014.
[70] A. Afsharinejad, A. Davy, and B. Jennings, "Dynamic channel allocation in electromagnetic nanonetworks for high resolution monitoring of plants," *Nano Communication Networks*, 2015.
[71] S. Balasubramaniam and J. Kangasharju, "Realizing the internet of nano things: challenges, solutions, and applications," *Computer*, no. 2, pp. 62–68, 2013.
[72] E. Gul, B. Atakan, and O. B. Akan, "Nanons: A nanoscale network simulator framework for molecular communications," *Nano Communication Networks*, vol. 1, no. 2, pp. 138–156, 2010.
[73] I. Llatser, I. Pascual, N. Garralda, A. Cabellos-Aparicio, and E. Alarcón, "N3sim: a simulation framework for diffusion-based molecular communication," 2011.
[74] Á. Tóth, D. Bánky, and V. Grolmusz, "3-d brownian motion simulator for high-sensitivity nanobiotechnological applications," *NanoBioscience, IEEE Transactions on*, vol. 10, no. 4, pp. 248–249, 2011.
[75] A. Akkaya and T. Tugcu, "dmcs: distributed molecular communication simulator," in *Proceedings of the 8th International Conference on Body Area Networks*. ICST (Institute for Computer Sciences, Social-Informatics and Telecommunications Engineering), 2013, pp. 468–471.
[76] L. Felicetti, M. Femminella, and G. Reali, "A simulation tool for nanoscale biological networks," *Nano Communication Networks*, vol. 3, no. 1, pp. 2–18, 2012.
[77] J. Suzuki, H. Budiman, T. A. Carr, and J. H. DeBlois, "A simulation framework for neuron-based molecular communication," *Procedia Computer Science*, vol. 24, pp. 103–113, 2013.

[78] G. Piro, L. A. Grieco, G. Boggia, and P. Camarda, "Nano-sim: simulating electromagnetic-based nanonetworks in the network simulator 3," in *Proceedings of the 6th International ICST Conference on Simulation Tools and Techniques*. ICST (Institute for Computer Sciences, Social-Informatics and Telecommunications Engineering), 2013, pp. 203–210.

[79] G. Piro, K. Yang, G. Boggia, N. Chopra, L. Grieco, and A. Alomainy, "Terahertz communications in human tissues at the nanoscale for healthcare applications," *Nanotechnology, IEEE Transactions on*, vol. 14, no. 3, pp. 404–406, May 2015.

[80] "NS-3 platform," https://www.nsnam.org/.

Chapter 3

Fundamentals of Electromagnetic Waves for Nano-Network Communication

Since the concept of nano-network was proposed, increasing number of papers appear to discuss the communication paradigm at nano-scale [1–3], most of which put their emphasis on the molecular communication because it is totally bio-compatible and easy to fabricate [4]. However, like coins have two sides, the molecular communication also has disadvantages: the actual communication distance is short; the time delay of the channel is quite large; and the channel is not stable because the molecules diffused by random motion [4, 5], which would be addressed by the EM communication. Therefore, some papers start to study the performance of the EM communication [6–9], which will be discussed in details later in this chapter.

The possibility of the application of EM communication is investigated in [8] and the THz band is considered as the most promising candidate frequency band for nano-EM communication. At the same time, another method based on electromechanical CNT transceiver is presented [10]. After the validation of the application of the THz

band, the performance of THz channel are studied in many papers [6, 11–13]. In this chapter, a brief review of the recent development of the in-body communication will be made, followed by an overview of the recent development in THz communication of nano-network.

3.1 Recent Developments in In-Body Communication

3.1.1 Antennas for In-Body Communication

The antenna plays an essential part in robust communication links. Recently, the allocation of the Medical Implant Communication System (MICS) band (402∼405 MHz), with the ISM and UWB bands, boosted the research on the design of optimised implantable antennas.

So far, so many ways has been adopted to reduce the antenna size to make it comfortable to implant in human body. The simplest way is to use the spiral and meander planar antenna which has a long arm in the limited area [14, 15]. Then, the multilayered stacked structure is applied [16, 17]. At the same time, the combination of fractal and inverted-F design, one example of 3D design, is also a good way to balance the desired performance and the size requirements [18]. Miniaturized cavity slot antennas working in ISM band are discussed in [19, 20], shown in Fig. 3.1.

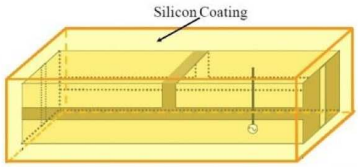

Figure 3.1: Miniaturized cavity slot antennas (reproduced from [19])

In most cases, packaging requirements get priority over the antenna requirements; but if the antenna design can take advantage of the package structure, the problem would be easily to solve. A PIFA is investigated in [21] focusing on pacemaker applications in the MedRadio frequency range while a circumference planar inverted-F antenna is studied [22]. A meandered dipole antenna using the insulation as the supporting structure is proposed in [23], shown in Fig. 3.2, which makes the whole system

as small as $11 \times 26\ mm^2$. Later, the designs with such technology are realised and proposed in [24–26], shown in Fig. 3.3. In [27], a much more special case is discussed which uses the cardiovascular stents as the antenna for short range communication at $2.45\ GHz$.

(a) Top view

(b) Side view

Figure 3.2: Conformal chandelier meandered dipole antenna (reproduce from [23])

3.1.2 Human Body Models

In order to predict the effects of the human body on the performance of the implanted antennas and the channel characteristics, an extremely broad selection of body phantoms has been proposed and investigated. Extensive work for the numerical analysis and the physical realisations have been done by Ito [28]. Particular attention is paid to the fact that the human body is highly lossy for the propagation of RF waves. The dielectric properties of the human tissues can be obtained from [29] from 10 Hz to 100 GHz, which are derived from the pioneering work of Gabriel [30].

Among all the phantoms, canonical geometries are the simplest, which not only allows reducing the simulation time but also provides easy-to-realise conditions for the radiator formulae. A rectangular cuboid (box) phantoms are considered in [20], while the cylindrical one, modelled in [31, 32], is recommended as a standard by the European Telecommunications Standards Institute (ETSI) [33]. Furthermore, a lossy cylinder was also used in the first experimental validations of theoretical studies on the EM wave propagation through a lossy medium (sea water) in [34]. Spherical geometries are always used to mimic the head [35–37] but can also be used to model the whole body [38]. Canonical geometries can be combined for a better representation of the human body. Human body models made of boxes or cylinders are modelled in [39] at $2.4GHz$ for on-body applications, shown in Fig. 3.4. Another example is

Figure 3.3: Bio-compatible capsule with embedded antenna (reproduced from [26])

illustrated in [27], where a cylinder is used to mimic the human torso integrated with a realistic lung. It should be pointed that for the pilot study such simple models are good enough because it would be time-efficient and memory-efficient. However, if the more precise results are required, the detailed phantoms should be applied.

The most detailed human body phantoms are obtained from high-resolution scan data of the human body, for instance, the U.S. Visible Human Project [40]. To complete the database, cryosection MRI and CT image data of the head of a 72 years old male were built at 0.174mm intervals and photographed at a resolution of 1056×1528 pixels at first. Later, a male cadaver was cut in the axial plane at 1mm intervals while the female intervals are 0.33mm. These body phantoms are used in [41–44] with ideal sources, and in [45] with a helical antenna, to evaluate the EM propagation within the body. Other complete male models are introduced in [46, 47], respectively. In particular, the latter two are considered to compare the performances of implanted antennas in [18, 35, 48]. Also based on medical data, complete Japanese male and female models are developed in [49], including the possibility of modifying their postures [50].

The Virtual Family and Virtual Classroom are shown in [51, 52] consisting of high-resolution models of a complete family and of four kids based on magnetic resonance

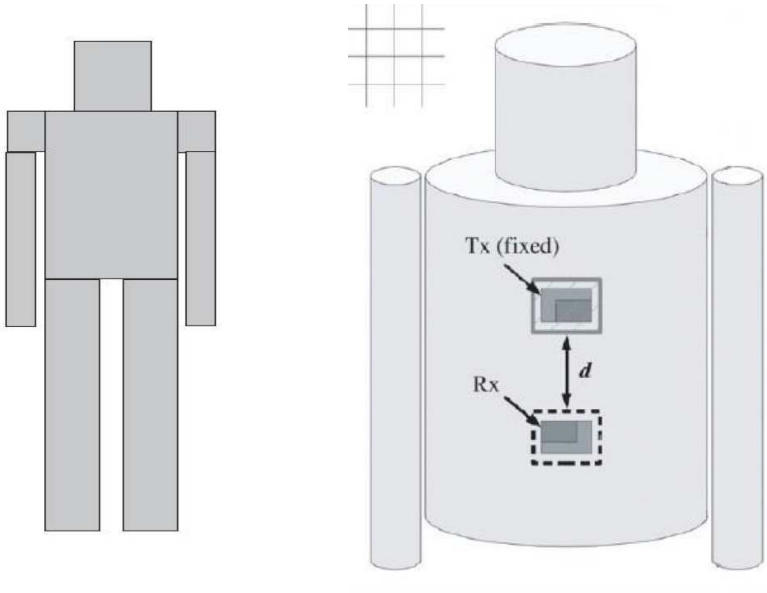

(a) Box [39]

(b) Cylindrical [27]

Figure 3.4: Approximations of a complete human model combining canonical geometries

images. These phantoms describe accurately the human body geometry with different organs for different people with various genders and ages but also allow for the investigations of different body constitutions (according to age and gender). Some postures of these models are illustrated in Fig. 3.5.

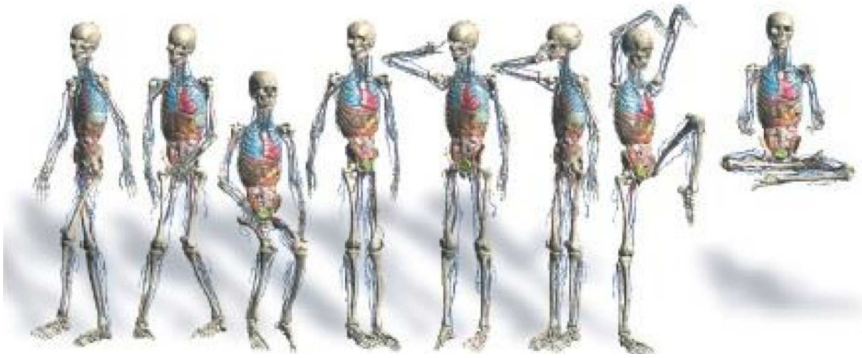

Figure 3.5: Examples of different body postures for the Virtual Family Models (reproduced from [52])

From the above, we can see that for the initial study of nano-communication, the simple phantoms should be used at first and then if needed, more detailed elements can be added step by step.

3.1.3 Channel Characterisation

The path loss in free space between a transmitter and a receiver as a function of the distance separating them can be expressed by the Friis transmission equation [53]. This equation can also be used to model radio propagation in some of the BAN scenarios by adding a term to represent the random variations around the mean path loss value. Those variations are known as shadowing, which is caused by the movement of the body or surrounding objects, and, in the case of implant channel, by varying dielectric properties of the different organs (heart, lung, liver, etc.) along the propagation path.

Fig. 3.6 shows the scatter plot for the path loss as a function of the transmitter-receiver separation for deep tissue implant to body surface scenarios at MICS band with the central frequency locating at 403.5 MHz. The mean value of the random path loss has been displayed by the solid line. This is obtained by fitting a least squares linear regression line through the scatter of measured path loss sample points in dB such that the root mean square deviation (8.18 here) of sample points about the regression line is minimized.

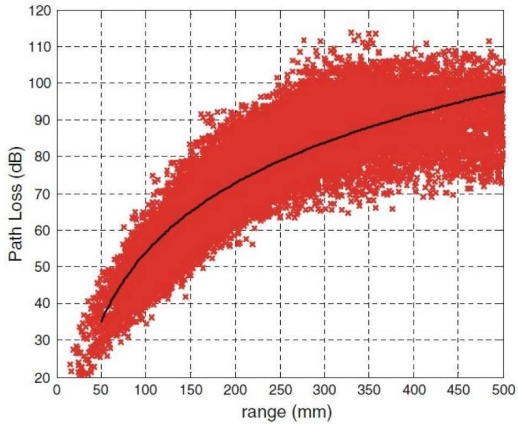

Figure 3.6: Scatter plot of the path loss vs. distance for deep tissue implant to another implant (reproduced from [54])

The scatter plot of the path loss in the 1-6 GHz band for implant to body surface is shown in Fig. 3.7 [55]. To obtain the scatter plot, the chest was exposed to an incoming plane wave from the front while ideal 595 electric field probes were placed inside the chest, arranged in seven planes consisting of 85 probes each and parallel to the skin. The plane wave was excited with a 2nd derivative Gaussian pulse with duration of $420\ ps$ in order to have most of the pulse energy within $1 \sim 6\ GHz$. The received signal

strength at every probe location was obtained and recorded. This model predicts an RMS delay spread below 1 ns, which is in agreement with the results in [56].

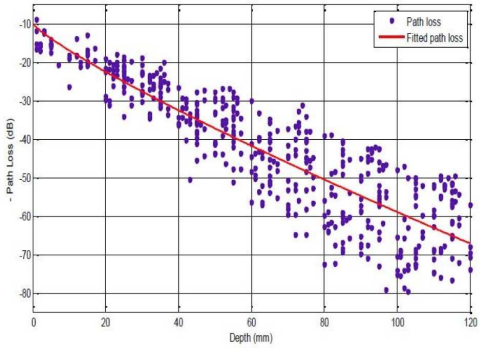

Figure 3.7: Scatter plot of the path loss in the 1-6 GHz band for implant to body surface (reproduced from [55])

From both numerical and statistical studies of path loss model at lower frequency band, it can be hypothesised that the path loss to THz wave for body-centric nano-communication can be divided into two parts: i) the part caused by the propagation of the wave; ii) the part caused by shadowing and scattering.

3.2 Recent Developments in THz Communication

3.2.1 Graphene/CNT as the Elements of THz System

Despite numerous papers on nano-technology are being published every year, enabling the EM communication between nano-devices is still a major challenge, which is mainly related to the development of nano-antennas and the corresponding electromagnetic transceivers. Reducing the size of the traditional antenna down to a few hundreds of nanometers would lead to extremely high operating frequencies, which compromises the feasibility of electromagnetic wireless communication among nano-devices. However, it has been proved that such limitation can be overcome by adopting the graphene as the building materials to fabricate the antennas because the wave propagation velocity in CNTs and GNRs can be up to one hundred times below the speed of light in vacuum depending on the structure geometry, temperature and Fermi energy [57], leading to the fact that the resonant frequency of nano-antennas made of

graphene can be up to two orders of magnitude below that of nano-antennas fabricated with other materials. Recent studies have already proved that CNT/graphene antenna can work at the THz band (*i.e.*, $0.1 - 10\ THz$); thus, the band of interest is the most promising candidate for the EM communication [8, 58, 59]. The CNT antenna was compared with classical dipoles by numerical analysis [60], while the possibility of CNT as dipole antenna was discussed, giving a mathematical framework [61]. [62] first demonstrated the performance of the propagation of EM waves on a graphene sheet. GNR-based nano patch antenna and CNT-based nano dipole antenna were compared [63], showing that graphene-based antenna with the length of 1 μm can radiate EM wave at THz band, which agreed with the prediction in [64].

An example of THz antenna made of plasmonic resonant graphene sheets is shown in Fig. 3.8 with its radiation pattern [65] from which it can be seen that the radiation pattern is similar to the traditional Hertzian dipole. In the paper, the comparison with typical metal implementations in terms of return loss and radiation efficiency was conducted and the result showed the great potential of the graphene. Later, the reconfigurable capability was studied in [66].

In addition to the antenna, graphene is also considered as the building material of novel nano-devices able to operate at Terahertz Band frequencies. Graphene-based nano-systems for Terahertz wave generation have been analytically and experimentally proved in [67–69]. Modulators for Terahertz Band signals have also been experimentally shown in [70, 71], which take advantage of the intra-band transitions in the conductivity of graphene at Terahertz Band frequencies. Similarly, filters and polarizers [72] and frequency mixers and multipliers [73–76] for Terahertz Band operation have been analytically and experimentally demonstrated. Moreover, Terahertz Band signal detection with graphene devices has been demonstrated in [77].

3.2.2 Channel Modelling of the THz Communication for Nano-Network

Because of the limitations such as size, complexity and energy consumption, EM communication between nano-devices have been thought impossible [78]. However, with the advent of the carbon-based materials like graphene and CNT, attention has been moved to the EM communication [8, 10] slowly. With the consideration that the communication is at nanoscale, the study of the communication between very short range

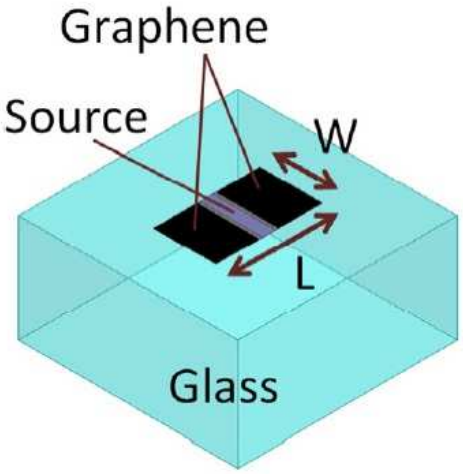

(a) antenna structure

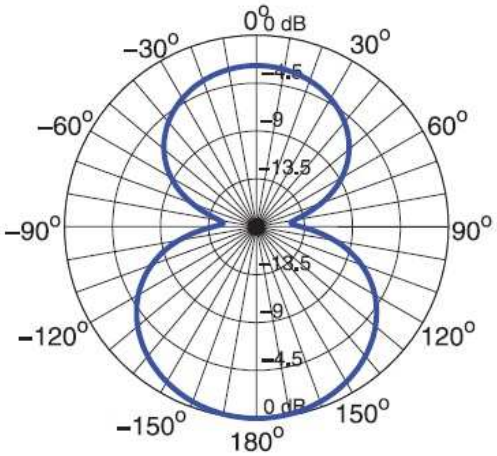

(b) E-plane

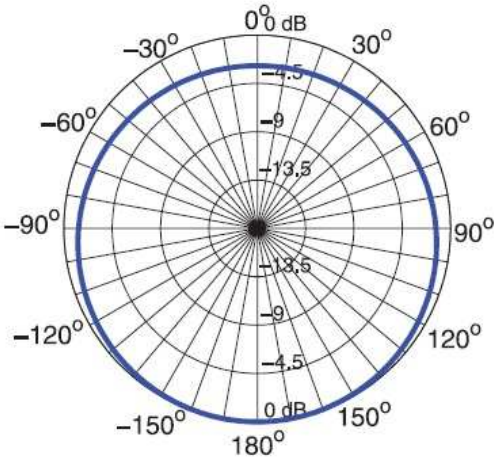

(c) H-plane

Figure 3.8: Graphene-sheet resonant plasmon antenna and its radiation pattern [65]

is essential [6, 7]. In this section, the details of the channel model will be investigated.

A modified Friis equation has been proposed by Jornet et al. in [6] to calculate the path loss of the THz channel in water vapor, which can be divided into two parts: the spread path loss and the absorption path loss. Later, a more detailed model of THz communication is proposed with the consideration of multi-ray scenario; thus, the propagation models for reflection, scattering and diffraction is considered [79]. At the same time, the scattering effects of small particles was discussed with the analysis frequency and the impulse responses [80]. Also, the Finite Difference Time-Domain and the Ray-Tracing technique were compared to evaluate the reception quality in nano-network with the consideration of two cases: LOS one and multiple objects dispersed near the LOS [81]; then, the conclusion is drawn that at the THz band RT performs as good as FDTD. Meanwhile, a discussion of the use of VHF band is conducted with the study of the bit error rate (BER) performance of the nano-receiver made of a carbon nano-tube (CNT) [82]. Similarly, the path loss in human tissues was also studied in [83].

The noise power of the channel can be obtained:

$$\begin{aligned} P_n(f,d) &= \int_B N(f,d)df = k_B \int_B T_{noise}(f,d)df \\ &\simeq k_B \int_B T_{mol}(f,d)df \end{aligned} \tag{3.1}$$

where, $T_{mol} = T_o(1 - e^{-4\pi f d\kappa/c})$ is the equivalent noise temperature due to molecular absorption; k_B is the Boltzmann constant; T_o is the reference temperature; d is the travelling distance; c stands for the light speed in the free space; f is the frequency; κ stands for the extinction coefficient of the air.

Fig. 3.9 and 3.10 show the path loss and noise temperature of the air with different water vapour concentration, individually.

The capacity of the channel was also studied to evaluate the potential of the EM paradigm. Fig. 3.11 shows the corresponding capacity for four different power spectral densities: optimal p.s.d., flat p.s.d., the Gaussian pulse and the p.s.d. for the case of the transmission window at 350 GHz, from which it can be easily seen that for the very short communication range, quite high transmission bit-rates can be supported, up to Terabits per second indicating the promising future of the application of the EM

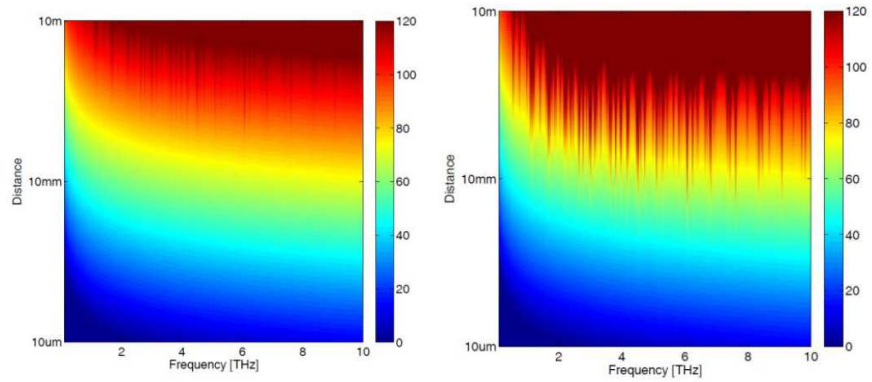

(a) 0.1% **(b)** 10%

Figure 3.9: Total path loss in dB for two different water vapour concentrations [6]

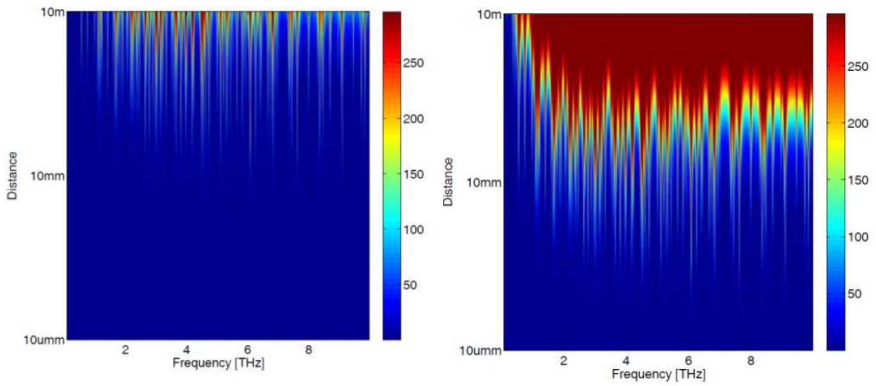

(a) 0.1% **(b)** 10%

Figure 3.10: Molecular absorption noise temperature in K for two different water vapor concentrations [6]

mechanism for nano-communication [6].

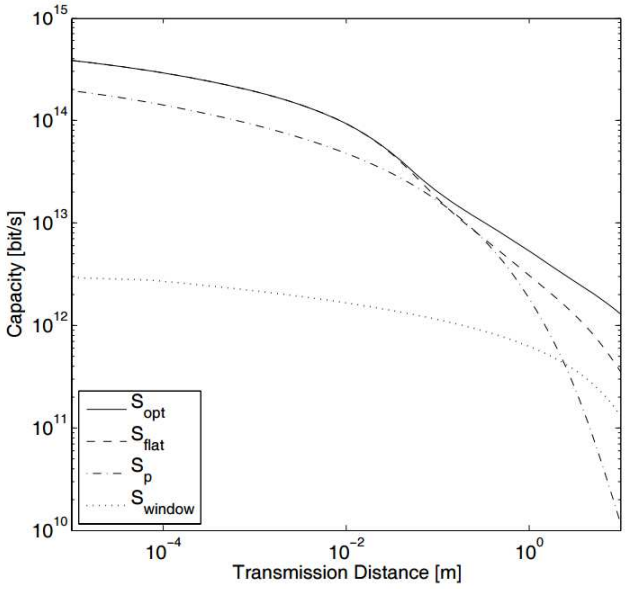

Figure 3.11: Capacity as a function of the distance for four different power spectral densities [6]

3.2.3 Other Aspects of the THz Communication for Nano-Network

The peculiar channel performances indicate the fact that new information encoding and modulation techniques should be introduced. In [13], a new communication paradigm named TS-OOK is presented and femtosecond pulse is suggested to complete the communication between the nano-devices [8]. [84] gave a thorough analysis on this pulse-based modulation which is based on the transmission of the pulse with 100 fs length by obeying an asymmetric On-Off Keying modulation Spread in Time. At the same time, the channel access scheme for nano networks at THz band was proposed and analysed to meet the requirement of the channel and the signal generators and detectors. In the paper, the cases of single user in an interference-free scenario and multi-user with interference were investigated. Finally, the whole model was evaluated by COMSOL Multi-physics [85] showing that the nano-networks can support a very large number of nano-devices communication simultaneously and the achievable rates range from a few Gbps to a few Tbps, depending on the TS-OOK parameters and nano- device density.

Because of the simple structure of nano-nodes, reducing power consumption is

challenging. To save the trasmitted energy, various coding methods were proposed. Fixed-length codewords with a constant weight were applied to mitigate interference in [86], which also reduces the transmitted energy. Kocaoglu *et al.* [87, 88] studied the design of fixed-length coding to keep the necessary Hamming distance between codewords while minimising the Average Code Weight (ACW). Based on the study of the dependence of the performance of fixed-length codes on the ACW and the code length [89], the problems of variable-length low weight codes for OOK modulation was investigated by Chi *et al.*in [90], aiming to minimise the transmission energy but guarantee the desired throughput at the same time. Based on the characteristics of the codes, two algorithms, *i.e.*, Binary Tree-based Weight Decreasing (BT-WD) and Binary Tree-based Length Decreasing (BT-LD), were proposed to dealt with the integer nonlinear programming problem, both of which performed well in average code word weight.

To support the extremely high density of nano-devices in nano-network, Jornet *et. al.* proposed a novel PHysical Layer Aware MAC protocol for Electromagnetic nanonetworks in the Terahertz Band (PHLAME) in 2012 [91], based on a novel pulse-based communication scheme, Rate Division Time-Spread OnOff Keying (RD TS-OOK). In this protocol the nano-transmitter and nano-receiver jointly select the optimal communication parameters and channel coding scheme to minimize the interference and maximize the probability of successfully decoding the received information. The results showed that by using such protocol, the network are able to support tens of Gbps throughput. Later, an energy and spectrum aware MAC protocol to achieve perpetual network was proposed [92], where a novel important system design parameter, namely, the critical packet transmission ratio (CTR) was derived. The CTR is the maximum allowable ratio of the transmission time to the energy harvesting time, below which the nano-sensor node can obtain more energy than the consumed one. By using this term, a symbol-compression solution was introduced and a packet-level timeline scheduling algorithm, built on a theoretical bandwidth-adaptive capacity-optimal physical layer, is proposed in order to keep the balance between single-user throughput and limited network lifetime. The results showed that the proposed simple scheduling algorithms would enable nano-sensors to transmit with high speed perpetually without draining the limited energy.

3.3 Summary

In this chapter, the emphasis was moved to the EM paradigm by briefly browsing the fundamentals and current development of the body-centric communication. It should be pointed out that because of the characteristics of CNT and graphene, THz band was chosen as the most suitable candidate for nano-communication. After the study of the CNT/graphene antennas, people started focusing on the channel characteristics, modulation, coding and *etc.*. Although the research is still at its early phase, its huge potential remains attractive to numerous academic groups.

References

[1] L. P. Giné and I. F. Akyildiz, "Molecular communication options for long range nanonetworks," *Computer Networks*, vol. 53, no. 16, pp. 2753–2766, 2009.

[2] M. Kuscu and O. B. Akan, "A physical channel model and analysis for nanoscale molecular communications with förster resonance energy transfer (fret)," *Nanotechnology, IEEE Transactions on*, vol. 11, no. 1, pp. 200–207, 2012.

[3] T. Hogg and R. A. Freitas Jr, "Acoustic communication for medical nanorobots," *Nano Communication Networks*, vol. 3, no. 2, pp. 83–102, 2012.

[4] S. F. Bush, *Nanoscale Communication Networks*. Artech House, 2010.

[5] I. F. Akyildiz, F. Brunetti, and C. Blázquez, "Nanonetworks: A new communication paradigm," *Computer Networks*, vol. 52, no. 12, pp. 2260–2279, 2008.

[6] J. M. Jornet and I. F. Akyildiz, "Channel modeling and capacity analysis for electromagnetic wireless nanonetworks in the terahertz band," *Wireless Communications, IEEE Transactions on*, vol. 10, no. 10, pp. 3211–3221, 2011.

[7] ——, "Channel capacity of electromagnetic nanonetworks in the terahertz band," in *Communications (ICC), 2010 IEEE International Conference on*. IEEE, 2010, pp. 1–6.

[8] I. F. Akyildiz and J. M. Jornet, "Electromagnetic wireless nanosensor networks," *Nano Communication Networks*, vol. 1, no. 1, pp. 3–19, 2010.

[9] R. Piesiewicz, T. Kleine-Ostmann, N. Krumbholz, D. Mittleman, M. Koch, J. Schoebel, and T. Kurner, "Short-range ultra-broadband terahertz communications: Concepts and perspectives," *Antennas and Propagation Magazine, IEEE*, vol. 49, no. 6, pp. 24–39, 2007.

[10] C. E. Koksal and E. Ekici, "A nanoradio architecture for interacting nanonetworking tasks," *Nano Communication Networks*, vol. 1, no. 1, pp. 63–75, 2010.

[11] Y. Kadoya, M. Onuma, S. Yanagi, T. Ohkubo, N. Sato, and J. Kitagawa, "Thz wave propagation on strip lines: devices, properties and applications," *Radioengineering*, vol. 17, no. 2, pp. 48–55, 2008.

[12] S. Priebe, C. Jastrow, M. Jacob, T. Kleine-Ostmann, T. Schrader, and T. Kürner, "Channel and propagation measurements at 300 ghz," *Antennas and Propagation, IEEE Transactions on*, vol. 59, no. 5, pp. 1688–1698, 2011.

[13] J. M. Jornet and I. F. Akyildiz, "Information capacity of pulse-based wireless nanosensor networks," in *Sensor, Mesh and Ad Hoc Communications and Networks (SECON), 2011 8th Annual IEEE Communications Society Conference on*. IEEE, 2011, pp. 80–88.

[14] P. Soontornpipit, C. M. Furse, and Y. C. Chung, "Design of implantable microstrip antenna for communication with medical implants," *Microwave Theory and Techniques, IEEE Transactions on*, vol. 52, no. 8, pp. 1944–1951, 2004.

[15] ——, "Miniaturized biocompatible microstrip antenna using genetic algorithm," *Antennas and Propagation, IEEE Transactions on*, vol. 53, no. 6, pp. 1939–1945, 2005.

[16] W.-C. Liu, F.-M. Yeh, and M. Ghavami, "Miniaturized implantable broadband antenna for biotelemetry communication," *Microwave and Optical Technology Letters*, vol. 50, no. 9, pp. 2407–2409, 2008.

[17] A. Kiourti, M. Christopoulou, S. Koulouridis, and K. S. Nikita, "Design of a novel miniaturized implantable pifa for biomedical telemetry," in *Wireless Mobile Communication and Healthcare*. Springer, 2011, pp. 127–134.

[18] M. Z. Azad and M. Ali, "A miniature implanted inverted-f antenna for gps application," *Antennas and Propagation, IEEE Transactions on*, vol. 57, no. 6, pp. 1854–1858, 2009.

[19] K. Ito, W. Xia, M. Takahashi, and K. Saito, "An implanted cavity slot antenna for medical communication systems," in *Antennas and Propagation, 2009. EuCAP 2009. 3rd European Conference on*. IEEE, 2009, pp. 718–721.

[20] W. Xia, K. Saito, M. Takahashi, and K. Ito, "Performances of an implanted cavity slot antenna embedded in the human arm," *Antennas and Propagation, IEEE Transactions on*, vol. 57, no. 4, pp. 894–899, 2009.

[21] T. Houzen, M. Takahashi, K. Saito, and K. Ito, "Implanted planar inverted f-antenna for

cardiac pacemaker system," in *Antenna Technology: Small Antennas and Novel Metamaterials, 2008. iWAT 2008. International Workshop on*. IEEE, 2008, pp. 346–349.
[22] A. Johansson, "Wireless communication with medical implants: antennas and propagation," Ph.D. dissertation, Lund University, 2004.
[23] P. M. Izdebski, H. Rajagopalan, and Y. Rahmat-Samii, "Conformal ingestible capsule antenna: A novel chandelier meandered design," *Antennas and Propagation, IEEE Transactions on*, vol. 57, no. 4, pp. 900–909, 2009.
[24] H. Yu, G. Irby, D. Peterson, M.-T. Nguyen, G. Flores, N. Euliano, and R. Bashirullah, "Printed capsule antenna for medication compliance monitoring," *Electronics Letters*, vol. 43, no. 22, pp. 1179–1181, 2007.
[25] H. Yu, G. Flores, S. Reza, G. Irby, C. Batich, R. Bashirullah, V. Meka, D. M. Peterson, and N. Euliano, "Feasibility study of printed capsule antennas for medication compliance monitoring," in *Biomedical Circuits and Systems Conference, 2007. BIOCAS 2007. IEEE*. IEEE, 2007, pp. 41–44.
[26] R. Bashirullah and N. Euliano, "Capsule antennas for medication compliance monitoring," in *Radio and Wireless Symposium, 2009. RWS'09. IEEE*. IEEE, 2009, pp. 123–126.
[27] E. Y. Chow, Y. Ouyang, B. Beier, W. J. Chappell, and P. P. Irazoqui, "Evaluation of cardiovascular stents as antennas for implantable wireless applications," *Microwave Theory and Techniques, IEEE Transactions on*, vol. 57, no. 10, pp. 2523–2532, 2009.
[28] K. Ito, "Human body phantoms for evaluation of wearable and implantable antennas," in *The Second European Conference on Antennas and Propagation, EuCAP 2007*, 2007.
[29] IFAC-CNR, "Dielectric properties of body tissues in the frequency range 10 hz - 100 ghz." [Online]. Available: http://niremf.ifac.cnr.it/tissprop/
[30] C. Gabriel, "Compilation of the dielectric properties of body tissues at rf and microwave frequencies." DTIC Document, Tech. Rep., 1996.
[31] Y. Koyanagi, H. Kawai, K. Ogawa, and K. Ito, "Consideration of the local sar and radiation characteristics of a helical antenna using a cylindroid whole body phantom at 150 mhz," *Electronics and Communications in Japan (Part I: Communications)*, vol. 87, no. 1, pp. 48–60, 2004.
[32] T. Dissanayake, K. P. Esselle, and M. R. Yuce, "Dielectric loaded impedance matching for wideband implanted antennas," *Microwave Theory and Techniques, IEEE Transactions on*, vol. 57, no. 10, pp. 2480–2487, 2009.
[33] ETSI, "Electromagnetic compatibitily and radio specrum matters (erm); short range devices (srd); ultra low power active medical implants (ulp-ami) and peripherals (ulp-ami-p) operating in the frequency range 402 mhz to 405 mhz," 2009.
[34] W. Blair, "Experimental verification of dipole radiation in a conducting half-space," *Antennas and Propagation, IEEE Transactions on*, vol. 11, no. 3, pp. 269–275, 1963.
[35] J. Kim and Y. Rahmat-Samii, "Implanted antennas inside a human body: Simulations, designs, and characterizations," *Microwave Theory and Techniques, IEEE Transactions on*, vol. 52, no. 8, pp. 1934–1943, 2004.
[36] C. M. Rappaport and F. R. Morgenthaler, "Optimal source distribution for hyperthermia at the center of a sphere of muscle tissue," *Microwave Theory and Techniques, IEEE Transactions on*, vol. 35, no. 12, pp. 1322–1327, 1987.
[37] K. S. Nikita, G. S. Stamatakos, N. K. Uzunoglu, and A. Karafotias, "Analysis of the interaction between a layered spherical human head model and a finite-length dipole," *Microwave Theory and Techniques, IEEE Transactions on*, vol. 48, no. 11, pp. 2003–2013, 2000.
[38] J. C. Lin, A. W. Guy, and C. C. Johnson, "Power deposition in a spherical model of man exposed to i-20-mhz electromagnetic fields," *Microwave Theory and Techniques, IEEE Transactions on*, vol. 21, no. 12, pp. 791–797, 1973.
[39] C. Miry, T. Alves, R. Gillard, J.-M. Laheurte, R. Loison, and B. Poussot, "Analysis of the transmission between on-body devices using the bilateral dual-grid fdtd technique," *Antennas and Wireless Propagation Letters, IEEE*, vol. 9, pp. 1073–1075, 2010.
[40] U. National Library of Medicine, "T.V.H. project." [Online]. Available: http://www.nlm.nih.gov/research/visible/visible_human.html

[41] W. G. Scanlon, J. B. Burns, and N. E. Evans, "Radiowave propagation from a tissue-implanted source at 418 mhz and 916.5 mhz," *Biomedical Engineering, IEEE Transactions on*, vol. 47, no. 4, pp. 527–534, 2000.

[42] L. C. Chirwa, P. Hammond, S. Roy, D. R. Cumming *et al.*, "Electromagnetic radiation from ingested sources in the human intestine between 150 mhz and 1.2 ghz," *Biomedical Engineering, IEEE Transactions on*, vol. 50, no. 4, pp. 484–492, 2003.

[43] A. Alomainy and Y. Hao, "Modeling and characterization of biotelemetric radio channel from ingested implants considering organ contents," *Antennas and Propagation, IEEE Transactions on*, vol. 57, no. 4, pp. 999–1005, 2009.

[44] J.-H. Jung, S.-W. Kim, Y.-S. Kim, and S.-Y. Kim, "Electromagnetic propagation from the intestine-ingested source in the human body model," *Antennas and Propagation, IEEE Transactions on*, vol. 58, no. 5, pp. 1683–1688, 2010.

[45] L. Xu, M. Q. Meng, and Y. Chan, "Effects of dielectric parameters of human body on radiation characteristics of ingestible wireless device at operating frequency of 430 mhz," *Biomedical Engineering, IEEE Transactions on*, vol. 56, no. 8, pp. 2083–2094, 2009.

[46] P. Dimbylow, "Current densities in a 2 mm resolution anatomically realistic model of the body induced by low frequency electric fields," *Physics in medicine and biology*, vol. 45, no. 4, p. 1013, 2000.

[47] I. G. Zubal, C. R. Harrell, E. O. Smith, Z. Rattner, G. Gindi, and P. B. Hoffer, "Computerized three-dimensional segmented human anatomy," *Medical physics*, vol. 21, no. 2, pp. 299–302, 1994.

[48] Z. N. Chen, G. C. Liu, and T. S. See, "Transmission of rf signals between mics loop antennas in free space and implanted in the human head," *Antennas and Propagation, IEEE Transactions on*, vol. 57, no. 6, pp. 1850–1854, 2009.

[49] T. Nagaoka, S. Watanabe, K. Sakurai, E. Kunieda, S. Watanabe, M. Taki, and Y. Yamanaka, "Development of realistic high-resolution whole-body voxel models of japanese adult males and females of average height and weight, and application of models to radio-frequency electromagnetic-field dosimetry," *Physics in medicine and biology*, vol. 49, no. 1, p. 1, 2004.

[50] T. Nagaoka and S. Watanabe, "Postured voxel-based human models for electromagnetic dosimetry," *Physics in medicine and biology*, vol. 53, no. 24, p. 7047, 2008.

[51] A. Christ, W. Kainz, E. G. Hahn, K. Honegger, M. Zefferer, E. Neufeld, W. Rascher, R. Janka, W. Bautz, J. Chen *et al.*, "The virtual familydevelopment of surface-based anatomical models of two adults and two children for dosimetric simulations," *Physics in medicine and biology*, vol. 55, no. 2, p. N23, 2010.

[52] I. Fundation, "High-resolution whole-body human models of the virtual population." [Online]. Available: http://www.itis.ethz.ch/services/human-and-animalmodels/human-models/

[53] K. Y. Yazdandoost, K. Sayrafian-Pour *et al.*, "Channel model for body area network (ban)," *IEEE P802*, vol. 15, 2009.

[54] K. Sayrafian-Pour, W.-B. Yang, J. Hagedorn, J. Terrill, K. Y. Yazdandoost, and K. Hamaguchi, "Channel models for medical implant communication," *International Journal of Wireless Information Networks*, vol. 17, no. 3-4, pp. 105–112, 2010.

[55] A. Khaleghi, R. Chavez-Santiago, and I. Balasingham, "An improved ultra wideband channel model including the frequency-dependent attenuation for in-body communications," in *Engineering in Medicine and Biology Society (EMBC), 2012 Annual International Conference of the IEEE*. IEEE, 2012, pp. 1631–1634.

[56] J. Wang and Q. Wang, "Channel modeling and ber performance of an implant uwb body area link," in *Applied Sciences in Biomedical and Communication Technologies, 2009. ISABEL 2009. 2nd International Symposium on*. IEEE, 2009, pp. 1–4.

[57] S. Datta, *Electronic transport in mesoscopic systems*. Cambridge university press, 1997.

[58] G. Zhou, M. Yang, X. Xiao, and Y. Li, "Electronic transport in a quantum wire under external terahertz electromagnetic irradiation," *Physical Review B*, vol. 68, no. 15, p. 155309, 2003.

[59] M. R. da Costa, O. Kibis, and M. Portnoi, "Carbon nanotubes as a basis for terahertz emitters and detectors," *Microelectronics Journal*, vol. 40, no. 4, pp. 776–778, 2009.
[60] G. W. Hanson, "Fundamental transmitting properties of carbon nanotube antennas," *Antennas and Propagation, IEEE Transactions on*, vol. 53, no. 11, pp. 3426–3435, 2005.
[61] P. J. Burke, S. Li, and Z. Yu, "Quantitative theory of nanowire and nanotube antenna performance," *Nanotechnology, IEEE Transactions on*, vol. 5, no. 4, pp. 314–334, 2006.
[62] G. W. Hanson, "Dyadic greens functions and guided surface waves for a surface conductivity model of graphene," *Journal of Applied Physics*, vol. 103, no. 6, p. 064302, 2008.
[63] J. M. Jornet and I. F. Akyildiz, "Graphene-based nano-antennas for electromagnetic nanocommunications in the terahertz band," in *Antennas and Propagation (EuCAP), 2010 Proceedings of the Fourth European Conference on*. IEEE, 2010, pp. 1–5.
[64] Y.-M. Lin, C. Dimitrakopoulos, K. A. Jenkins, D. B. Farmer, H.-Y. Chiu, A. Grill, and P. Avouris, "100-ghz transistors from wafer-scale epitaxial graphene," *Science*, vol. 327, no. 5966, pp. 662–662, 2010.
[65] M. Tamagnone, J. Gomez-Diaz, J. Mosig, and J. Perruisseau-Carrier, "Analysis and design of terahertz antennas based on plasmonic resonant graphene sheets," *Journal of Applied Physics*, vol. 112, no. 11, p. 114915, 2012.
[66] M. Tamagnone, J. Gomez Diaz, J. Perruisseau-Carrier, and J. R. Mosig, "High-impedance frequency-agile thz dipole antennas using graphene," in *Antennas and Propagation (EuCAP), 2013 7th European Conference on*. Ieee, 2013, pp. 533–536.
[67] T. Otsuji, T. Watanabe, A. El Moutaouakil, H. Karasawa, T. Komori, A. Satou, T. Suemitsu, M. Suemitsu, E. Sano, W. Knap *et al.*, "Emission of terahertz radiation from two-dimensional electron systems in semiconductor nano-and hetero-structures," *Journal of Infrared, Millimeter, and Terahertz Waves*, vol. 32, no. 5, pp. 629–645, 2011.
[68] T. Otsuji, S. B. Tombet, A. Satou, H. Fukidome, M. Suemitsu, E. Sano, V. Popov, M. Ryzhii, and V. Ryzhii, "Graphene-based devices in terahertz science and technology," *Journal of Physics D: Applied Physics*, vol. 45, no. 30, p. 303001, 2012.
[69] T. Otsuji, S. B. Tombet, A. Satou, M. Ryzhii, and V. Ryzhii, "Terahertz-wave generation using graphene: Toward new types of terahertz lasers," *Selected Topics in Quantum Electronics, IEEE Journal of*, vol. 19, no. 1, pp. 8 400 209–8 400 209, 2013.
[70] S. H. Lee, M. Choi, T.-T. Kim, S. Lee, M. Liu, X. Yin, H. K. Choi, S. S. Lee, C.-G. Choi, S.-Y. Choi *et al.*, "Switching terahertz waves with gate-controlled active graphene metamaterials," *Nature materials*, vol. 11, no. 11, pp. 936–941, 2012.
[71] B. Sensale-Rodriguez, R. Yan, M. M. Kelly, T. Fang, K. Tahy, W. S. Hwang, D. Jena, L. Liu, and H. G. Xing, "Broadband graphene terahertz modulators enabled by intraband transitions," *Nature communications*, vol. 3, p. 780, 2012.
[72] H. Yan, X. Li, B. Chandra, G. Tulevski, Y. Wu, M. Freitag, W. Zhu, P. Avouris, and F. Xia, "Tunable infrared plasmonic devices using graphene/insulator stacks," *Nature Nanotechnology*, vol. 7, no. 5, pp. 330–334, 2012.
[73] H. Wang, D. Nezich, J. Kong, and T. Palacios, "Graphene frequency multipliers," *Electron Device Letters, IEEE*, vol. 30, no. 5, pp. 547–549, 2009.
[74] H. Wang, A. Hsu, J. Wu, J. Kong, and T. Palacios, "Graphene-based ambipolar rf mixers," *Electron Device Letters, IEEE*, vol. 31, no. 9, pp. 906–908, 2010.
[75] H. Wang, A. Hsu, K. K. Kim, J. Kong, and T. Palacios, "Gigahertz ambipolar frequency multiplier based on cvd graphene," in *Electron Devices Meeting (IEDM), 2010 IEEE International*. IEEE, 2010, pp. 23–6.
[76] Y.-M. Lin, A. Valdes-Garcia, S.-J. Han, D. B. Farmer, I. Meric, Y. Sun, Y. Wu, C. Dimitrakopoulos, A. Grill, P. Avouris *et al.*, "Wafer-scale graphene integrated circuit," *Science*, vol. 332, no. 6035, pp. 1294–1297, 2011.
[77] G. Deligeorgis, F. Coccetti, G. Konstantinidis, and R. Plana, "Radio frequency signal detection by ballistic transport in y-shaped graphene nanoribbons," *Applied Physics Letters*, vol. 101, no. 1, p. 013502, 2012.
[78] S. Luryi, J. Xu, and A. Zaslavsky, *Future trends in microelectronics: up the nano creek*. John Wiley & Sons, 2007.

[79] C. Han, A. Bicen, and I. Akyildiz, "Multi-ray channel modeling and wideband characterization for wireless communications in the terahertz band," *Wireless Communications, IEEE Transactions on*, vol. PP, no. 99, pp. 1–1, 2015.

[80] J. Kokkoniemi, J. Lehtomaki, K. Umebayashi, and M. Juntti, "Frequency and time domain channel models for nanonetworks in terahertz band," *Antennas and Propagation, IEEE Transactions on*, vol. 63, no. 2, pp. 678–691, Feb 2015.

[81] K. Kantelis, S. Amanatiadis, C. Liaskos, N. Kantartzis, N. Konofaos, P. Nicopolitidis, and G. Papadimitriou, "On the use of fdtd and ray-tracing schemes in the nanonetwork environment," *Communications Letters, IEEE*, vol. 18, no. 10, pp. 1823–1826, Oct 2014.

[82] J. Lehtomaki, A. Bicen, and I. Akyildiz, "On the nanoscale electromechanical wireless communication in the vhf band," *Communications, IEEE Transactions on*, vol. 63, no. 1, pp. 311–323, Jan 2015.

[83] K. Yang, A. Pellegrini, M. Munoz, A. Brizzi, A. Alomainy, and Y. Hao, "Numerical analysis and characterization of thz propagation channel for body-centric nano-communications," *Terahertz Science and Technology, IEEE Transactions on*, vol. 5, no. 3, pp. 419–426, May 2015.

[84] J. M. Jornet and I. F. Akyildiz, "Femtosecond-long pulse-based modulation for terahertz band communication in nanonetworks," *Communications, IEEE Transactions on*, vol. 62, no. 5, pp. 1742–1754, 2014.

[85] COMSOL, "COMSOL Multiphysics Simulation Software," http://www.comsol.com/products/multiphysics/.

[86] J. M. Jornet and I. F. Akyildiz, "Low-weight channel coding for interference mitigation in electromagnetic nanonetworks in the terahertz band," in *Communications (ICC), 2011 IEEE International Conference on*. IEEE, 2011, pp. 1–6.

[87] M. Kocaoglu and O. B. Akan, "Minimum energy coding for wireless nanosensor networks," in *INFOCOM, 2012 Proceedings IEEE*. IEEE, 2012, pp. 2826–2830.

[88] ——, "Minimum energy channel codes for nanoscale wireless communications," *Wireless Communications, IEEE Transactions on*, vol. 12, no. 4, pp. 1492–1500, 2013.

[89] K. Chi, Y.-h. Zhu, X. Jiang, and X.-z. Tian, "Energy optimal coding for wireless nanosensor networks," in *Wireless Communications and Networking Conference (WCNC), 2013 IEEE*. IEEE, 2013, pp. 998–1002.

[90] K. Chi, Y.-h. Zhu, X. Jiang, and V. Leung, "Energy-efficient prefix-free codes for wireless nano-sensor networks using ook modulation," *Wireless Communications, IEEE Transactions on*, vol. 13, no. 5, pp. 2670–2682, 2014.

[91] J. M. Jornet, J. C. Pujol, and J. S. Pareta, "Phlame: A physical layer aware mac protocol for electromagnetic nanonetworks in the terahertz band," *Nano Communication Networks*, vol. 3, no. 1, pp. 74–81, 2012.

[92] P. Wang, J. M. Jornet, M. A. Malik, N. Akkari, and I. F. Akyildiz, "Energy and spectrum-aware mac protocol for perpetual wireless nanosensor networks in the terahertz band," *Ad Hoc Networks*, vol. 11, no. 8, pp. 2541–2555, 2013.

Chapter 4

Numerical Modelling of THz Wave Propagation in Human Tissues

To enable electromagnetic paradigm realisable, the characterization of the frequency band at which nano-devices communicate is essential. In this chapter, a new channel model for body-centric, especially in-body communication at THz band (0.1 THz to 10 THz) was proposed by investigating the path loss and noise model on the basis of the previous work where the concept of molecular absorption and noise was revisited. Additionally, the channel capacity was calculated to investigate the potential of the THz band by applying different power allocation. Finally, simple models were simulated in CST to evaluate the channel model.

4.1 Motivation and Related Work

As shown in Chapter 3, graphene-based plasmonic nano-antennas are expected to work at THz band [1–3]; thus, THz band is considered as a promising candidate for nano-communication. At the same time, a substantial amount of work has been performed on the channel characterisation and modelling for body-centric wireless communications at microwave frequencies and mm-wave band [4]. Statistical on-body

path loss models for different links and body scenarios have been developed by analysing the measurement data from on-body propagation with two patch antennas working at 2.45 GHz in an anechoic and lab environment [5]. The path loss model of radio propagation in human tissues was presented in [6] and subsequently compared to experimental results for muscle, validating the reliability of the numerical simulation at 2.45 GHz. A numerical modelling method using parallel FDTD was applied to study the radio propagation and system performance of the wireless body area network at UWB band [7], proving that both channel performance and system performance are subject-specific. The path loss model for mm-wave was studied by comparing the numerical results from Remcom XGTD and measured data in [8], which indicated the path loss model for on-body communication at 94 GHz was closely related to the body shape and garments. At the same time, several papers on THz indoor communications have been published [9, 10]. In addition, the optical parameters of human tissues up to 2.5 THz have been empirically characterized in [11], [12] following the discussion of the possibility of applying EM waves in nano-networks [13]. The channel model for THz wave propagating in the air with different concentration of the water vapor was presented in [14] and the corresponding channel capacity was also studied. Based on the characteristics of the channel, a new physical- layer aware medium access control (MAC) protocol, Time Spread On-Off Keying (TS-OOK), was proposed [15]. Meanwhile, the applications of THz technology in imaging and medical field [16, 17] has also achieved great development and the biological effects of THz radiation are reviewed in [18] showing minimum effect on the human body and no strong evidence of hazardous side effects. However, most work presented in the open literature does not explicitly investigate the EM channel modelling at THz for the body-centric nano-networks, which would be the main contribution of this chapter.

4.2 Channel Modelling of Human Tissues at THz Band

4.2.1 Relationship of Optical Parameters to Electromagnetic Parameters

At optical frequencies, all the information is usually delivered in terms of refractive index or index of refraction:

$$\tilde{n}(f) = n_r(f) - jn_i(f) \tag{4.1}$$

The real part n_r can be usually obtained directly from the measurement while the imaginary part n_i (which would also be referred to as κ, named extinction coefficient) can be calculated from the absorption coefficient α. The relationship between the two can be given by

$$n_i(f) = \frac{\alpha(f)\lambda_o}{4\pi} \tag{4.2}$$

where, $\lambda_o = c/f$ is the wavelength in free-space.

From $\tilde{n}$, we can obtain the relative permittivity constant ϵ as

$$\begin{aligned} \epsilon(f) &= \tilde{n}(f)^2 \\ &= n_r(f)^2 - \kappa(f)^2 - j2n_r(f)\kappa(f) \end{aligned} \tag{4.3}$$

Thus, we can obtain:

$$\begin{cases} \epsilon' = n_r(f)^2 - \kappa(f)^2 \\ \epsilon'' = 2n_r(f)\kappa(f) \end{cases} \tag{4.4}$$

where, ϵ' and ϵ'' are the real and imaginary part of the relative permittivity ϵ.

The absorption coefficient of some human tissues, *i.e.* blood, skin and fat, is shown in Fig. 4.1a ([11], [12]) while the EM parameters, *i.e.*, permittivity of the corresponding tissues, calculated from Eq. 4.4, were shown in Fig. 4.1b and 4.1c. [1]

4.2.2 Path Loss

A modified Friis equation has been proposed by Jornet et al. in [14] to calculate the path loss of the THz channel in water vapor, which can be divided into two parts: the spread path loss PL_{spr} and the absorption path loss PL_{abs}. Similarly, the path loss in

[1] The refractive index n_r is 1.97, 1.73 and 1.58 for blood, skin and fat, respectively.

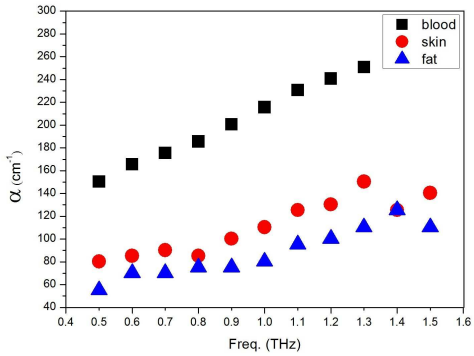

(a) Measured absorption coefficient α (Reproduced from [11, 12])

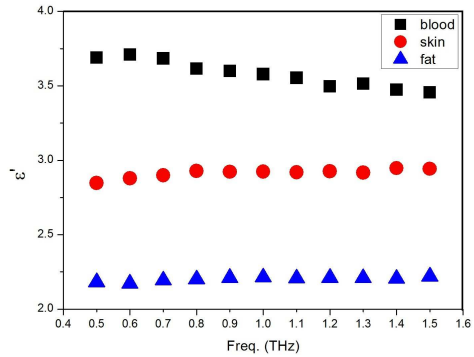

(b) Real part of the relative permittivity (calculated from Eq. 4.4)

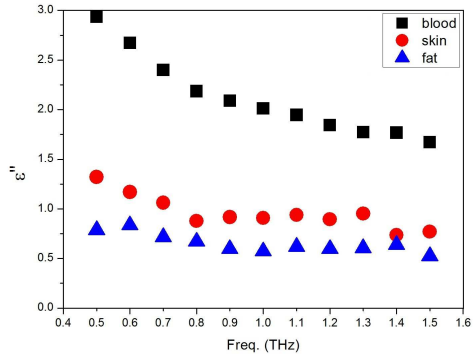

(c) Imaginary part of the relative permittivity (calculated from Eq. 4.4)

Figure 4.1: Optical and electromagnetic parameters of human tissues (blood, skin and fat)

human tissues can also be divided into two parts:

$$PL_{total}[dB] = PL_{spr}(f,d)[dB] + PL_{abs}(f,d)[dB] \tag{4.5}$$

where, f stands for the frequency while d is the path length.

The spread path loss is introduced by the expansion of the wave in the medium, which is defined as:

$$PL_{spr}(f,d) = (\frac{4\pi d}{\lambda_g})^2 \tag{4.6}$$

where $\lambda_g = \lambda_o/n_r$ stands for the wavelength in medium with free-space wavelength λ_o, and d is the travelling distance of the wave. In this study, the electromagnetic power is considered to spread spherically.

The absorption path loss accounts for the attenuation caused by the molecular absorption of the medium, where part of the energy of the propagating wave is converted into internal kinetic energy of the excited molecules in the medium. The absorption loss can be obtained from the transmittance of the medium $\tau(f,d)$:

$$PL_{abs} = \frac{1}{\tau(f,d)} = e^{\alpha(f)d} \tag{4.7}$$

The dependence of the channel path loss for blood, skin and fat on the distance and frequency is shown in Fig. 4.2. It is demonstrated that there are some fluctuations in each individual figure due to the fact that absorption path loss is related to the extinction coefficient, κ, which is not an analytical function along the required frequency band, in addition to the expected increase in path loss values with larger distances and higher frequency components. For different tissues, the path loss varies: with blood experiencing the highest losses, followed by the skin due to the water concentration, which contributes a significant absorption path loss. At the level of the millimeters, the path loss of the blood is around 120 dB, while the skin is around 90 dB and the fat is around 70 dB. Compared with the channel attenuation of the molecular communication [19], the future of the EM paradigms is promising because at 1 kHz (here, the frequency is the operation frequency of the RC circuit which depicted the emission and absorption process of the diffusion-based particle communication) and at a distance of 0.05 mm the molecular channel attenuation is above 140 dB which

is substantially higher than the case for blood at the distance of $1mm$ applying THz EM communication mechanism. In [20], the capacity was also compared between the two paradigms, showing that the EM communication keeps extremely high data rate until the distance is up to $10mm$ while the molecular communication scheme provides much lower capabilities.

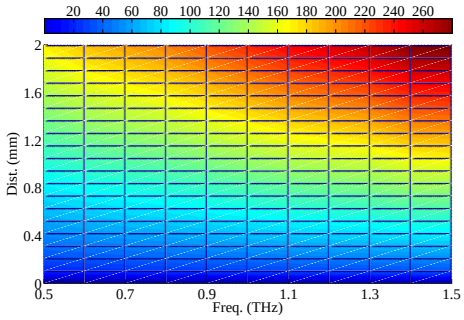

(a) Blood

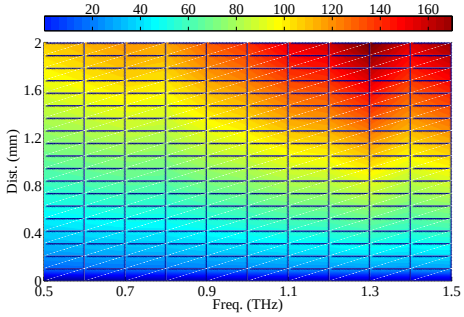

(b) Skin

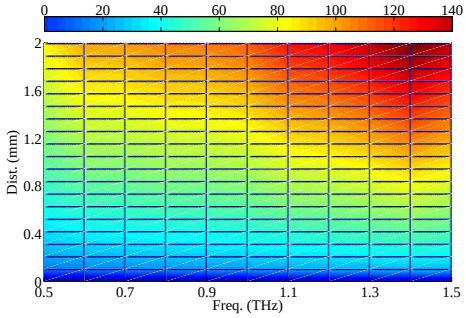

(c) Fat

Figure 4.2: Total path loss as a function of the distance and frequency for different human tissues

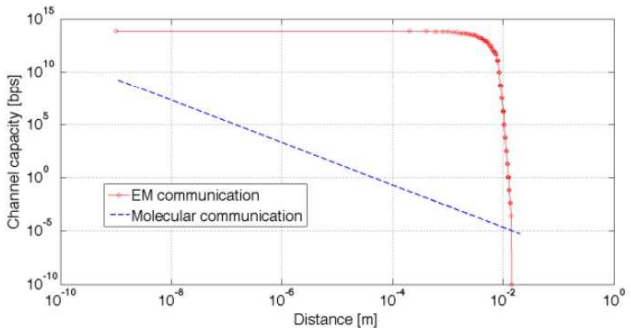

Figure 4.3: Channel capacity comparison between EM and molecular communication [20]

4.2.3 Delay

As the name indicates, the propagation delay is the length of time it takes for waves travelling from the origin:

$$D = \frac{d}{\nu} \tag{4.8}$$

where, d is the path distance while $\nu = c/n_r$ is the wave speed in the medium.

The delay of blood, skin and fat are all at the order of pico-second along the frequency which indicates that the effect of the frequency on the delay can be ignored since the refractive index is considered as the same over this band. At the same time, for different tissues the delay would be different because the refractive index would change. From Fig. [11, 12] it can be concluded that waves in fat took the shortest time while the wave in blood will travel for the longest time.

4.2.4 Noise

The molecules along the path not only introduce the attenuation of the wave but also introduce the noise because their internal vibration, provoked by the incident wave, would turn into the emission of EM radiation at the same frequency [21], which can be measured by the parameter of the emissivity of the channel, ξ :

$$\xi(f, d) = 1 - \tau(f, d) \tag{4.9}$$

Where, $\tau(f, d) = e^{-\alpha(f)d}$ is the transmissivity of the medium, f is the frequency of the EM wave, d stands for the path length.

Thus, the equivalent noise temperature due to molecular absorption can be obtained:

$$T_{mol}(f,d) = T_0\xi(f,d) \tag{4.10}$$

where T_0 is the reference temperature, f is the frequency of the EM wave, d stands for the path length, ξ refers to the emissivity of the channel given by Eq. 4.9. It should be noted that this kind of noise only appears around the frequencies in which the molecular absorption is quite high.

The total noise temperature of the system T_{noise} is composed of the system electronic noise temperature, T_{sys}, and the total antenna noise temperature, T_{ant}, which includes not only the molecular absorption noise temperature, T_{mol}, but also other contributions from several sources, T_{other}, such as the noise created by surrounding nano-devices or the same device.

$$T_{noise} = T_{sys} + T_{ant} = T_{sys} + T_{mol} + T_{other} \tag{4.11}$$

For a given bandwidth, B, the total system noise power at the receiver can be calculated as follows:

$$P_n(f,d) = \int N(f,d)df = k_B \int T_{noise}(f,d)df \tag{4.12}$$

Where, N stands for the noise power spectral density; k_B is the Boltzmann constant; T_{noise} is the equivalent noise temperature.

Because the electronic noise temperature of the system is assumed to be low due to the electron transport properties of graphene [22], the main factor affecting the channel performance will be the molecular absorption noise temperature, which indicates $T_{noise} \approx T_{mol}$.

The molecular absorption noise temperature is shown in Fig. 4.4. It can be seen that the noise temperature increases with the rise of the frequency and distance, which will lead to the rise of the noise power. At the level of millimeters, the molecular noise temperature reaches 310 K, the normal human temperature.

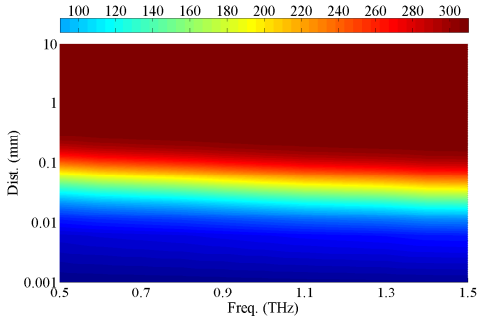

(a) Blood

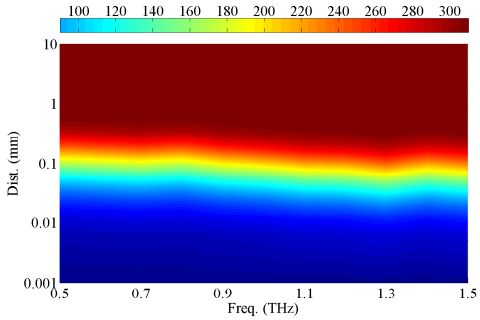

(b) Skin

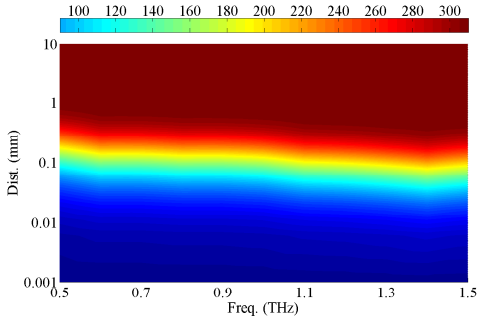

(c) Fat

Figure 4.4: Noise temperature as a function of the distance and frequency for different human tissues

4.3 Channel Capacity of Human Tissues at THz Band

In order to evaluate the potential of the Terahertz Band, the channel capacity would be used as the performance metric. In the analysis, THz Band is considered as a single transmission window which is almost 1 THz wide (from 0.5 THz to 1.5 THz) because of the limit of the current database for human tissues at THz band [11, 12].

According to the *Shannons theory*, the channel capacity can be obtained as follows [23]:

$$C = Blog_2(1 + \frac{S}{N}) \tag{4.13}$$

where B is the whole bandwidth of the system while $\frac{S}{N}$ stands for the signal-noise-ratio.

From the previous investigation, the channel is frequency-selective and the noise is non-white, thus the whole bandwidth need to be divided into many narrow sub-bands which can be chosen small enough to make the channel appear non-selective and the noise power spectrum distribution locally flat [23]. The ith sub-band is centred at f_i with the bandwidth $\Delta f (i = 1, 2, 3...)$. Then, the Eq. 4.13 can be rewritten as

$$C(d) = \sum_i \Delta f log_2[1 + \frac{S(f_i)}{PL(f_i, d)S_N(f_i, d)}] \tag{4.14}$$

where, $S(f_i)$ is the power spectral density of the transmitted signal while Δf is fixed to 0.1 THz; $PL(f_i, d)$ is the path loss over the sub-band; $S_N(f_i, d)$ is the noise power spectral density over the sub-band. And here the frequency band covering from 0.5 THz to 1.5 THz with 1 THz bandwidth is considered.

From Eq. 4.13, it can be easily seen that besides the effect of both path loss and noise temperature communication capabilities are also strictly influenced by the way how the transmitted power, P_{tx}, is distributed in the frequency domain. In line with [14], three communication schemes (*i.e.*, *flat*, *pulse-based*, and *optimal*) are considered in this work and characterised in what follows.

Flat Communication

The total power transmission, P_{tx}, is uniformly distributed over the entire operating band. Thus, the corresponding power spectral density is:

$$S_f(f) = \begin{cases} S_0 = P_{tx}/B & \text{if } f_m \leq f \leq f_M \\ \\ 0 & \text{otherwise} \end{cases} \tag{4.15}$$

where, obviously, $\int_{f_m}^{f_M} S_f(f)df = P_{tx}$, that is, $S_0 = P_{tx}/B$.

Pulse-Based Communication

Taking into account capabilities of graphene-based nanoelectronic, the pulse generated by a nano-device, i.e., the wave form used to transmit the logical '1', can be modelled with a n-th derivative of a Gaussian-shape, i.e., $\phi(f) = (2\pi f)^{2n} e^{(-2\pi\sigma f)^2}$ [14]. Hence, the power spectral density can be expressed as:

$$S_p(f) = a_0^2 \cdot \phi(f)\ , \tag{4.16}$$

where σ, and a_0^2 are the standard deviation of the Gaussian pulse and a normalising constant, respectively.

Considering that $\int_{f_m}^{f_M} S_p(f)df = P_{tx}$, a_0^2 is given by:

$$a_0^2 = P_{tx} \Big/ \int_{f_m}^{f_M} \phi(f)\ \ . \tag{4.17}$$

Optimal Communication

This scheme aims at maximising the overall channel capacity by optimally adapting the power allocation as a function of frequency-selective properties of the channel. The optimal transmission scheme can be obtained by solving the following optimisation

problem with the consideration of Eq. 4.14:

$$\begin{cases} \max \left\{ \sum_i \Delta f \log_2 \left[1 + \frac{S_o(f_i)}{PL(f_i,d)N(f_i,d)} \right] \right\} \\ \\ \text{subject to} \quad \sum_i S_o(f_i)\Delta f = P_{tx} \end{cases} \tag{4.18}$$

As known, the maximum value of a concave function, like the one in Eq. (4.18), can be done by using Lagrange multiplier, λ. Thus, the optimisation problem can be rewritten as:

$$\max \left\{ \sum_i \Delta f \left(\log_2 \left[1 + \frac{S_o(f_i)}{PL(f_i,d)N(f_i,d)} \right] + \lambda S_o(f_i) \right) - P_{tx} \right\} \tag{4.19}$$

The maximum is found by equating to zero the derivative of the argument of Eq. 4.19 with respect to $S_o(f_i)$ and λ. This produces:

$$\frac{1}{\ln(2)[S_o(f_i) + PL(f_i,d)N(f_i,d)]} = \lambda \qquad \forall i \, . \tag{4.20}$$

That is, the overall channel capacity is maximised when:

$$S_o(f_i) + PL(f_i,d)N(f_i,d) = \beta, \tag{4.21}$$

where β is a constant to be evaluated.

The problem can be solved by using the *water-filling* principle, which adopts an iterative procedure for finding the most suitable power distribution on available sub-bands. In details, at the n-th step, β is computed as:

$$\beta(n) = \frac{1}{L(n)} \left[\frac{P_{tx}}{\Delta f} + \sum_i PL(f_i,d)N(f_i,d) \right] \tag{4.22}$$

where $L(n)$ is the number of sub-bands at the n-th step.

In particular, considering the i-th sub-band, the power spectral density is set as $S_o(f_i) = \beta - A(f_i,d)N(f_i,d)$. If it results $S_o(f_i) \leq 0$, then the corresponding power spectral density is set to 0 and Eq. (4.22) should be computed again (without considering the identified sub-band) as long as there are no sub-bands with a negative $S_o(f_i)$. At the end, the procedure optimally distributes the total power transmission over the available sub-bands by assigning higher power spectral density values to sub-bands

offering better channel conditions (i.e., lower path loss and lower noise power).

Fig. 4.5 shows the capacity for different tissues with different power allocations. From the figure, it can be seen that with the increase of the distance the capacity will keep almost the same at first and then drop significantly at some point (for different tissues and different power allocation, the point changes). And also we can see that the optimal one always occupies the top while the performance of the pulse-based one is not as good as the other two but the differences between them is not very huge. By comparing the three figures listed, we can see that the capacity of fat is better than the other two.

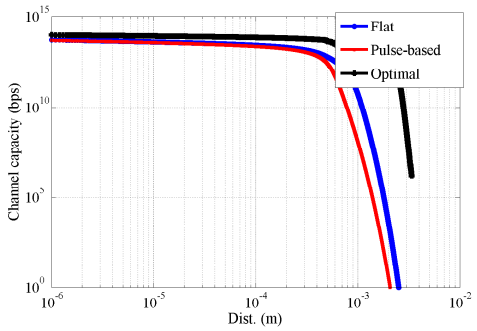

(a) blood

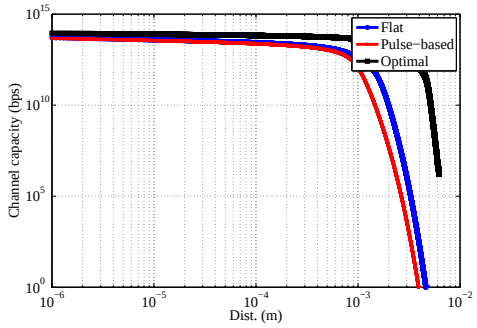

(b) skin

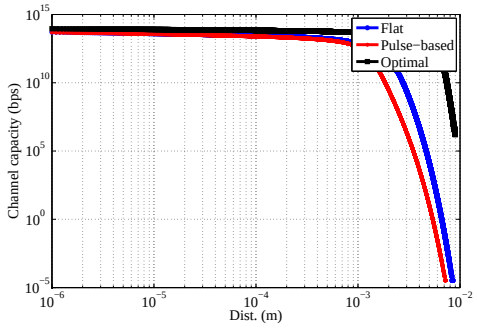

(c) fat

Figure 4.5: Capacity for different tissues with different power allocations

4.4 Numerical Models and the Corresponding Results

In the previous section, the theoretical model of path loss was proposed where a new term, absorption path loss, was introduced. In this section, a validation through simulation would be conducted and then the layered model would be built to investigate the wave propagation at THz band.

4.4.1 Homogeneous Model

A simple model, shown in Fig. 4.6, is set up in CST Microwave Studio [24] to obtain the path loss due to the absorption of the human tissues [25]. As generally known, the magnitude of the electric field of the plane wave does not vary when propagating in free space but attenuates propagating in the lossy material, thus the plane wave propagating in the tissue is studied to obtain the absorption path loss. As shown in the Fig. 4.6, a dielectric cube, at the level of mm^3, is built first. This assumption is valid considering the THz range wavelength in comparison to the examined tissue size ($7mm \times 7mm \times 7mm$). By aligning the dielectric constants to the cube, the homogeneous human tissue can be modelling, which can be obtained from Fig. 4.1b and 4.1c and shown in table 4.1, calculated from the optical parameters in [11], [12] by Eq. 4.4.

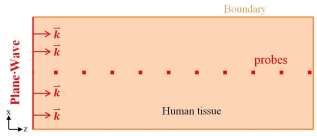

(a) 2D Cross-Section of the simplified model of the propagation of the plane wave in human tissues

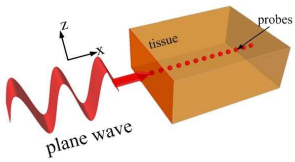

(b) 3-D Schematics of the simplified model of the propagation of the plane wave in human tissues

Figure 4.6: Schematics of the simplified model of the propagation of the plane wave in human tissues

As shown in the figure, several probes have been equally spaced in order to monitor the variation of the E-field with the distance from the source. A PML (Perfect

Tissues	Blood	Skin	Fat
ϵ'	3.5781	2.9240	2.2130
ϵ''	2.0109	0.9085	0.5732

Table 4.1: The Dielectric parameters of blood, skin and fat at 1 THz

Matched Layer) has been considered as the boundary condition in the direction of propagation and the periodic conditions in other directions. A plane wave has been defined as the propagating wave travelling in the direction of +z while E-field is pointing to +x.

Eq. 4.7 is used to calculate the absorption path loss and the comparison of the analytical and numerical results with the corresponding difference are demonstrated in Fig. 4.7. It can be easily observed that the results agree well, indicating the reliability of the numerical model thus paving the road to the further study of the THz wave for body-centric nano-communication.

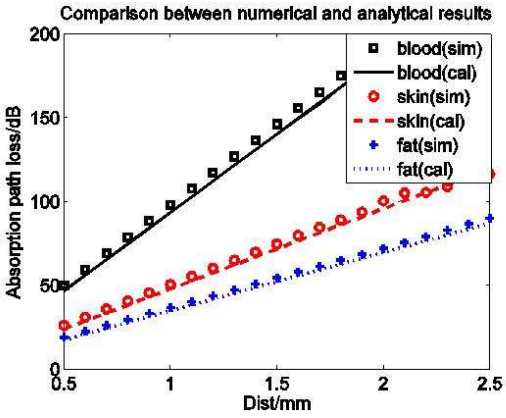

Figure 4.7: Absorption path loss vs. distance at 1 THz for different human tissues

4.4.2 Layered Model

To investigate the effect of the layered structures, the model shown in Fig. 4.8 is numerically simulated in CST Microwave Studio. It can be seen that a traditional 3-layered human model is built - skin, fat and muscle, whose thickness are 1.5 mm, 5 mm and 1.9 mm, respectively - with the PML as the boundary. Two dipoles working at the band of $0.8THz \sim 1.2THz$ are allocated for two different scenarios: one dipole in skin with another one in fat (vertical simulation, shown in Fig. 4.8a); both dipoles in skin allocated along the direction of the interface (horizontal simulation, shown in

Fig. 4.8b). By changing the distance between two dipoles, the power loss, *i.e.*, S_{21} can be obtained. From Table 4.1 it can be seen that the permittivity of skin and fat are very close to each other in values in the frequency range of interest; therefore the power loss caused by the interface is minimum. The comparison between the simulated power loss (vertical simulation and horizontal simulation) and calculated path loss is shown in Fig. 4.9, from which it can be easily concluded that the effect of the layered structure on power loss is quite limited.

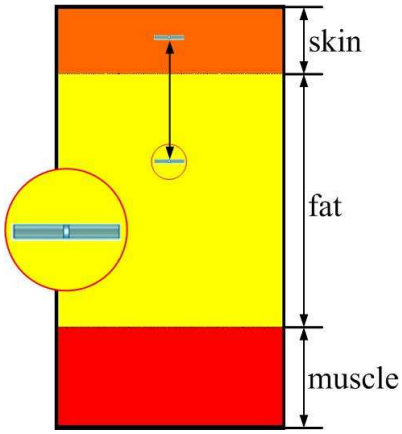

(a) 2D Displany of planar layered model of human body with dipole aligned vertically

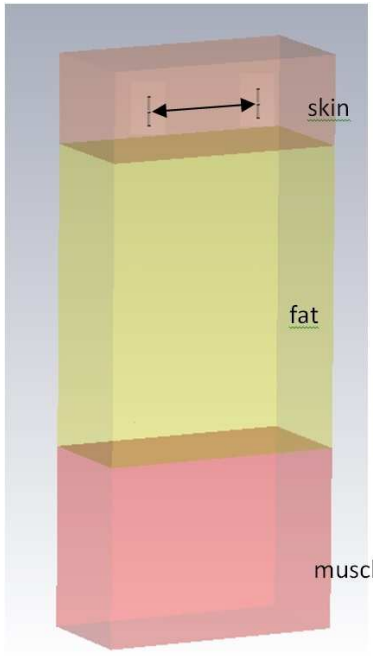

(b) 3-D Display of planar layered model of human body with dipoles aligned horizontally

Figure 4.8: Planar layered models of human body with dipoles aligned in

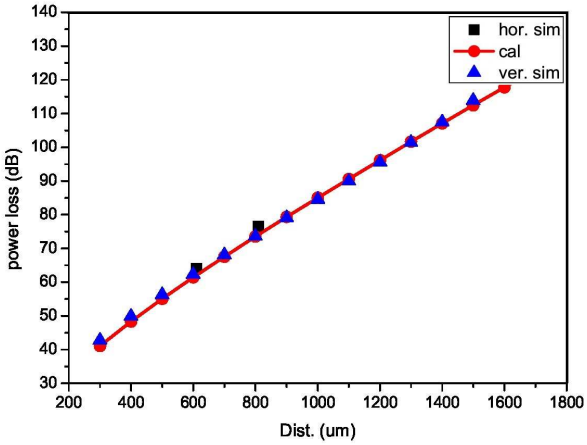

Figure 4.9: Comparison of the calculated power loss with the simulated one of different dipole allocation for the layered structure (hor. sim. is the short form of horizontal simulation; ver. sim. is the short for vertical simulation; cal. means the results calculated from theory)

4.5 Summary

In this chapter, a new channel model was proposed to compute the path loss and noise at THz band. Then, the corresponding channel capacity was investigated by discussing the effect of different tissues and power allocation schemes. The results showed that THz band channel was strongly dependent on both the type of the medium and the distance where the concentration of water had a lot of influence because it not only caused attenuation to the THz wave but also introduced non-white noise. In the very short distance, i.e., at the distance of millimeters, the capacity can reach as high as 100 Terabits per second ($Tbps$) depending on the environment and exciting pulse types. And in the end of the chapter, two 3-D numerical models of THz nano-communication channel have been applied for in-body scenarios and validated by the analytical model. In summary, the proposed models pave the way to the further studies considering more body structures and tissue properties.

References

[1] S. Luryi, J. Xu, and A. Zaslavsky, *Future Trends in Microelectronics: Frontiers and Innovations*. John Wiley & Sons, 2013.

[2] M. Dragoman, A. Muller, D. Dragoman, F. Coccetti, and R. Plana, "Terahertz antenna based on graphene," *Journal of Applied Physics*, vol. 107, no. 10, p. 104313, 2010.

[3] I. Llatser, C. Kremers, A. Cabellos-Aparicio, J. M. Jornet, E. Alarcón, and D. N. Chigrin, "Graphene-based nano-patch antenna for terahertz radiation," *Photonics and Nanostructures-Fundamentals and Applications*, vol. 10, no. 4, pp. 353–358, 2012.

[4] P. S. Hall and Y. Hao, *Antennas and Propagation for Body-Centric Wireless Communication*. Artech House, 2012.

[5] A. Alomainy, Y. Hao, A. Owadally, C. G. Parini, Y. Nechayev, C. C. Constantinou, and P. S. Hall, "Statistical analysis and performance evaluation for on-body radio propagation with microstrip patch antennas," *Antennas and Propagation, IEEE Transactions on*, vol. 55, no. 1, pp. 245–248, 2007.

[6] D. Kurup, W. Joseph, G. Vermeeren, and L. Martens, "In-body path loss model for homogeneous human tissues," *Electromagnetic Compatibility, IEEE Transactions on*, vol. 54, no. 3, pp. 556–564, 2012.

[7] Q. H. Abbasi, A. Sani, A. Alomainy, and Y. Hao, "Numerical characterization and modeling of subject-specific ultrawideband body-centric radio channels and systems for healthcare applications," *Information Technology in Biomedicine, IEEE Transactions on*, vol. 16, no. 2, pp. 221–227, 2012.

[8] A. Brizzi, A. Pellegrini, L. Zhang, and Y. Hao, "Statistical path-loss model for on-body communications at 94 ghz," *Antennas and Propagation, IEEE Transactions on*, vol. 61, no. 11, pp. 5744–5753, 2013.

[9] Y. Choi, J.-W. Choi, and J. M. Cioffi, "A geometric-statistic channel model for thz indoor communications," *Journal of Infrared, Millimeter, and Terahertz Waves*, vol. 34, no. 7-8, pp. 456–467, 2013.

[10] R. Piesiewicz, M. Jacob, M. Koch, J. Schoebel, and T. Kürner, "Performance analysis of future multigigabit wireless communication systems at thz frequencies with highly directive antennas in realistic indoor environments," *Selected Topics in Quantum Electronics, IEEE Journal of*, vol. 14, no. 2, pp. 421–430, 2008.

[11] A. Fitzgerald, E. Berry, N. Zinov'ev, S. Homer-Vanniasinkam, R. Miles, J. Chamberlain, and M. Smith, "Catalogue of human tissue optical properties at terahertz frequencies," *Journal of Biological Physics*, vol. 29, no. 2-3, pp. 123–128, 2003.

[12] E. Berry, A. J. Fitzgerald, N. N. Zinov'ev, G. C. Walker, S. Homer-Vanniasinkam, C. D. Sudworth, R. E. Miles, J. M. Chamberlain, and M. A. Smith, "Optical properties of tissue measured using terahertz-pulsed imaging," in *Medical Imaging 2003*. International Society for Optics and Photonics, 2003, pp. 459–470.

[13] I. F. Akyildiz and J. M. Jornet, "Electromagnetic wireless nanosensor networks," *Nano Communication Networks*, vol. 1, no. 1, pp. 3–19, 2010.

[14] J. M. Jornet and I. F. Akyildiz, "Channel modeling and capacity analysis for electromagnetic wireless nanonetworks in the terahertz band," *Wireless Communications, IEEE Transactions on*, vol. 10, no. 10, pp. 3211–3221, 2011.

[15] J. M. Jornet, J. C. Pujol, and J. S. Pareta, "Phlame: A physical layer aware mac protocol for electromagnetic nanonetworks in the terahertz band," *Nano Communication Networks*, vol. 3, no. 1, pp. 74–81, 2012.

[16] C. S. Joseph, A. N. Yaroslavsky, V. A. Neel, T. M. Goyette, and R. H. Giles, "Continuous wave terahertz transmission imaging of nonmelanoma skin cancers," *Lasers in Surgery and Medicine*, vol. 43, no. 6, pp. 457–462, 2011.

[17] E. Jung, H. Park, K. Moon, M. Lim, Y. Do, H. Han, H. J. Choi, B.-H. Min, S. Kim, I. Park *et al.*, "Thz time-domain spectroscopic imaging of human articular cartilage," *Journal of Infrared, Millimeter, and Terahertz Waves*, vol. 33, no. 6, pp. 593–598, 2012.

[18] G. J. Wilmink and J. E. Grundt, "Invited review article: current state of research on biological effects of terahertz radiation," *Journal of Infrared, Millimeter, and Terahertz Waves*, vol. 32, no. 10, pp. 1074–1122, 2011.
[19] M. Pierobon and I. F. Akyildiz, "A physical end-to-end model for molecular communication in nanonetworks," *Selected Areas in Communications, IEEE Journal on*, vol. 28, no. 4, pp. 602–611, 2010.
[20] S. Bush, J. Paluh, G. Piro, V. Rao, V. Prasad, and A. Eckford, "Defining communication at the bottom," *Molecular, Biological and Multi-Scale Communications, IEEE Transactions on*, vol. PP, no. 99, pp. 1–1, 2015.
[21] F. Box, "Utilization of atmospheric transmission losses for interference-resistant communications," *Communications, IEEE Transactions on*, vol. 34, no. 10, pp. 1009–1015, 1986.
[22] A. N. Pal and A. Ghosh, "Ultralow noise field-effect transistor from multilayer graphene," *Applied Physics Letters*, vol. 95, no. 8, p. 082105, 2009.
[23] A. Goldsmith, *Wireless Communication*. Cambridge University Press, 2005.
[24] C. M. Studio, "Cst microwave studio." [Online]. Available: https://www.cst.com
[25] K. Yang, A. Pellegrini, A. Brizzi, A. Alomainy, and Y. Hao, "Numerical analysis of the communication channel path loss at the thz band inside the fat tissue," in *Microwave Workshop Series on RF and Wireless Technologies for Biomedical and Healthcare Applications (IMWS-BIO), 2013 IEEE MTT-S International*. IEEE, 2013, pp. 1–3.

Chapter 5

Effects of Non-Flat Interfaces in Human Skin Tissues on the In-Vivo THz Communication Channel

Following the work of Chapter 4, a numerical computational studies would be conducted in this chapter to investigate the quality of the radio communication of nano-networks depending on the skin structure, where layered models of the human skin of various geometries in the scale of the THz wavelengths was considered. Additionally, the effects of the sweat duct would be considered and investigated.

5.1 Motivation and Related Work

The channel model of THz wave in human tissues has been investigated in Chapter 4, but to analyse the wave propagation in the human body, more accurate and finer model should be considered instead of the homogeneous one. In this chapter, detailed skin models would be introduced to observe the wave propagation and EM interaction with the finer skin structures.

According to the current researches, there are three main models to describe the skin structure: 1) 3 layered model; 2) 2 layered model and 3) model with detailed parts. For the 3-layer models, the skin is divided into 3 layers: stratum corneum layer (SC), epidermis and dermis layer (E-D) and subcutaneous fat layer (SCF)[1, 2]. In 2 layered models, the skin is modelled as the combination of epidermis and dermis [3, 4]. On the basis of these models, more sophisticated models with detailed parts are introduced to further study the skin performance [5, 6]. Furthermore, the helical sweat duct structure was inserted into the epidermis layer of a 3-layered stratified model to study its effects on electromagnetic (EM) reflection spectrum of skin in the frequency range of 100 GHz to 450 GHz [6]. The results have shown that the morphological features of the skin and the structure of the sweat ducts play an important role in the reflectance spectrum. It also pointed out that at the higher frequencies the roughness of the boundary should be incorporated into the model due to the same order of the magnitude of the wavelength and the roughness but the detailed studies were not considered. From the 3-D cross-sectional images depicting the different layers of the skin [7] [8], it can be seen that the interface between the layers was not flat and the roughness between the different layers of the skin was at the order of millimetre which was considerable to the wavelength of the applied THz band (300 GHz to 10 THz [9]) of Nano-Communication Network [6]; thus, it is evident that more detailed models of skin are required in order to understand the effects on EM wave propagation, which is the main concern of this chapter.

5.2 Applied Numerical Skin Models

5.2.1 Human Skin Structure

The skin is a complex heterogeneous and anisotropic medium, where the small parts, like blood vessel and pigment content, are spatially distributed in depth [10] [11], as shown in Fig. 5.1. Human skin can be generally divided into three main visible layers from the surface: the epidermis ($\sim$ 100 μm, blood-free layer), the dermis ($\sim$ 1 - 4 mm, vascularized layer) and the subcutaneous fat (from 1 to 6 mm dependent on the location) as shown in Fig. 5.1 [12]. The epidermis contains two sub-layers: stratum corneum with only dead quamous cells and the living epidermis layer, where

most of the skin pigmentation stay. The stratum corneum is a thin, stratified and highly specialized layer which is accumulated on the outermost skin surface. The dermis, supporting the epidermis, is thicker and mainly composed of collagen fibres and intertwined elastic fibres enmeshed in a gel-like matrix. The subcutaneous fat layer is composed of the packed cells with considerable fat, where the boundary is not well demarcated; thus the thickness of this layer varies widely for different part of human body [13].

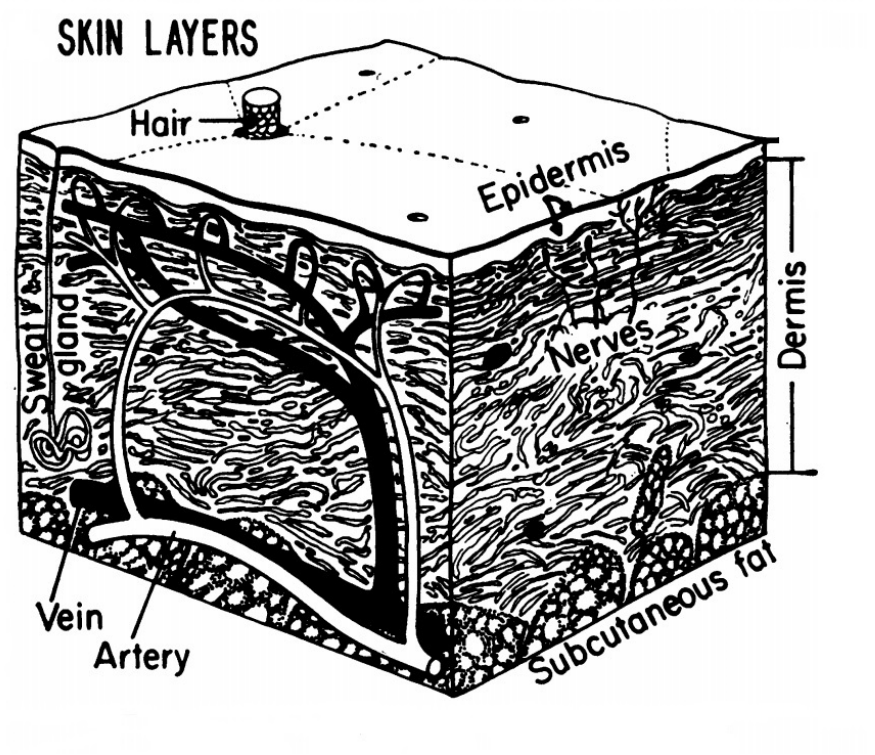

Figure 5.1: General 3-layer skin model [14]

5.2.2 Numerical Skin Models

Models with Rough Boundary

From the skin model shown in Fig. 5.1 [15], it can be observed that the interface between the layers is non-flat [6], and the dermal ridges prolong and penetrate into the epidermis. In this paper, the influence of rough interface between these two layers was studied, making the model more physiologically plausible. CST Microwave

Studio^{TM} software package using Finite Integration Technique was selected to simulate the propagation and interaction of THz wave in the three-dimensional (3-D) numerical model of skin, shown in Fig. 5.2 where the interfaces between the epidermis and dermis are 3-D sine and 3-D sinc wave, respectively. A cube, L μm wide and H μm high was built to model the skin cube, including a h_{epi} μm upper layer as the epedermis and a h_{derm} μm layer as the dermis. The bisected cross-section of both models are shown in Fig. 5.3 and the corresponding applied functions, depicting the 3-D surface were shown below:

$$z = \pm A cos(\frac{2\pi x}{S}) cos(\frac{2\pi y}{S}) \tag{5.1}$$

where, A and S are short for amplitude and span, respectively; "$+$" stands for the peak scenario while "$-$" refers to the valley case (in Fig. 5.3a, "$-$" is chosen).

$$z = \begin{cases} \pm A \frac{sin(\sqrt{(x-nS)^2+(y-nS)^2})}{\sqrt{(x-nS)^2+(y-nS)^2}}, & \text{when } -(2n-1)S/2 \leq x, y \leq (2n+1)S/2; \\ 0, & \text{else.} \end{cases} \tag{5.2}$$

where, A represents the amplitude of the sinc function while S is the span of sinc function shown in Fig. 5.3b; $n = L/S$ is the ratio of skin cube length to sinc functin span; "$+$" stands for the peak scenario while "$-$" refers to the valley case (Fig. 5.3b shows the case of "$+$").

The parameters of the two models in Fig. 5.2 are summarised in Table 5.1.[a]

model	Sine	Sinc
H	2105	1600
L	2100	2100
h_{epi}	$[405-105]$	$[40-240]$
h_{derm}	$[1000-1700]$	$[1260-1460]$

Table 5.1: Different parameters of simulated models using sine and sinc functions as the interface (unit: μm)

Two dipoles are also modelled as the nano-antennas, working at THz band. One is placed on the skin surface while the other is located within the skin. Two discrete

[a]For sine model the amplitude of the surface A is 350 μm while for sinc model the amplitude of the surface A is 200 μm.

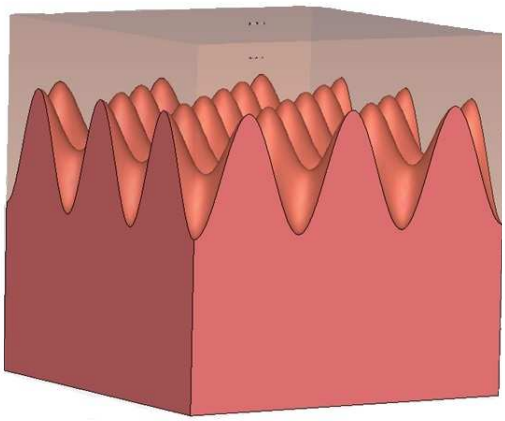

(a) Stratified skin model with 3D sine function as the interface

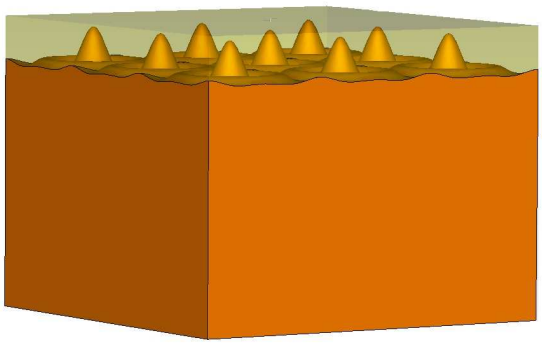

(b) Stratified skin model with 3D sinc function as the interface

Figure 5.2: Numerical models with different function interfaces, developed in CST Microwave Studio

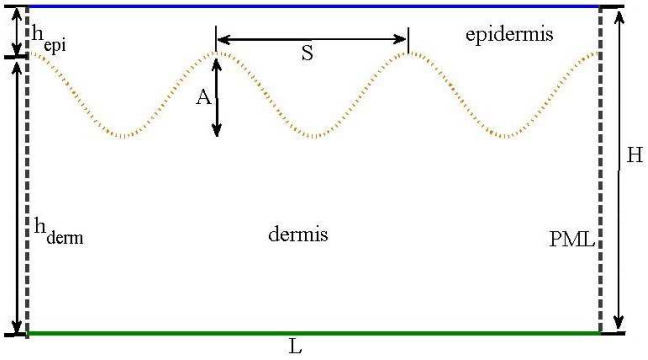

(a) Stratified skin model with 3D sine function as the interface in CST

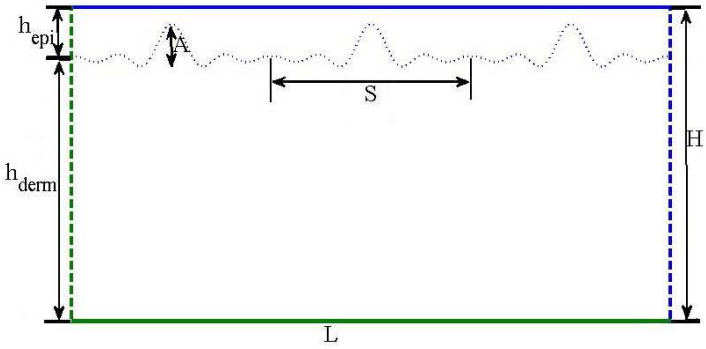

(b) Stratified skin model with 3D sinc function as the interface in CST

Figure 5.3: Cross section of the applied models in Fig. 5.2 (L is the cube length, H is the cube height, h_{epi} and h_{derm} is the thickness of epidermis and dermis, A is the amplitude of the surface while S is the span of the surface)

ports were applied to the dipoles and the tranmission coefficient, $S21$, was recorded to investigate the power loss. The dimensions of the dipoles are shown in Table 5.2, and they are optimised to ensure that the impedance matching is better than $-10\ dB$. The open boundary ,*i.e.*, Perfect Match Layer (PML) was applied to ensure that the reflections of the abruptly-cutting boundaries are neglectable. The nano-second long Gaussian pulse is applied in the Time-Domain simulation while hexahedral mesh type was applied. The permittivities applied to the different parts of skin are shown in Fig. 5.4 [16].

	dipole on the skin surface	dipole in the skin
arm length (μm)	43	36
radius (μm)	5	5

Table 5.2: Parameters of the dipole antennas used as transmit and receive elements for the EM propagation power loss study across and within the human skin tissue models

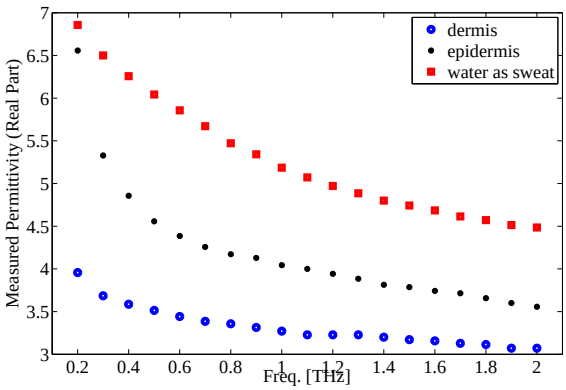

(a) Real part of the relative permittivity

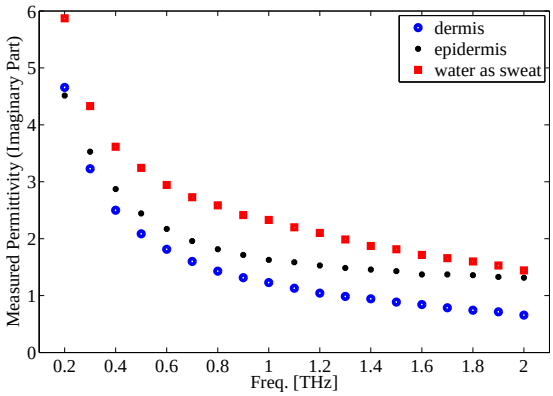

(b) Imaginary part of the relative permittivity

Figure 5.4: Permittivity of different skin layers and sweat at THz frequencies [16].

Skin Models with Sweat Ducts

For this part of the study, similar detailed skin model as shown in Fig. 5.2a was applied with the inclusion of sweat ducts, as shown in Fig. 5.5. The sweat duct is 265 μm in height and 40 μm in diameter. It includes three turns to be considered as a helical antenna (For helical antenna number of turns should be at least 3.). Only when the sweat duct contains sweat, containing 99% water and 1% salt and amino acid [17], it can be regarded as a conductor; and hence the permittivity of water at THz band was used to model sweat duct, as shown in Fig. 5.4.

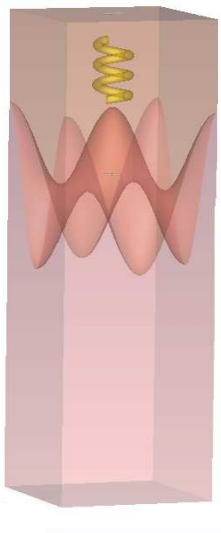

Figure 5.5: Numerical model of skin while including sweat ducts.

5.3 Analysis of Skin-Internal Non-flat Interfaces on the THz EM Channel

5.3.1 Effects of Different Shapes

Since the shape of the interface is determined by amplitude A and span S, to simplified the case one of these two variables is fixed and the other changed with equal difference. Four scenarios were investigated with model parameters as shown in Table 5.3.

The power loss for individual cases were recorded. Take the sine model as an example, the line array records are illustrated in Fig. 5.6. Based on the recorded power

Sine Model		Sinc Model	
S = 700	A=350	S = 700	A = 200
A	S	A	S
175	350	100	300
245	560	120	400
350	700	140	500
420	910	160	600
525	1050	180	700
		200	

Table 5.3: Amplitude and span change for the different interface models (unit: μm)

losses, the mean values and deviations of the power losses for each case are calculated with Matlab (as shown in Fig. 5.7). The obtained power losses for different distance are then compared with the power losses obtained from the common flat one and the homogeneous models, shown in Fig. 5.7. It can be seen that all values decrease due to the distance increment. The power loss of the flat model and the mean values of stratified models with 3-D sine and sinc surfaces are close to each other, pointing out that the influence of the rough interface could be neglected, when the general study is being conducted. Additionally, the deviation of the stratified model with 3-D sine interface is greater than the one with sinc interface. The biggest difference is around 2 dB and they both increases with the increasing distance. By comparing the results shown in Fig. 5.7a and Fig. 5.7b, it can be concluded that the span variation would cause more changes to the power loss because of its larger deviations, reaching around 10 dB (sine model) and 5 dB (sinc model) at the distance of 600 μm, respectively, while the deviation of the amplitude is always less than 1 dB.

5.3.2 Effects of the Antenna Location

The impact of the location of the antennas are also studied. In one of the scenarios, both antennas are placed along the line going through the peak of the 3-D wave as shown in Fig. 5.8a while another going through valley of the wave as shown in Fig. 5.9a. The field distribution for both cases of the sine model are shown in Fig. 5.8 and 5.9. It can be easily seen that the applied PML boundary has no effect to the performance of the antenna and the interface between the epidermis and dermis barely affect the wave propagation. The results shown in Fig. 5.10 agree well indicating

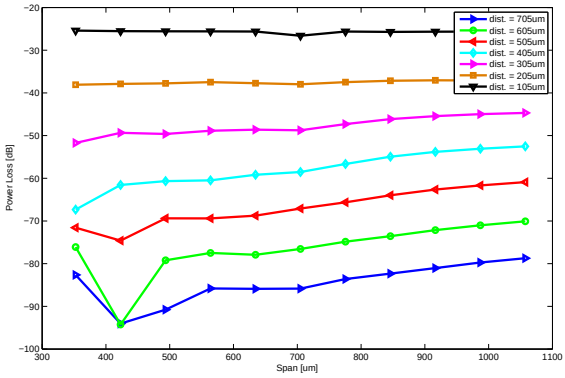

(a) Power loss of different span values when A is set to 350 μm

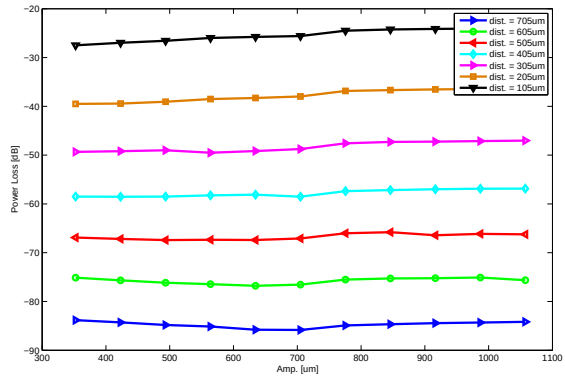

(b) Power loss of different amplitude values when S is set to 700 μm

Figure 5.6: Effects of parameter changes on power loss for sine-wave model listed in Table 5.3

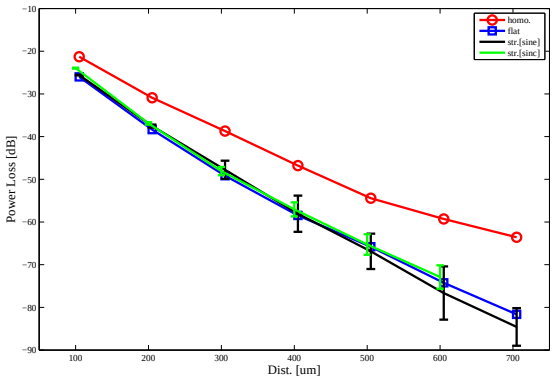

(a) Influence of span change on power loss

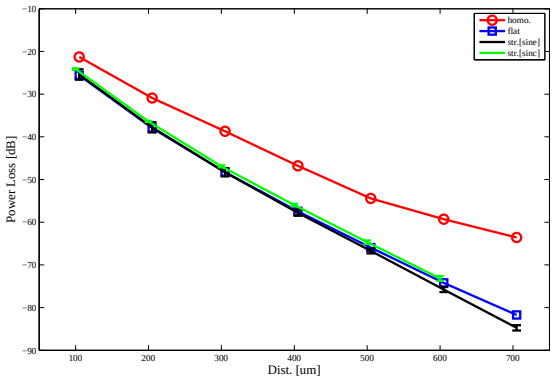

(b) Influence of amplitude change on power loss

Figure 5.7: Dependance of the power loss on the distance for different models

that the effect of the antenna location can be ignored, when the antennas are located above/below the peak/valley boundary for the 3-D sine model. However, when the span and amplitude values go beyond 300 μm, the difference between the power losses is noticeable with a 5 dB difference at 600 μm (as shown in Fig. 5.11). The power loss for the scenario that two dipoles locates above/below the peak is larger for the one with the valley scenario because for the peak scenario the second antenna would be in the dermis most of the time.

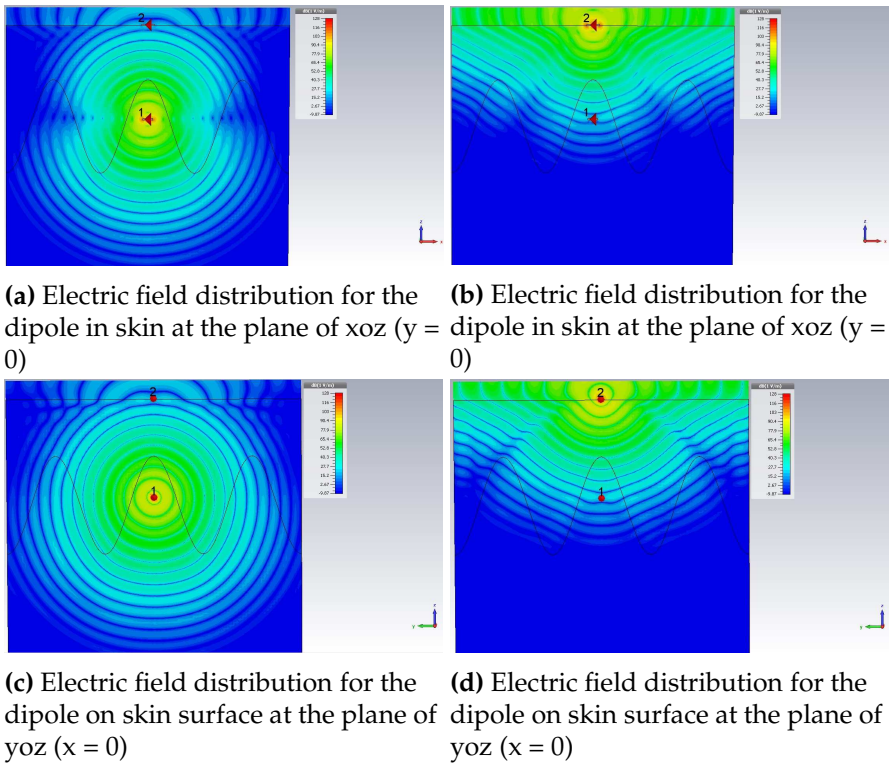

(a) Electric field distribution for the dipole in skin at the plane of xoz (y = 0)

(b) Electric field distribution for the dipole in skin at the plane of xoz (y = 0)

(c) Electric field distribution for the dipole on skin surface at the plane of yoz (x = 0)

(d) Electric field distribution for the dipole on skin surface at the plane of yoz (x = 0)

Figure 5.8: Electric field distribution of the dipoles at 1 THz for the peak scenario of the sine wave model

5.3.3 Effects of the Sweat Duct

The effects of the sweat duct for the sine wave model was investigated, shown in Fig. 5.12. It is observed that with the increase of the distance the power loss increases, as predicted. When PEC was applied to the sweat duct to make it as the ideal conductor, the power loss is 5 dB less than the case of water applied to the sweat duct, which shares similar power loss with the model without sweat duct. This indicates that if sweat duct is working as PEC, the power loss would be reduced; however, in most

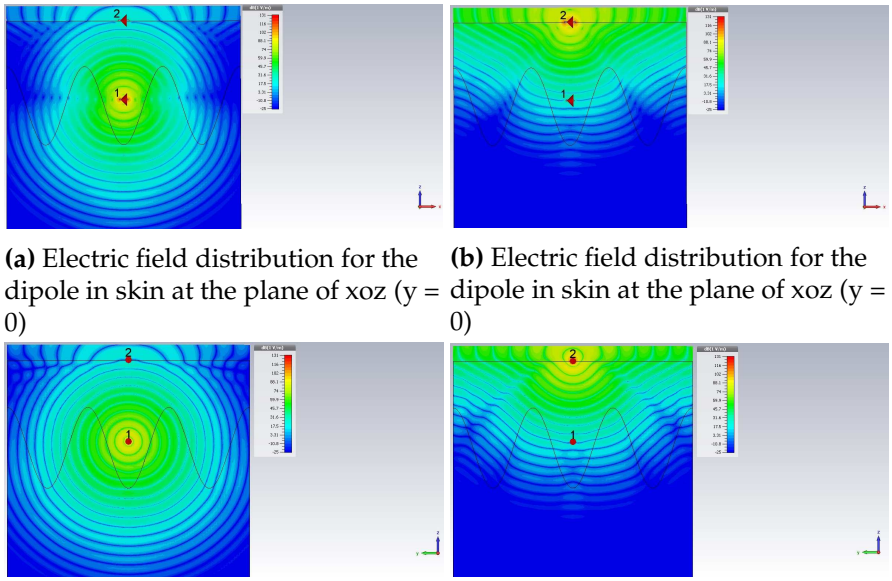

(a) Electric field distribution for the dipole in skin at the plane of xoz (y = 0)

(b) Electric field distribution for the dipole in skin at the plane of xoz (y = 0)

(c) Electric field distribution for the dipole on skin surface at the plane of yoz (x = 0)

(d) Electric field distribution for the dipole on skin surface at the plane of yoz (x = 0)

Figure 5.9: Electric field distribution of the dipoles at 1 THz for the valley scenario of the sine wave model

cases, the sweat duct is full of sweat containing 99% water, which has limited influence on the overall communication link quality. Analysis clearly shows the importance of the study of the parameters of the human tissue, especially at THz band.

5.4 Summary

In this chapter a new model with a 3-D sinc interface was first proposed to increase the randomness of the model while the mean and deviation of the power loss for all models are compared with the common flat model. The results show that the power loss is around -80 dB at 700 μm. Although there are no systems with the dynamic range more than 80 dB nowadays, we would like to highlight that for nano-networks the 700 μm range is considered large specifically with the cooperative and dense nano-sensor networks predicted to be used for the applications described in the introduction. Additionally, the influence of the antenna location was studied, which shows that the influence of the model with sine wave interface is negligible; however, the antenna location would cause some changes when the sinc wave interface was applied where the difference can go up to 4 dB with distance of 600 μm between the transmitting

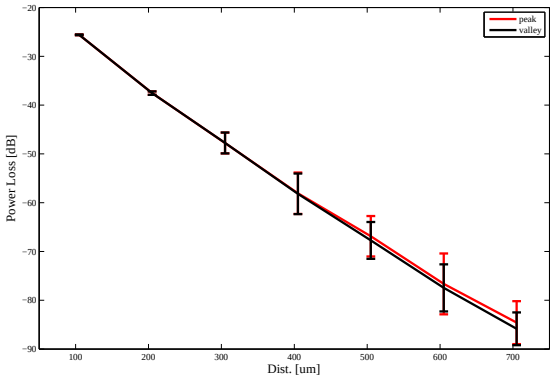

(a) Effects of span alteration on the power loss with respect to distance.

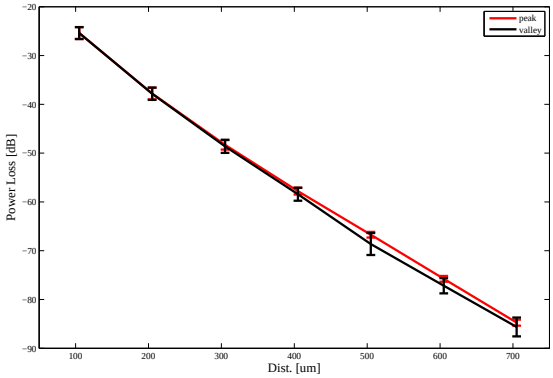

(b) Effects of amplitude alteration on the power loss with respect to distance.

Figure 5.10: Comparison between the two Scenarios: two dipoles located above/beneath the peak and valley of the interface for the model with 3-D sine function as the interface.

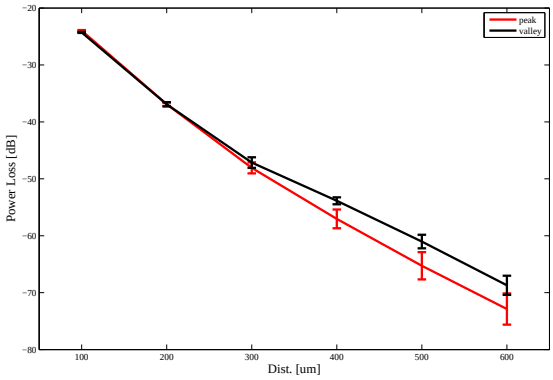

(a) Effects of span alteration on the power loss with respect to distance.

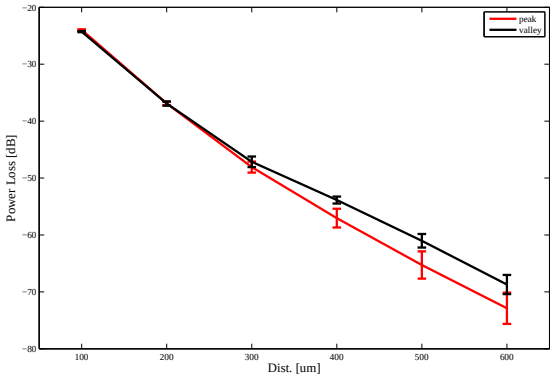

(b) Effects of amplitude alteration on the power loss with respect to distance.

Figure 5.11: Comparison between the two Senarios: two dipoles located above/beneath the peak and valley of the interface for the model with 3-D sinc function as the interface.

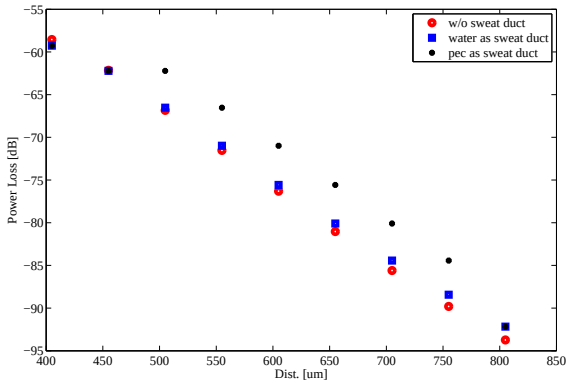

Figure 5.12: Power loss at 1 THz for three scenario: a) without the sweat duct in epidermis; b) water is considered as the sweat in sweat duct; c) the sweat duct is considered as PEC

and receiving antennas. Finally, the effects of the sweat duct were investigated by applying two different materials (PEC and water) and compared to the case without the sweat duct presence. Result shows that when PEC is considered as a material for sweat duct, the power loss reduction is around 5 dB, while the power loss is negligible, when water is considered as a material for sweat duct at THz band.

References

[1] R. Aminzadeh, M. Saviz, and A. A. Shishegar, "Dielectric properties estimation of normal and malignant skin tissues at millimeter-wave frequencies using effective medium theory," in *Electrical Engineering (ICEE), 2014 22nd Iranian Conference on*. IEEE, 2014, pp. 1657–1661.

[2] S. Huclova, J. Frohlich, L. Falco, F. Dewarrat, M. S. Talary, and R. Vahldieck, "Validation of human skin models in the mhz region," in *Engineering in Medicine and Biology Society, 2009. EMBC 2009. Annual International Conference of the IEEE*. IEEE, 2009, pp. 4461–4464.

[3] K. H. Chan, S. W. Leung, Y. L. Diao, Y. M. Siu, and K. T. Ng, "Analysis of millimeter wave radiation to human body using inhomogeneous multilayer skin model," in *Electromagnetic Compatibility (APEMC), 2012 Asia-Pacific Symposium on*. IEEE, 2012, pp. 721–724.

[4] C. So-Ling and L. Li, "A multi-layered reflection model of natural human skin," in *Computer Graphics International 2001. Proceedings*. IEEE, 2001, pp. 249–256.

[5] H. Nugroho, A. F. M. Hani, R. Jolivot, and F. Marzani, "Melanin type and concentration determination using inverse model," in *National Postgraduate Conference (NPC), 2011*. IEEE, 2011, pp. 1–7.

[6] I. Hayut, A. Puzenko, P. Ben Ishai, A. Polsman, A. J. Agranat, and Y. Feldman, "The helical structure of sweat ducts: Their influence on the electromagnetic reflection spectrum of the skin," *Terahertz Science and Technology, IEEE Transactions on*, vol. 3, no. 2, pp. 207–215, 2013.

[7] P.-L. Hsiung, Y. Chen, T. Ko, J. Fujimoto, C. de Matos, S. Popov, J. Taylor, and V. Gapontsev, "Optical coherence tomography using a continuous-wave, high-power, raman continuum light source," *Optics express*, vol. 12, no. 22, pp. 5287–5295, 2004.

[8] P. Cimalla, J. Walther, M. Mehner, M. Cuevas, and E. Koch, "Simultaneous dual-band optical coherence tomography in the spectral domain for high resolution in vivo imaging," *Optics express*, vol. 17, no. 22, pp. 19 486–19 500, 2009.

[9] I. F. Akyildiz, F. Brunetti, and C. Blázquez, "Nanonetworks: A new communication paradigm," *Computer Networks*, vol. 52, no. 12, pp. 2260–2279, 2008.

[10] W. Montagna, *The Structure and Function of Skin 3E*. Elsevier, 2012.

[11] G. F. Odland, "Structure of the skin," *Physiology, biochemistry, and molecular biology of the skin*, vol. 1, pp. 3–62, 1991.

[12] A. Bashkatov, E. Genina, V. Kochubey, and V. Tuchin, "Optical properties of human skin, subcutaneous and mucous tissues in the wavelength range from 400 to 2000 nm," *Journal of Physics D: Applied Physics*, vol. 38, no. 15, p. 2543, 2005.

[13] Q. H. Abbasi, A. Sani, A. Alomainy, and Y. Hao, "Numerical characterization and modeling of subject-specific ultrawideband body-centric radio channels and systems for healthcare applications," *Information Technology in Biomedicine, IEEE Transactions on*, vol. 16, no. 2, pp. 221–227, 2012.

[14] R. F. Rushmer, K. J. Buettner, J. M. Short, and G. F. Odland, "The skin," *Science*, vol. 154, no. 3747, pp. 343–348, 1966.

[15] A. Knu, S. Bonev, W. Knaak *et al.*, "New method for evaluation of in vivo scattering and refractive index properties obtained with optical coherence tomography," *Journal of biomedical optics*, vol. 9, no. 2, pp. 265–273, 2004.

[16] K. Yaws, D. Mixon, and W. Roach, "Electromagnetic properties of tissue in the optical region," in *Biomedical Optics (BiOS) 2007*. International Society for Optics and Photonics, 2007, pp. 643 507–643 507.

[17] G. Shafirstein and E. G. Moros, "Modelling millimetre wave propagation and absorption in a high resolution skin model: the effect of sweat glands," *Physics in medicine and biology*, vol. 56, no. 5, p. 1329, 2011.

Chapter 6

Characteristics and Modelling of Electromagnetic Parameters of Human Skin at THz band

During the study of the channel performance of THz wave for nano communication, it is found that there is a lack of the data-base of EM parameters of human tissues. In this chapter, the collagen, main constitute of skin has been cultivated and measured to obtain the optical/electromagnetic parameters at the THz band of interest. Then, a double Debye model would be investigated, followed by the validation of the theoretical model produced in previous chapters.

6.1 Motivation and Related Work

From the previous discussion, it can be easily seen that the papers on EM/Optical parameters of human tissues are quite limited in the THz band of interest [1–3]. Pulse THz spectroscopy was first used to measure the absorbtance of DNA, bovine serum albumin and collagen at the band of 0.06 to 2.0 THz [4], showing that the absorption

would increase with hydration and denaturing. Later, animal tissues, such as pork skin, pork fat and rat skin, were measured to study the power absorption and far-infrared signal transmission at THz band [5]. Because the performance of the cancer is different from the healthy tissue at THz band, more and more studies are conducted on the characterisation of the human tissues at these bands. The healthy liver and liver cancer were studied to indicate the possibility of the application of THz Fiber-scanning Near-Field Imaging technology to diagnose the cancer [6]. Recently, spectroscopy measurements of normal and cancer breast tissue in the range of 0.1 to 4 THz were conducted by Tyler Bowman and *et. al.* [7], demonstrating the potential of THz spectroscopy for the recognisation of the cancer cell while the dielectric model of human breast tissue in THz band was built by A.J. Fitzgerald [8], where the average complex permittivity of health tumour, healthy fibrous breast tissue and healthy fat breast tissue from [9] were compared. However, most of the researches are still restricted to KHz or GHz of range [10–13] because the biological material in this range is believed to have little scattering and the radiation is readily absorbed and transmitted through depending on the size and inherent properties of the material [14] and the study of the tissue parameters at THz band is at its early phase. To enrich the database of the parameters for biological tissues at THz band, the human tissue samples cultivated in Blizard Institute would be measured with the THz Time Domain Spectroscopy (THz-TDS) system at Queen Mary University of London [a].In this chapter, the skin tissue, especially collagen, the main constitute of epidermis, would be the main focus to investigate if it is enough to use the parameters of collagen as the epidermis at the band of interest by studying both dielectric constants.

6.2 Principles of the Measurement

6.2.1 THz-TDS System Set-up

To obtain information of complex refractive index of measured samples because of the nature of THz, Grischkowsky and his co-workers introduced the first THz-TDS [15]. Although current THz-TDS systems are more advanced in the aspect of techniques such as scanning time, beam generation, detection methods and *etc.*, the fundamental

[a]Ethics Number: East London & The City REC Alpha 09/H0704/69

principle of operation remains. A schematic illustration of the set-up of a THz-TDS in transmission mode is shown in Fig. 6.1. The pulsed titanium-Sapphire laser produces femto-second pulses, which are then redirected into two separate optical paths by a beam-splitter. One beam becomes the receiver pulse (a measurement using the receiver is possible only when a femto-second pulse is incident on the receiver), while the other is used to excite THz wave at the emitter. Parabolic mirrors are used to focus and collimate the THz pulses travelling through the sample and onto the detector. The detector only conducts when it is struck by the femtosecond pulse from the detection beam line. When the detector is photo-excited, the THz pulses electric field causes an electric current to flow inside the detector. Using a time delay on the detector beam line to control the relative time delay between the THz pulse and when the detector can conduct, the electric field of the THz pulse can be plotted over time.

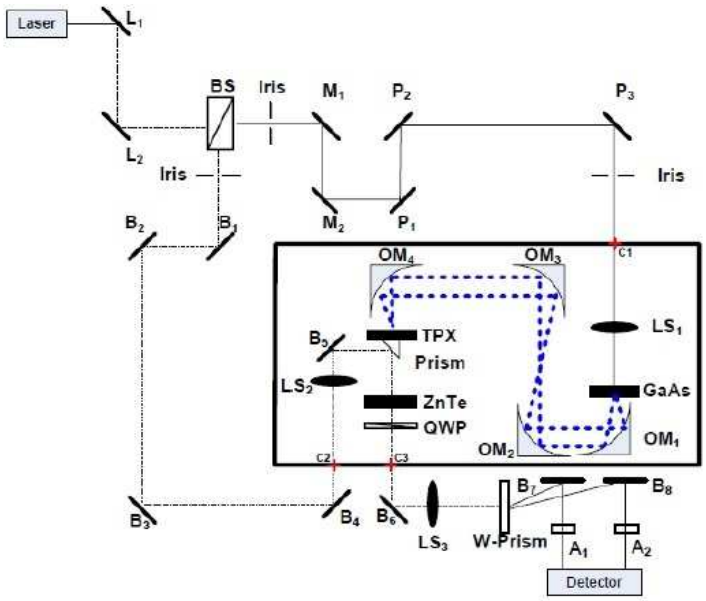

Figure 6.1: Schmatic diagram of a THz-TDS system operating in transmission mode

The photo of the THz-TDS installed at QMUL is shown in Fig. 6.2. The system shown here is operating in transmission mode. The main features and characteristics of this spectrometer are [16]:

- Typical operating frequency domain: $0.1 - 4.0\ THz$;
- Maximum dynamic range is $25 - 30\ dB$, SNR is normally around $25\ dB$;
- Motorized delay stage maximum travelling distance is $15\ cm$;

- Typical resolution is $14\,GHz$ (scan size $10.24\,mm$, step $10\,\mu m$); maximum achievable resolution is $1-2\,GHz$;

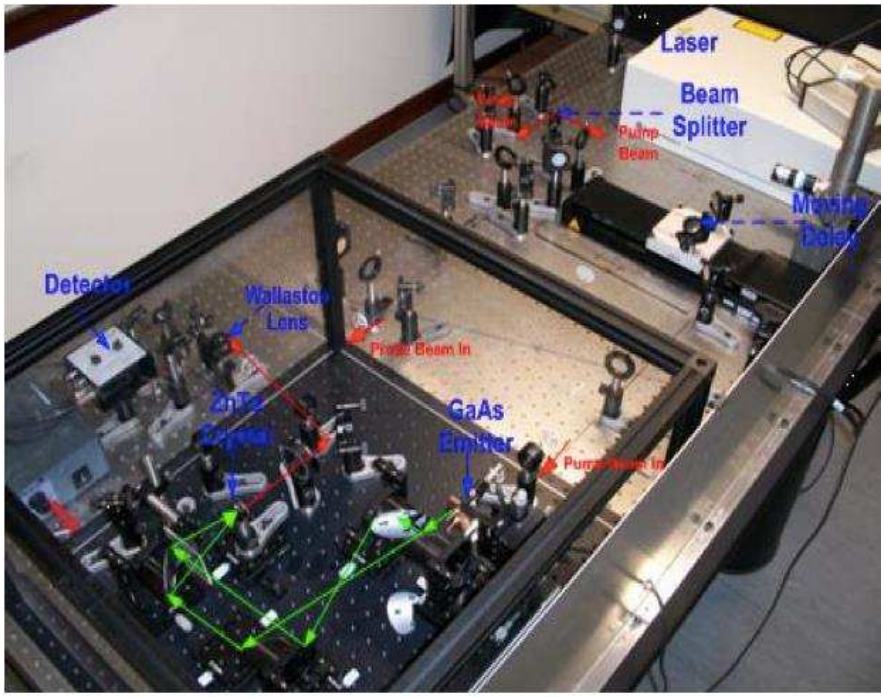

Figure 6.2: THz-TDS system in Queen Mary University of London [16]

The photo of the sample holder with the stand is shown in Fig. 6.3. It was made of poly-4-methyl pentene-1 (TPX) because of its non-dispersive characteristics at the band of interest that its absorption is very low, $\leq 1cm^{-1}$ and the refraction index is 1.46 over $0.1 \sim 4\,THz$.

6.2.2 Data-Processing [17, 18]

The original measurement data from the THz-TDS system were the received electric field $\vec{E}$. The complex spectra of air measured by TDS system is shown in Fig. 6.4.

Conventionally, the rate of the sample spectra to the reference one, which is served by the absence of the sample, usually the air, is used to calculate the complex refractive index $\tilde{n} = n - i\kappa$. Thus, the measured transfer function is:

$$\tilde{H}_{measure}(f) = \frac{\tilde{E}_{sam}(f)}{\tilde{E}_{ref}(f)} \tag{6.1}$$

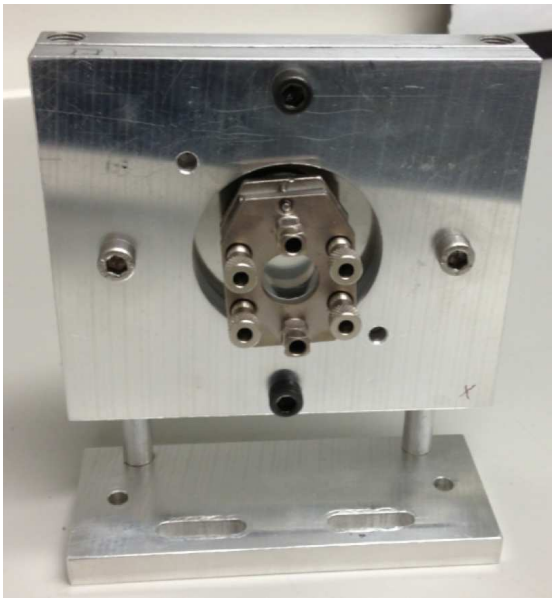

Figure 6.3: Sample holder with the stand

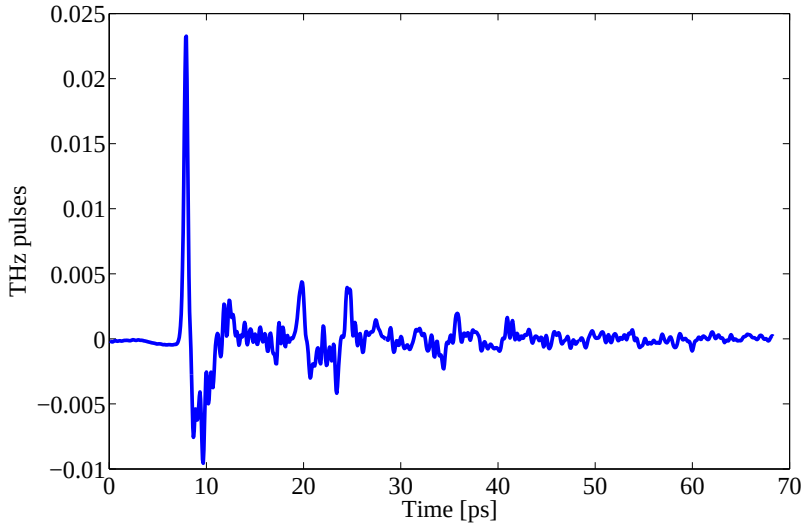

Figure 6.4: Received THz pulse of air from TDS system

where, $\tilde{E}_{sam}(f)$ and $\tilde{E}_{ref}(f)$ are the complex spectra of the sample and reference, obtained from the Fourier Transform of the corresponding time-domain response.

Since the THz wave arriving at the sample is regarded as the TE wave, thus the propagation of the wave through the sample can be described by:

$$\tilde{A} = e^{-\frac{i2\pi f\tilde{n}d}{c}} \tag{6.2}$$

where, f is the frequency; $\tilde{n}$ is the complex refractive index; d is the sample thickness; c is the speed of light in free space.

Therefore, the analytical transfer function can be obtained:

$$\tilde{H}(f) = \tilde{t}_{12}(f)\tilde{t}_{21}(f)e^{-\frac{i2\pi f(\tilde{n}-n_{air})d}{c}} \tag{6.3}$$

where, f is the frequency; $\tilde{n}$ is the complex refractive index; n_{air} is the refractive index of air because air is usually taken as the reference; d is the sample thickness; c is the free-space light speed; $\tilde{t}_{12}(f)$ and $\tilde{t}_{21}(f)$ are the Fresnel transmission coefficients associated with the front and back boundary interfaces between sample and holder medium.

According to [17], there are three ways to do the data-processing to obtain the refractive index.

First, assuming that the Fresnel coefficients in Eq. 6.3 are both real number while there is no internal reflections and Fabry-Perot effect; thus the refractive index n and extinction coefficient κ can be obtained:

$$\begin{cases} n(f) = 1 + \frac{c}{2\pi fd}(\phi_{sam}(f) - \phi_{ref}(f)) \\ \kappa(f) = -\frac{c}{2\pi fd}ln(\frac{|\tilde{E}_{sam}(f)|}{|\tilde{E}_{ref}(f)|}\frac{(1+n(f))^2}{4n(f)}) \end{cases} \tag{6.4}$$

where, $\phi_{sam}(f)$ and $\phi_{ref}(f)$ are the unwrapped phase of the sample and reference spectra.

Second, the internal reflections and complex Fresnel coefficients are considered, thus the Fresnel coefficients in Eq. 6.3 can be obtained:

$$\begin{cases} \tilde{t}_{12}(f) = \frac{2n_{air}}{\tilde{n}(f)+n_{air}} \\ \tilde{t}_{21}(f) = \frac{2\tilde{n}(f)}{\tilde{n}(f)+n_{air}} \end{cases} \tag{6.5}$$

and an additional term $\sum[\tilde{r}^2(f)e^{-\frac{i4d\pi f\tilde{n}(f)}{c}}]$ would be added, where $\tilde{r}(f) = \frac{\tilde{n}(f)-n_{air}}{\tilde{n}(f)+n_{air}}$. To obtain the refractive index $\tilde{n}$, the non-linear regression algorithm should be applied.

Third, all the effects including the complex Fresnel coefficients, internal reflection and Fabry-Perot effect are taken into account, where the following term is added to Eq. 6.3 [19]:

$$\begin{aligned} FP(f) &= 1 + r^2(f)A^2(f) + r^4(f)A^2(f) + ... \\ &= \sum_{i=0}^{\infty}(r^2(f)A^2(f))^i \\ &= (1 - r^2(f)A^2(f))^{-1} \end{aligned} \tag{6.6}$$

Thus, Eq. 6.3 becomes:

$$H(f) = \frac{\tilde{t}_{12}(f)_{21}(f)e^{-\frac{i2\pi fd(\tilde{n}(f)-n_{air})}{c}}}{1 - r^2(f)e^{-\frac{i4\pi fd\tilde{n}(f)}{c}}} \tag{6.7}$$

Similar to second approximation, the non-linear regression algorithm is also adopted to get the refractive index [20–22].

6.3 Measured Results and Discussions

The collagen samples are cultivated in Blizard Institute and then measured with the THz TDS system at QMUL. First, the system without the holder is measured to get the time-domain pulse response of the air and then the response of system with empty holder is measured. At the end, the holder with samples is measured. For each sample with different thickness, 3 measurements would be conducted and the mean value would be adopted. Fig. 6.5 shows the time response of air, empty holder and the holder with the sample for just one measurement, from which we can see that the inclusion of holder causes considerable delay and attenuation of the pulse compared to the air while the sample introduced slight delay and attenuation compared to the empty holder. By doing the *Fourier Transform* and related data-processing shown in Section 6.2.2, the refractive index and extinction coefficient can be obtained, as shown in Fig. 6.6. The Matlab code is shown in Appendix B. We can see that with the rise of the frequency the refractive index and extinction coefficient both go down. Before

$0.5\ THz$, both parameters descend steeply while after $0.5\ THz$ both parameters drop slightly.

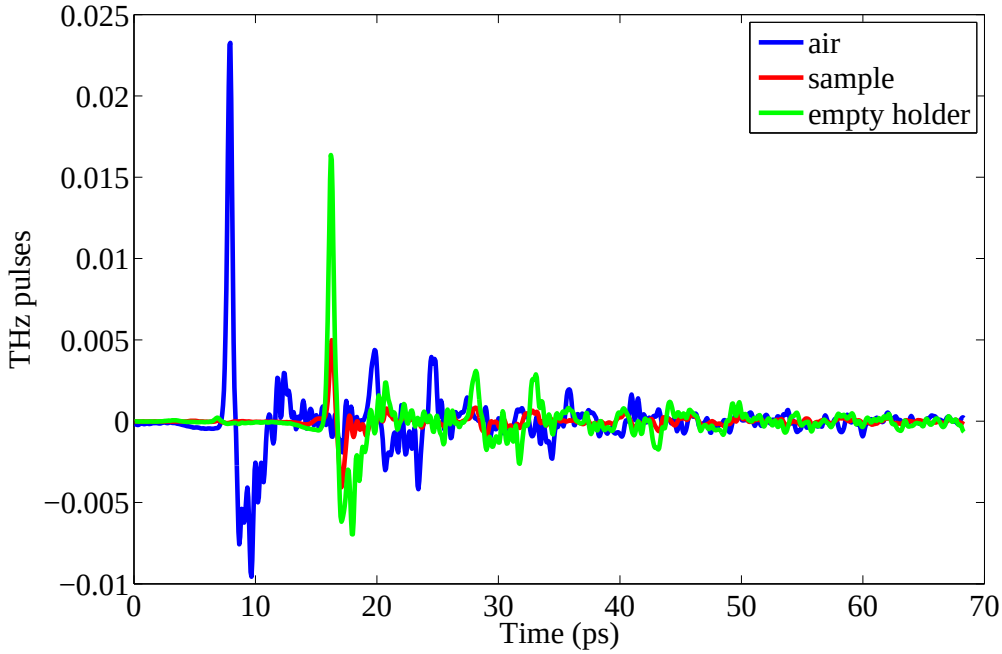

Figure 6.5: Time response of air, empty holder and the holder with the sample measured by THz-TDS system

Using the following relationship between the EM parameters to the optical parameters, Eq. 6.8, the permittivity of the collagen can be obtained, as shown in Fig. 6.7. Similar to the optical parameters, the permittivity falls with the increase of the frequency and there is also a frequency point, $0.5\ THz$ approximately, where the trend of both curves change.

$$\begin{cases} \epsilon' = n_r(f)^2 - \kappa(f)^2 \\ \epsilon'' = 2n_r(f)\kappa(f) \end{cases} \tag{6.8}$$

where, ϵ' and ϵ'' are the real and imaginary part of the permittivity ϵ.

The comparison between the measured results with the data shown in [23], [24] and [25] is shown in Fig. 6.8. From the figure, it can be easily seen that although the trend of the three curves are similar, the permittivity of the measured collagen is less than the others' data, demonstrating that the collagen is not enough to represent the epidermis at the band of interest. Also, it can be easily noticed that the trend of data in [24] is different from others in the lower frequency band, which is mainly due to the

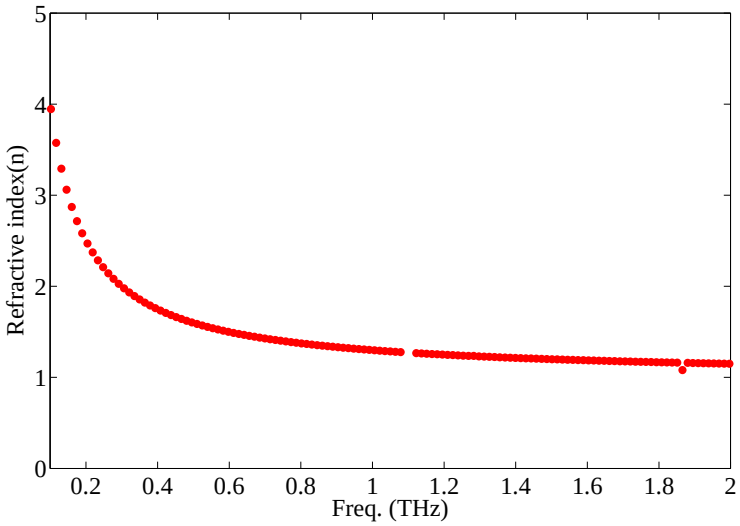

(a) Relative refractive index measured by THz-TDS system

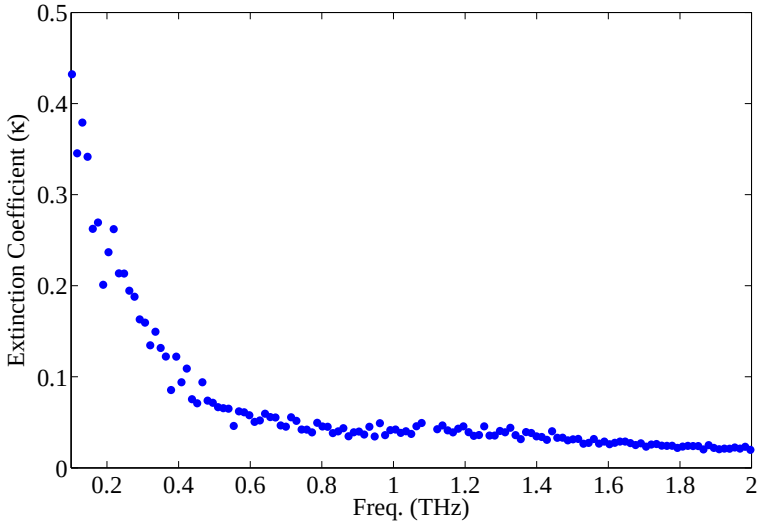

(b) Extinction coefficient measured by THz-TDS system

Figure 6.6: Measured optical parameters of collagen from THz-TDS system

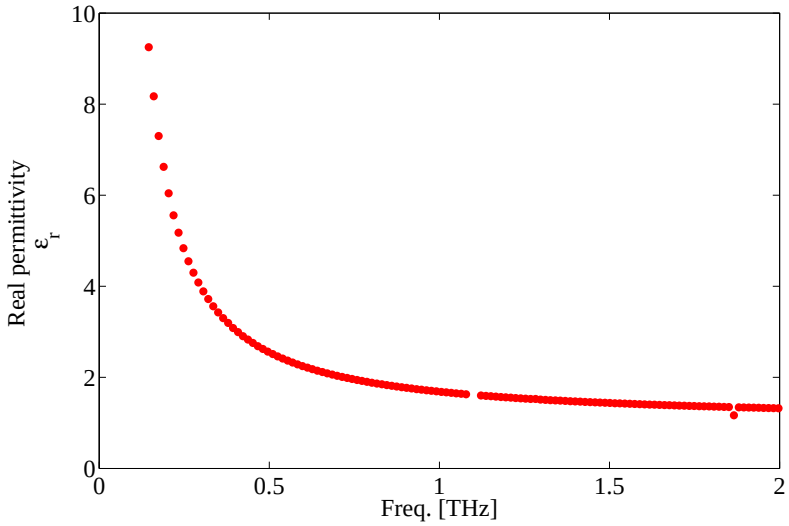

(a) Real part of the dielectric constant measured by THz-TDS system

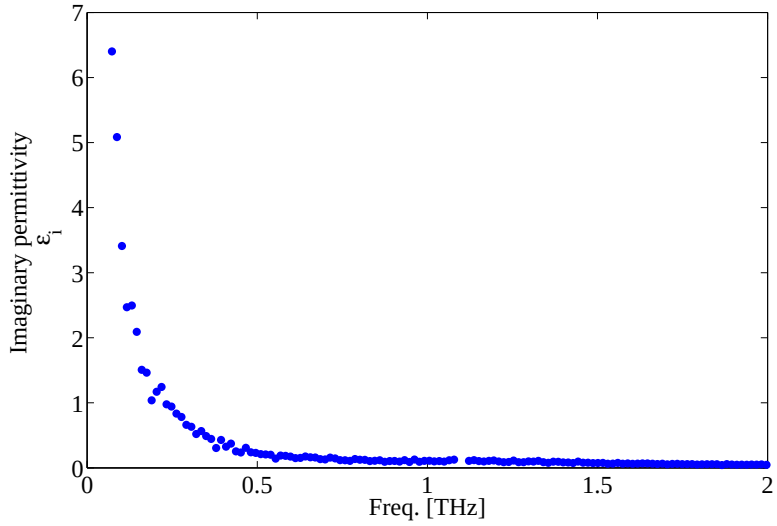

(b) Imaginary part of the dielectric constant measured by THz-TDS system

Figure 6.7: Calculated complex dielectric constant of collagen from Eq. 6.8

fact that the samples applied are dehydrated.

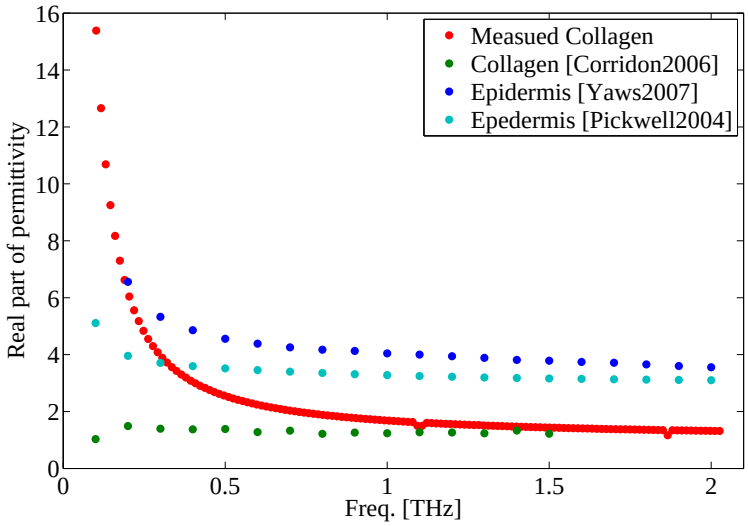

(a) Comparison of the real part of the dielectric constants of skin

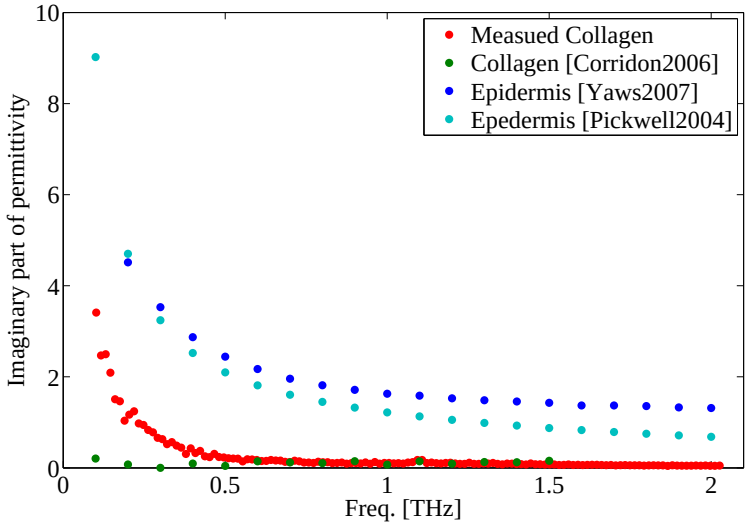

(b) Comparison of the imaginary part of the dielectric constants of skin

Figure 6.8: Comparison between the measured results with other avaiblable data from [23–25]

6.4 Modelling of the Measured Results

6.4.1 Dielectric Model of Collagen at THz Band

As stated before, human tissue is always considered as a dispersive material; thus, relative permittivity and conductivity should be both included in the model. And

from the previous section, it can be easily seen that the frequency rise will cause steep drop of the permittivity. Therefore, Debye model, shown in Eq. 6.9 would be appropriate to express the dependence of dielectric properties on the frequency. Complex permittivity of human tissue in the very low frequency range is well-described by the single-debye relaxation model, while its responses in higher frequencies above 0.1 THz require extra Debye relaxation process [26] because of the higher water content of various human tissues [13].

$$\epsilon_\omega = \epsilon_\infty + \sum_n \frac{\Delta\epsilon_n}{1 + j\omega\tau_n} \tag{6.9}$$

where $\Delta\epsilon_n$ is the difference between static permittivity and permittivity at higher frequencies $\epsilon_s - \epsilon_\infty$, indicating the permittivity dispersion of the nth-Debye relaxation process; ω is the angular frequency and ϵ_∞, τ_n are the permittivity at infinite frequency and relaxation time.

The double-Debye model, shown in Eq. 6.10 was first applied to describe the dielectric function of water, and then has been widely used for highly hydrated mixtures [27–29]. In [30], it has already been used as the function to describe the interaction of THz radiation with human skin tissue.

$$\epsilon_\omega = \epsilon_\infty - \frac{\Delta\epsilon_1}{1 + j\omega\tau_1} + \frac{\Delta\epsilon_2}{1 + j\omega\tau_2} \tag{6.10}$$

where ϵ_∞ is the permittivity at infinite frequency , larger than the vacuum permittivity ϵ_0. $\Delta\epsilon_1$ represents the dispersion in amplitude of the slow relaxation processes, where the bulk bonding between hydrogen molecules is released to equilibrium state under the impact of external electric field. $\Delta\epsilon_2$ describes the fast relaxation process, where hydrogen-bond formation and decomposition occur. τ_1 is the relaxation time of the slow process and τ_2 is the relaxation time of the fast process [28, 31]. ω is the angular frequency.

6.4.2 Fitting Algorithm

To obtain the parameters of *Double-Debye Model*, the Euclidean distance [32] between the raw data input and the Eq. 6.10 output was employed, shown in Eq. 6.11:

$$e = \frac{1}{N}\sum_{i=1}^{N}[(\frac{\epsilon'_{\omega_i} - \hat{\epsilon}'_{\omega_i}}{median[\epsilon'_{\omega_i}]})^2 + (\frac{\epsilon''_{\omega_i} - \hat{\epsilon}''_{\omega_i}}{median[\epsilon''_{\omega_i}]})^2] \tag{6.11}$$

where ϵ'_{ω_i} and ϵ''_{ω_i} are the real and imaginary part of measured dielectric properties. $\hat{\epsilon}'_{\omega_i}$ and $\hat{\epsilon}''_{\omega_i}$ represent the output of the Debye equation for real and imaginary part of the dielectric properties, respectively, and N is the number of points picked across the frequency range of 0.1 THz to 1.5 THz (almost 212 for this study).

The optimisation problem can be summarised below:

$$\begin{aligned} \min_{\epsilon_\infty,\Delta\epsilon_1,\Delta\epsilon_2,\tau_1,\tau_2} & \frac{1}{N}\sum_{i=1}^{N}[(\frac{\epsilon'_{\omega_i} - \hat{\epsilon}'_{\omega_i}}{median[\epsilon'_{\omega_i}]})^2 + (\frac{\epsilon''_{\omega_i} - \hat{\epsilon}''_{\omega_i}}{median[\epsilon''_{\omega_i}]})^2] \\ \text{subject to} \quad & \epsilon_\infty \geq 1 \\ & \Delta\epsilon_1 \geq 0, \Delta\epsilon_2 \geq 0 \\ & \tau_1 \geq 0, \tau_2 \geq 0 \end{aligned} \tag{6.12}$$

To solve this problem, particle swarm optimization (PSO) [33–35] was applied, which would return all Double Debye variables for the five set of parameters if the Euclidean distance is smaller than the threshold of 0.0012.

The number of particles chosen in the PSO algorithm here was 500. The algorithm would end after 1000 iterations if the threshold were not reached before this point. The final parameters of the Double Debye Model are shown in Table 6.1 and Fig. 6.9 demonstrates the comparison between the complex permittivity calculated from the double debye model and the measured data for collagen, showing that the proposed dielectric model mimics very well the dielectric properties of collagen not only at the high range of frequency beyond 1 THz but also at the lower band.

ϵ_∞	$\Delta\epsilon_1$	τ_1 (ps)	$\Delta\epsilon_2$	τ_2 (ps)
1.63	500	17.7	100	3.64

Table 6.1: Parameters of double Debye model optimised by PSO algorithm

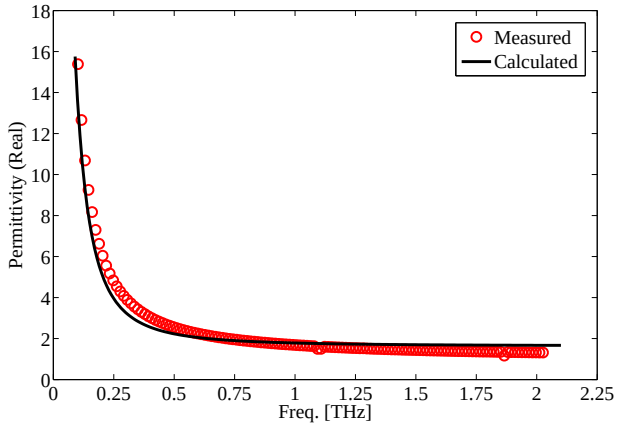

(a) Real part of the permittivity

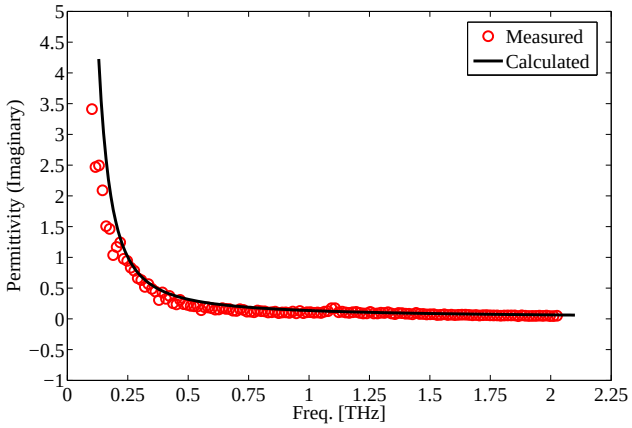

(b) Imaginary part of the permittivity

Figure 6.9: Measured complex permittivity of collagen and its fitting model

6.5 Comparison with the Proposed Model

This section is a supplement of the work in Chapter 4. Based on the previous work, the absorption coefficient of collagen at the band of interest can be obtained. Then using the equation $10lge^{\alpha d}$ with d as $1mm$, the corresponding path loss can be calculated, shown in Fig. 6.10. Also, the rough power loss can be obtained by the equation: $20lg\frac{E_{sample}}{Eholder}$ through the measured data, also shown in Fig. 6.10. Then using the least square optimisation method,the fitting models of both results can be obtained, also shown in Fig. 6.10. We can see that the differences between both losses go larger with the rise of the frequency. It is mainly due to the fact that when the frequency goes up, the SNR would fall down which would introduce more error. On the other hand, the theoretical losses do not include the reflection loss of the air-TPX interfaces and the TPX-sample interfaces.

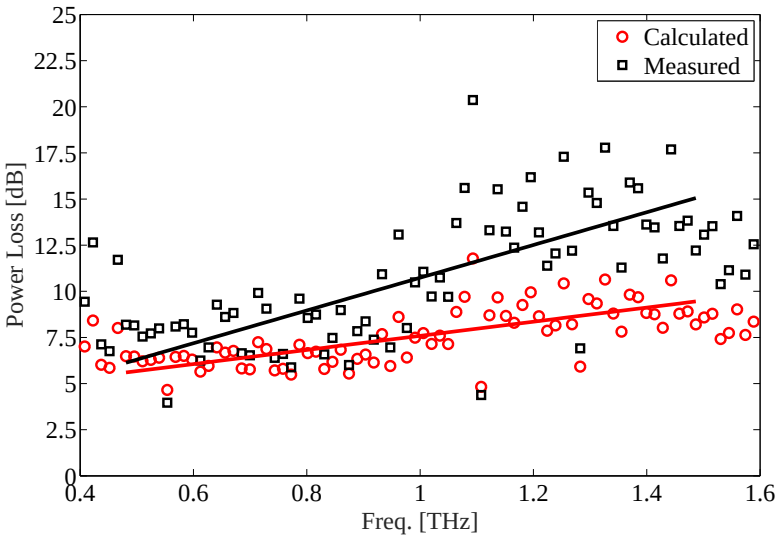

Figure 6.10: Comparison of the measured power losses to the theoretical ones of the sample with thickness of 1 mm with their fitting models

6.6 Summary

In this chapter, the EM/optical parameters of cultivated collagen are measured with the THz Time Domain Spectroscopy (THz-TDS) system and compared with the available data, showing that the collagen is not enough to represent the performance of the epidermis at the band of interest. At the same time, a double Debye model of collagen

at THz band was also introduced by studying the measured results, followed by the validation of the model proposed in previous chapters.

References

[1] A. Fitzgerald, E. Berry, N. Zinov'ev, S. Homer-Vanniasinkam, R. Miles, J. Chamberlain, and M. Smith, "Catalogue of human tissue optical properties at terahertz frequencies," *Journal of Biological Physics*, vol. 29, no. 2-3, pp. 123–128, 2003.

[2] E. Berry, A. J. Fitzgerald, N. N. Zinov'ev, G. C. Walker, S. Homer-Vanniasinkam, C. D. Sudworth, R. E. Miles, J. M. Chamberlain, and M. A. Smith, "Optical properties of tissue measured using terahertz-pulsed imaging," in *Medical Imaging 2003*. International Society for Optics and Photonics, 2003, pp. 459–470.

[3] D. Lipscomb, I. Echchgadda, X. G. Peralta, and G. J. Wilmink, "Determination of the optical properties of melanin-pigmented human skin equivalents using terahertz time-domain spectroscopy," vol. 8585, 2013.

[4] A. Markelz, A. Roitberg, and E. Heilweil, "Pulsed terahertz spectroscopy of dna, bovine serum albumin and collagen between 0.1 and 2.0 thz," *Chemical Physics Letters*, vol. 320, no. 1, pp. 42–48, 2000.

[5] M. He, A. K. Azad, S. Ye, and W. Zhang, "Far-infrared signature of animal tissues characterized by terahertz time-domain spectroscopy," *Optics Communications*, vol. 259, no. 1, pp. 389–392, 2006.

[6] C. Hua, M. Shi-Hua, Y. Wen-Xing, W. Xiu-Mei, and W. Xiao-Zhou, "The diagnosis of human liver cancer by using thz fiber-scanning near-field imaging," *Chinese Physics Letters*, vol. 30, no. 3, p. 030702, 2013.

[7] T. Bowman, M. El-Shenawee, and S. G. Sharma, "Terahertz spectroscopy for the characterization of excised human breast tissue," in *Microwave Symposium (IMS), 2014 IEEE MTT-S International*. IEEE, 2014, pp. 1–4.

[8] B. C. Truong, H. D. Tuan, A. J. Fitzgerald, V. P. Wallace, and H. T. Nguyen, "A dielectric model of human breast tissue in terahertz regime," *Biomedical Engineering, IEEE Transactions on*, vol. 62, no. 2, pp. 699–707, 2015.

[9] P. C. Ashworth, E. Pickwell-MacPherson, E. Provenzano, S. E. Pinder, A. D. Purushotham, M. Pepper, V. P. Wallace *et al.*, "Terahertz pulsed spectroscopy of freshly excised human breast cancer," *Optics express*, vol. 17, no. 15, pp. 12 444–12 454, 2009.

[10] R. Pethig, "Dielectric properties of biological materials: Biophysical and medical applications," *Electrical Insulation, IEEE Transactions on*, no. 5, pp. 453–474, 1984.

[11] C. Gabriel, S. Gabriel, and E. Corthout, "The dielectric properties of biological tissues: I. literature survey," *Physics in medicine and biology*, vol. 41, no. 11, p. 2231, 1996.

[12] S. Gabriel, R. Lau, and C. Gabriel, "The dielectric properties of biological tissues: Ii. measurements in the frequency range 10 hz to 20 ghz," *Physics in medicine and biology*, vol. 41, no. 11, p. 2251, 1996.

[13] ——, "The dielectric properties of biological tissues: Iii. parametric models for the dielectric spectrum of tissues," *Physics in medicine and biology*, vol. 41, no. 11, p. 2271, 1996.

[14] C. C. Johnson and A. W. Guy, "Nonionizing electromagnetic wave effects in biological materials and systems," *Proceedings of the IEEE*, vol. 60, no. 6, pp. 692–718, 1972.

[15] D. Grischkowsky, S. Keiding, M. Van Exter, and C. Fattinger, "Far-infrared time-domain spectroscopy with terahertz beams of dielectrics and semiconductors," *JOSA B*, vol. 7, no. 10, pp. 2006–2015, 1990.

[16] O. Sushko, "Terahertz dielectric study of bio-molecules using time-domain spectrometry and molecular dynamics simulations," Ph.D. dissertation, School of Electronic Engineering and Computer Science, Queen Mary University of London, March 2014.

[17] O. Sushko, K. Shala, R. Dubrovka, and R. Donnan, "Revised metrology for enhanced accuracy in complex optical constant determination by thz-time-domain spectrometry," *JOSA A*, vol. 30, no. 5, pp. 979–986, 2013.

[18] H. C. B. Skjeie, "Terahertz time-domain spectroscopy," July 2012.

[19] M. Born and E. Wolf, *Principles of optics: electromagnetic theory of propagation, interference and diffraction of light*. Cambridge university press, 1999.

[20] L. Duvillaret, F. Garet, and J.-L. Coutaz, "A reliable method for extraction of material

parameters in terahertz time-domain spectroscopy," *Selected Topics in Quantum Electronics, IEEE Journal of*, vol. 2, no. 3, pp. 739–746, 1996.
[21] ——, "Highly precise determination of optical constants and sample thickness in terahertz time-domain spectroscopy," *Applied optics*, vol. 38, no. 2, pp. 409–415, 1999.
[22] W. Withayachumnankul, B. Ferguson, T. Rainsford, S. Mickan, and D. Abbott, "Simple material parameter estimation via terahertz time-domain spectroscopy," *Electronics Letters*, vol. 41, no. 14, pp. 800–801, 2005.
[23] K. Yaws, D. Mixon, and W. Roach, "Electromagnetic properties of tissue in the optical region," in *Biomedical Optics (BiOS) 2007*. International Society for Optics and Photonics, 2007, pp. 643 507–643 507.
[24] P. M. Corridon, R. Ascázubi, C. Krest, and I. Wilke, "Time-domain terahertz spectroscopy of artificial skin," in *Biomedical Optics 2006*. International Society for Optics and Photonics, 2006, pp. 608 007–608 007.
[25] E. Pickwell, B. Cole, A. Fitzgerald, M. Pepper, and V. Wallace, "In vivo study of human skin using pulsed terahertz radiation," *Physics in Medicine and Biology*, vol. 49, no. 9, p. 1595, 2004.
[26] H. J. Liebe, G. A. Hufford, and T. Manabe, "A model for the complex permittivity of water at frequencies below 1 thz," *International Journal of Infrared and Millimeter Waves*, vol. 12, no. 7, pp. 659–675, 1991.
[27] S. Smye, J. Chamberlain, A. Fitzgerald, and E. Berry, "The interaction between terahertz radiation and biological tissue," *Physics in medicine and biology*, vol. 46, no. 9, p. R101, 2001.
[28] E. Pickwell, B. Cole, A. Fitzgerald, V. Wallace, and M. Pepper, "Simulation of terahertz pulse propagation in biological systems," *Applied Physics Letters*, vol. 84, no. 12, pp. 2190–2192, 2004.
[29] J. Kindt and C. Schmuttenmaer, "Far-infrared dielectric properties of polar liquids probed by femtosecond terahertz pulse spectroscopy," *The Journal of Physical Chemistry*, vol. 100, no. 24, pp. 10 373–10 379, 1996.
[30] B. C. Truong, H. D. Tuan, H. H. Kha, and H. T. Nguyen, "Debye parameter extraction for characterizing interaction of terahertz radiation with human skin tissue," *Biomedical Engineering, IEEE Transactions on*, vol. 60, no. 6, pp. 1528–1537, 2013.
[31] J. Barthel and R. Buchner, "High frequency permittivity and its use in the investigation of solution properties," *Pure and Applied Chemistry*, vol. 63, no. 10, pp. 1473–1482, 1991.
[32] M. Lazebnik, D. Popovic, L. McCartney, C. B. Watkins, M. J. Lindstrom, J. Harter, S. Sewall, T. Ogilvie, A. Magliocco, T. M. Breslin *et al.*, "A large-scale study of the ultrawideband microwave dielectric properties of normal, benign and malignant breast tissues obtained from cancer surgeries," *Physics in Medicine and Biology*, vol. 52, no. 20, p. 6093, 2007.
[33] T. Yilmaz, R. Foster, and Y. Hao, "Towards accurate dielectric property retrieval of biological tissues for blood glucose monitoring," *Microwave Theory and Techniques, IEEE Transactions on*, vol. 62, no. 12, pp. 3193–3204, Dec 2014.
[34] M. Clerc, *Particle swarm optimization*. John Wiley & Sons, 2010, vol. 93.
[35] R. C. Eberhart and Y. Shi, "Particle swarm optimization: developments, applications and resources," in *Evolutionary Computation, 2001. Proceedings of the 2001 Congress on*, vol. 1. IEEE, 2001, pp. 81–86.

Chapter 7

Conclusion and Future Work

7.1 Conclusion

Nano communication has driven great research interests since its proposal in 2008 as it will enable a plenty of applications in many fields, not only healthcare and monitoring, but also industrial development and environment-protection. Although the study of Nano-Network Communication is still at its early phase, it is generally believed that the research work on the hardware-oriented research and communication-focused investigations on EM communication paradigm of Nano-Communication is essential which could pave the road and make the future work much more convenient.

In this thesis, the main focus was put on the fundamental study of the body-centric nano-communication, especially the in-body one. Based on this aim, the channel model of THz wave in human tissues was studied and investigated, showing the potential of THz band ($0.1 - 10\ THz$) as the working band for EM paradigm. It is generally believed that when the operation band goes higher, the skin model with roughness interfaces should be investigated because both the wavelength and roughness will be of the same order of magnitude; thus, a new model with 3-D sinc interface was proposed based on the study of the similar one with 3-D sine interface. During the study, we found the data-base of the parameters of human tissues was not sufficient,

so the measurement of parameters of human tissues was conducted.

7.2 Key Contributions

The major contributions of this work are summarised as follows:

- In chapter 4, a 3-D numerical model of THz nano-communicational channel has been applied for in-body scenarios and validated by the analytical model. Channel characteristics and the system capacity for different human tissues have been calculated. The comparison between the numerical and analytical results are conducted, showing a good agreement compared with the total path loss and the reliability of the proposed numerical model. Meanwhile, the proposed model paves the way to the further studies considering more body structures and tissue properties. In the meantime, the noise model has been applied to calculate the capacity for different power allocation which indicates that for the Gaussian shaped pulse the capacity can reach and maintain 100 Tbps for the distance up to several millimetres which indicates the promising future of the application of the EM paradigm to the body-centric nano-communication.

- In chapter 5, 3-D stratified skin models are built to investigate the wave propagation from the under-skin to skin surface. Then, the influence of the rough interface between different skin layers is investigated by introducing two detailed skin models with different interfaces (i.e.,3-D sine function and 3-D sinc function). The mean and deviation of the power losses for both models are compared with the common flat model, showing that it is possible to transmit the signal through the skin since the power loss is just around -80 dB at 700 μm and the general flat model can be applied to do the rough research since the difference is always less than 4 dB. And the effects of the sweat duct on the wave propagation is also analysed. The results show great potential of the THz waves on sensing and communicating.

- In chapter 6, the EM/optical parameters of collagen, the main building material of skin are measured with the THz Time Domain Spectroscopy (THz-TDS)

system at Queen Mary University of London to obtain the electromagnetic parameters with the aim to enrich the database with the cooperation of Blizard Institute, London UK. At the same time, the double Debye model of the dielectric parameters at the band of interest was also studied and the validation of the proposed channel model was done.

7.3 Future Work

In line with the work presented, the future research directions which would make potential and natural progression to complete the studies in the thesis are summarised:

Measurement on the parameters of the human tissues

Although several optical parameters are provided, it is still not enough. First, the experiment was conducted long time ago and the number of tissues was limited. Second, the samples were mainly from one old male which lower the credibility of the results. Therefore, it is necessary to redo the experiments to get the parameters of interest by measuring more samples from different people.

Safety issues: heating problems of THz wave

Safety issue is always the main consideration when people talks about nano-network, especially when the nano-devices are applied to the in-body scenario. For THz communication, heating problem was the main concern in the academic field. Therefore, the study of the THz wave heating effects on the human tissue would be conducted to make the standard and requirement for communicating or sensing.

Interaction between the nano-devices and the surrounding environment

From the study of the models of nerve system and skin, it seems dispensable to study the detailed model when the size of the functional devices goes down to milli/nano-scale. The interaction between the environment and the devices should be study to make sure the devices function normal.

Simulating body-centric nano-networks using the state-of-art simulator

Although there are lots of communication paradigms for nano-communication, the study on interaction between each two different communications, for example the EM communication and the molecular communication, is still missing. It is generally believed that by emerging all the communications together the nano-network would be much more flexible and powerful. With the comprehensive simulator proposed in IEEE P1906.1 based on the ns-3 platform in mind, different communication schemes would be studied by comparing to the EM one. And at the same time, the relationship between them and EM method should be further studied.

Appendix A

Applications of Nano-Communication [1, 2]

There are a great numbers of potential applications of nano-networks, which can be mainly divided into four groups: biomedical, environmental, industrial and military [1, 2]. Additionally, the applications of nano-networks are not limited into these four domains; and they also can be used extensively into other fields like consumer electronics, life style and home appliances because nano-technologies have an essential role in the manufacturing process of several devices.

A.1 Biomedical Applications

A large number of direct applications of nano-networks are related to the biological field. Biological models encourage the use of nano-technologies to interact with organs and tissues because the most molecules, proteins, DNA and the major components of cells are almost at the nano-scale. Thus, it is clear that the advantages of nano-networks are in terms of the size, bio-compatibility and bio-stability of both the device and network. By controlling the system components at molecular level, nano-sensors can provide an interface between biological phenomenal and electronic nano-devices to complete the communication of nano-networks.

- Bio-hybrid implants: the aim is to support or substitute components such as

nervous tracks or some lost tissues [3, 4] because nano-networks can provide friendly interfaces between the implant and the human body. Restoration of central nervous system tracks is the most possible application of bio-hybrid implants.

- Genetic engineering: manipulation and modification of nano-structures such as molecular sequences and genes can be achieved by nano-machines; therefore, using nano-networks can expand the potential applications in genetic engineering.

- Immune system support: like the bio-immune system, the artificial immune system will help the organism fight against virus with the aid of a collection of nano, micro and macro systems, including sensors and actuators, acting in a coordinated way to identify and control foreign and pathogen elements. At the nano-network, nano-machines will be used to detect or eliminate procedures. They could realize tasks of localization and response to malicious agents and cells [5, 6], such as cancer cells, resulting in a less aggressive and invasive treatments compared to the existing ones.

- Health monitoring system: the concentration of sodium, glucose and oxygen in blood [7], cholesterol level [8], cancer bio-markers [9] or other infectious agents [10] can be checked by nano-sensors. For example, one can use a tattoo-like sensor to monitor the glucose level instead of pricking his finger several times a day [7]. [9] also provides an overview of the bio-sensor technology which are being developed and researched for cancer markers diagnosis. The need to deliver the information retrieved by these nano-sensors or systems to relevant actors require the set-up of nano-networks which can provide the proper level of connectivity to complete the communication between the nano-devices or deliver the sensed information from nano-systems to micro-systems.

- Drug delivery systems: nano-sensors can be utilized to monitor a specific substance, then nano-actuators can be used to carry out some simple tasks like releasing a specific drug in some unreachable areas of human body [11]. [1] describes the general idea: a distributed nano-networks of nano-sensors and nano-actuators can work cooperatively to decide whether or not to release a given

drug to control the intra-cranial pressure, a chemical compound to dissolve a clot in an artery, or an engineered antibody to improve the immunologic system of humans in front of new diseases; and they work with cooperative schemes to make the decision on the fly. At the same time, all these data can be collected and remotely monitored by doctors. For instance, if the system is used to compensate metabolism diseases like diabetes, nano-sensors and smart glucose reservoirs or producers can work in a cooperative way to support regulating mechanisms [12]. This system can also be used to help mitigate the effects of neuro-degenerative diseases by delivering neurotransmitters or specific drugs [13].

A.2 Environmental Applications

It is said that the original idea of nano-networks is from biological systems found in nature, so the nano-sensor or nano-actuator can be applied to achieve some goals which current technologies could not deal with. Some possible applications are as follows:

- Bio-degradation: take the garbage handling, a thorny problem around the world, as an example, with the aid of the nano-networks, the garbage can be sensed and tagged by different material so that it can be located and processed by the smart nano-actuators [1].

- Bio-control: it is well-known that plants can release some chemical composites to the air to attract the predators of the insect or regulate their blooming among different plantation [14, 15]. Nano-chemical sensors can be used to detect such chemical composites to monitor the on-going process in the field. When insects appear, nano-actuators can be used to release the natural volatiles to attract the predators of the insects or to release the chemical composites to control the behaviour of the insects because some pheromone can trigger certain behaviour on animals in nature.

- Air pollution control: like bio-degradation, nano-networks can be used to monitor the air. If possible, nano-filters can be applied to purify the air [16].

A.3 Industrial Applications

The emphasis is put on the intra-body application of nano-network; but at the same time, nano-networks can also be used in industries ranging from flexible and stretchable electronic devices [17] to new fictionalized nano-materials for intelligent self-cleaning anti-microbial textiles [18].

- Product quality control: Similar to health monitoring applications, nano-networks can be applied to the product quality control. Nano-sensors can be used to detect small bacterial and toxic components which cannot be detected by the traditional technologies [19] while the nano-actuator can be used to kill them or removing them.

- Intelligent office: The interconnection of nano-devices with existing communication networks, ultimately Internet, will supply new interceding applications which will have great influence on the way we live. If everything is attached with a nano-sensor which is allowed to connect to the Internet permanently, the user can keep track of all its professional and personal belongings in an effortless way. Ultimately, these nano-sensors can be connected seamlessly to create a smart working environment or living environment.

A.4 Military Applications

Communication among the nano-device makes the applications of nanotechnology in military field practical, which are shown as follows:

- Nuclear, biological and chemical defences: nano-sensors can be deployed over the battlefield or targeted areas to detect aggressive chemical and biological agents and coordinate with the nano-actuators to make accurate defensive response [20]. Nano-networks can also be used in Customer to detect if there is unauthorized entrance of chemical, biological or radiological materials.

- Nano-fictionalized equipment: similar to the environment control, nano-networks can be taken advantage of in the uniform or the camouflage. For example, equipment can be manufactured with advanced materials containing nano-networks

that can self-regulate the temperature underneath soldiers' clothes [21] and even detect whether the soldier has been injured to take initial treatment, or change the color of the cloth to camouflage the soldier like the lizard.

References

[1] I. F. Akyildiz and J. M. Jornet, "Electromagnetic wireless nanosensor networks," *Nano Communication Networks*, vol. 1, no. 1, pp. 3–19, 2010.

[2] I. F. Akyildiz, F. Brunetti, and C. Blázquez, "Nanonetworks: A new communication paradigm," *Computer Networks*, vol. 52, no. 12, pp. 2260–2279, 2008.

[3] K. E. Drexler, *Nanosystems: molecular machinery, manufacturing, and computation*. John Wiley & Sons, Inc., 1992.

[4] R. A. Freitas, "What is nanomedicine?" *Nanomedicine: Nanotechnology, Biology and Medicine*, vol. 1, no. 1, pp. 2–9, 2005.

[5] C.-J. Chen, D. Y. Haik, and J. Chatterjee, "Development of nanotechnology for biomedical applications," in *Emerging Information Technology Conference, 2005.* IEEE, 2005, pp. 4–pp.

[6] R. A. Freitas, "Nanotechnology, nanomedicine and nanosurgery," *International Journal of Surgery*, vol. 3, no. 4, pp. 243–246, 2005.

[7] J. M. Dubach, D. I. Harjes, and H. A. Clark, "Fluorescent ion-selective nanosensors for intracellular analysis with improved lifetime and size," *Nano Letters*, vol. 7, no. 6, pp. 1827–1831, 2007.

[8] J. Li, T. Peng, and Y. Peng, "A cholesterol biosensor based on entrapment of cholesterol oxidase in a silicic sol-gel matrix at a prussian blue modified electrode," *Electroanalysis*, vol. 15, no. 12, pp. 1031–1037, 2003.

[9] I. E. Tothill, "Biosensors for cancer markers diagnosis," in *Seminars in cell & developmental biology*, vol. 20, no. 1. Elsevier, 2009, pp. 55–62.

[10] P. Tallury, A. Malhotra, L. M. Byrne, and S. Santra, "Nanobioimaging and sensing of infectious diseases," *Advanced drug delivery reviews*, vol. 62, no. 4, pp. 424–437, 2010.

[11] R. Fernández-Pacheco, J. G. Valdivia, and M. R. Ibarra, "Magnetic nanoparticles for local drug delivery using magnetic implants," in *Micro and Nano Technologies in Bioanalysis*. Springer, 2009, pp. 559–569.

[12] R. A. Freitas, "Pharmacytes: An ideal vehicle for targeted drug delivery," *Journal of Nanoscience and Nanotechnology*, vol. 6, no. 9-10, pp. 2769–2775, 2006.

[13] B. Wowk, "Cell repair technology," *Cryonics, vol*, pp. 21–30, 1988.

[14] M. Heil and J. Ton, "Long-distance signalling in plant defence," *Trends in plant science*, vol. 13, no. 6, pp. 264–272, 2008.

[15] C. M. Pieterse and M. Dicke, "Plant interactions with microbes and insects: from molecular mechanisms to ecology," *Trends in plant science*, vol. 12, no. 12, pp. 564–569, 2007.

[16] J. Han, J. Fu, and R. B. Schoch, "Molecular sieving using nanofilters: past, present and future," *Lab on a Chip*, vol. 8, no. 1, pp. 23–33, 2008.

[17] J. Rogers, "Materials and mechanics for stretchable electronics-from electronic eye cameras to conformal brain monitors," in *Solid-State Sensors, Actuators and Microsystems Conference, 2009. TRANSDUCERS 2009. International*. IEEE, 2009, pp. 1602–1603.

[18] D. Tessier, I. Radu, and M. Filteau, "Antimicrobial fabrics coated with nano-sized silver salt crystals," in *NSTI Nanotech*, vol. 1, 2005, pp. 762–764.

[19] J. W. Aylott, "Optical nanosensorsan enabling technology for intracellular measurements," *Analyst*, vol. 128, no. 4, pp. 309–312, 2003.

[20] H. Dai, "Carbon nanotubes: Synthesis, structure, properties and application," *Topics in Applied Physics*, 2001.

[21] M. Endo, T. Hayashi, Y. A. Kim, and H. Muramatsu, "Development and application of carbon nanotubes," *Japanese Journal of Applied Physics*, vol. 45, no. 6R, p. 4883, 2006.

Appendix B

Matlab Code of Optical/EM Parameters Extraction

B.1 Principle of nlinfit( ) function

Nonlinear regression: $beta = nlinfit(X, Y, modelfun, beta0)$ returns a vector of estimated coefficients for the nonlinear regression of the responses in Y on the predictors in X using the model specified by $modelfun$. The coefficients are estimated using iterative least squares estimation, with initial values as $beta0$.

B.2 Matlab Code

```
% sample with both windows at both sides
clear all;
clc
clf
close all

c = 2.99e8;% in m/s
d_w = 2.71e-3;% in m
d_sam = 1e-3; % in m
step = 10e-6;% in m

L = 1024;
NFFT = 2^nextpow2(L);
T = 6.7e-14;              %%%%%%%%sampling time
fn = 1/T;

load Nish_holder.txt; %load the cell data in time domain;
Cell1 = (Nish_holder(:,2))';
Cell_FFT1 = fft(Cell1,NFFT)/L; %using FFT to get frequency signals;
Cell_phase = phase(Cell_FFT1);
Cell_unwrap_phase1 = unwrap(Cell_phase); %unwrapped the phase signal;
Cell_unwrap_phase = Cell_unwrap_phase1(2:513);
Cell_FFT2 = abs(Cell_FFT1);
Cell_FFT = Cell_FFT2(2:513);


load Nish_sample.txt; %load the sample data in time domain;
Sample1 = (Nish_sample(:,2))';
Sample_FFT1 = fft(Sample1,NFFT)/L; %using FFT to get frequency signals;
Sample_phase = phase(Sample_FFT1);
Sample_unwrap_phase1 = unwrap(Sample_phase); %unwrapped the phase signal;
Sample_unwrap_phase = Sample_unwrap_phase1(2:513);
Sample_FFT2 = abs(Sample_FFT1);
Sample_FFT = Sample_FFT2(2:513);


m=(1:1024);
scan_n=(m*(10*10^-6));      %%%%%%%%%%delay was 10um
tn=(2*(scan_n)/c);            %%%%%%%%%%%%%%2*stepsize/c

f = 0.5*fn*linspace(0, 1, NFFT/2+1);

figure(1)
plot (tn,Sample1,'r',tn,Cell1,'g')
xlabel('Time (s)');
ylabel('THz pulses');
legend('sample', 'empty holder')
```

```
nw = 1.43.*ones(size(f));
kw = 0.*ones(size(f));

phase_dif = Sample_unwrap_phase - Cell_unwrap_phase;
% the phase difference between the sample and the cell;
n_guess = 1+(phase_dif).*c./(2*pi.*f(2:513).*d_sam);
%%%%%nm = (phm*3e8./(2*pi*f*d)) + 1;
k_guess = -c./(2*pi.*f(2:513).*d_sam)*...
    log(Sample_FFT./Cell_FFT.*(1+n_guess).^2/(4.*n_guess));


T = Sample_FFT.*exp(-phase_dif.*1i)./Cell_FFT; % transfer function;

%%%%fitting the ns and ks using nlinfit%%%%%%
for p = 1:512

 y = T(p)';
 x = [f(p+1);nw(p);kw(p)]';

  beta0 = [n_guess(p);abs(k_guess(p))];            % regression coeficient;

  fun = @(beta,x)((((x(:, 2)-x(:, 3).*1i+1).^2).*(beta(1)-beta(2).*1i))./..
      ((x(:, 2)-x(:, 3).*1i+beta(1)-beta(2).*1i).^2).*...
      ((exp(2.*1i.*pi.*x(:, 1) .*d_sam./c)).*...
      (exp(-2.*1i.*pi.*x(:, 1) .*d_sam.*(beta(1)-beta(2).*1i)./c))));

   try beta = nlinfit(x,y,fun,beta0);

   catch err

   end

  rr = abs(real(beta));

  result(p) = mat2cell(rr,2,1)

end


ll = cell2mat(result);
ns = ll(1,:);
ks = ll(2,:);
%the fitting results of refreactive index and extinction coefficient

figure(2)
plot(f(2:513)/1e12,ns,'r');  %%%%%plotting ns
xlim([0.1 2])
```

```
xlabel('Freq. (THz)');
ylabel('Extinction Coefficient (\kappa)');


%%%%%%%%%epsilon calculation%%%%%%%%%
eps_r = ns.^2-ks.^2;
eps_i = 2.*ns.*ks;

pp(:,1) = f(8:140)';
pp(:,2) = eps_r(7:139)';
pp(:,3) = eps_i(7:139)';

save 'collagen_EMPara.txt' pp -ASCII;

figure(4)
plot(f(2:513)/1e12, eps_r, 'ro')
xlim([0 2])
ylim([0 10])
xlabel('Freq. [THz]');
ylabel('Real permittivity (\epsilon_r)');
figure(5)
plot(f(2:513)/1e12, eps_i, 'bo')
xlim([0 2])
ylim([0 10])
xlabel('Freq. [THz]')
ylabel('Imaginary permittivity (\epsilon_i)')
```